İSTANBUL TECHNICAL UNIVERSITY ★ GRADUATE SCHOOL OF SCIENCE ENGINEERING AND TECHNOLOGY

SYNTHESIZE AND CHARACTERIZATION OF MULTI-COMPONENT MAGNETIC NANO PARTICLES

M.Sc. THESIS

Mona NEJATPOUR

Department of Mechanical Engineering
Materials and Manufacture Program

JUNE 2016

İSTANBUL TECHNICAL UNIVERSITY ★ GRADUATE SCHOOL OF SCIENCE ENGINEERING AND TECHNOLOGY

SYNTHESIZE AND CHARACTERIZATION OF MULTI-COMPONENT MAGNETIC NANO PARTICLES

M.Sc. THESIS

Mona NEJATPOUR
(503141325)

Department of Mechanical Engineering

Materials and Manufacture Program

Thesis Advisor: Prof. Dr. Celaletdin Ergün

JUNE 2016

İSTANBUL TEKNİK ÜNİVERSİTESİ ★ FEN BİLİMLERİ ENSTİTÜSÜ

ÇOK BİLEŞENLİ MANYETİK NANO PARÇACIK SENTEZİ VE KARAKTERİZASYONU

YÜKSEK LİSANS TEZİ

Mona NEJATPOUR
(503141325)

Makina Mühendisliği Anabilim Dalı

Malzeme ve İmalat Programı

Tez Danışmanı: Prof. Dr. Celaletdin Ergün

HAZİRAN 2016

Mona Nejatpour, a M.Sc. student of İTU Graduate School of Science Engineering and Technology student ID **503141325**, successfully defended the thesis entitled "**SYNTHESIZE AND CHARACTERIZATION OF MULTI-COMPONENT MAGNETIC NANO PARTICLES**", which she prepared after fulfilling the requirements specified in the associated legislations, before the jury whose signatures are below.

Thesis Advisor: Prof. Dr. Celaletdin Ergün .....
İstanbul Technical University

Jury Members: Doç.Dr. Selçuk Aktürk .....
İstanbul Technical University

Doç.Dr. İbrahim Erden .....
Yıldız Technical University

Date of Submission : 02 May 2016
Date of Defense : 09 June 2016

FOREWORD

Special thnaks to Prof. Dr. Cellaletdin Ergun for his support and guidance and I thank him for all the things that he thought me during this two years. I also thank all my friends and our research group members, Selim Parlak and Elvan Aydın.

June 2016

Mona NEJATPOUR
Mechanical Engineer

TABLE OF CONTENTS

Page

FOREWORD ..... **vii**
TABLE OF CONTENTS ..... **ix**
ABBREVIATIONS ..... **xi**
SYMBOLS ..... **xiii**
LIST OF TABLES ..... **xv**
LIST OF FIGURES ..... **xvii**
SUMMARY ..... **xxiii**
ÖZET ..... **xxv**
1. INTRODUCTION **1**
1.1 Purpose of Thesis 2
1.2 Literature Review 2
1.2.1 Magnetism 2
1.2.1.1 Nanomagnetism 2
1.2.1.2 Physics of magnetism 4
1.2.1.3 Hystersis loop 4
1.2.1.4 Superparamagnetic magnetic nanoparticles 5
1.2.1.5 Heat dissipation mechanism 5
1.2.2 Synthesis methods of magnetic nanoparticles 7
1.2.2.1 Thermal decomposition 7
1.2.2.2 Microemulsion 8
1.2.2.3 Hydrothermal synthesis 8
1.2.2.4 Lases pyrolysis 8
1.2.2.5 Riverse Micelle method 9
1.2.2.6 Co-precipitation 9
1.2.3 Surface functionalization of magnetic nanoparticles 14
2. MATERIALS AND EQUIPMENTS **15**
2.1 Chemical Reagents 15
2.2 Devices for Nanoparticle Characterization 17
2.2.1 Bruker optics ALPHA-Transmittance FTIR spectrometer 17
2.2.2 Vibrating sample magnetometer (VSM) 17
3. METHODS **19**
3.1 Core Synthesizing 19
3.2 Magnetic Nanoparticles Surface Coating 23
3.2.1 Oleic acid coating 23
3.2.2 Silica coating and amination of the magnetic nanoparticles 23
3.2.3 Nanoparticle powder preparation for FTIR and VSM measurements 25
3.2.4 Making capsules out of nanoparticles for VSM 27
3.2.5 Sample preparation for SEM measurements 28
4. RESULTS AND DISCUSSION **31**
5. FUTURE WORK **37**
REFERENCES **39**

APPENDICES **49**
APPENDIX A 50
APPENDIX B 77
APPENDIX C 85
CURRICULUM VITAE **111**

ABBREVIATIONS

AC	: Alternating current
APTES	: (3-Aminopropyl)triethoxysilane
DI	: Deionised
FTIR	: Fourier transform infrared spectroscopy
MNP	: Magnetic nanopartivle
MRI	: Magnetic resonance imaging
NP	: Nanoparticle
PEG	: Polyethylene glycol
SEM	: Scanning electron microscope
SPION	: Superparamagnetic iron oxide nanoparticles
TEOS	: Tetraethyl orthosilicate
VSM	: Vibrating sample magnetometer

SYMBOLS

B	**:** Magnetic induction
H	**:** Magnetic field strength
$\mathbf{H_{apply}}$	**:** Strength of appliec AC magnetic field
K	**:** Anisotropy constant
M	**:** Magnetic moment per volume
P	**:** Heat dissipation
T	**:** Temperature
$\mathbf{V_H}$	**:** Hydrodynamic particle volume
$\mathbf{V_M}$	**:** Volume of particle
Z	**:** Viscosity
f	**:** AC magnetic field frequency
k	**:** Boltzmann constant
$\mathbf{\mu_o}$	**:** Permeability in vacuum
$\mathbf{\chi}$	**:** Volumetric magnetic susceptibility
$\mathbf{\chi''}$	**:** AC magnetic susceptibility (imaginary part)
$\mathbf{\tau}$	**:** Effective magnetic relaxation time
$\mathbf{\tau_B}$	**:** Brownian magnetic relaxation time
$\mathbf{\tau_N}$	**:** Neel magnetic relaxation time

LIST OF TABLES

Page

Table 1.1: Parameters for synthesizing Fe_3O_4 nanoparticles in different sizes using co-precipitation method available in literature.....10
Table 2.1: Materials used for synthesizing nanoparticle cores, silica coating and amination.....15
Table 3.1: Materials and parameters for synthesizing Fe_3O_4 nanoparticles. 20
Table 3.2: Materials and parameters for synthesizing $SrFe_{12}O_{19}$ nanoparticles. ..21
Table 3.3: Materials and parameters for synthesizing $BaFe_{12}O_{19}$ nanoparticles. .21
Table 3.4: Materials and parameters for synthesizing $MgFe_2O_4$ nanoparticles. ...21
Table 3.5: Materials and parameters for synthesizing $MnFe_2O_4$ nanoparticles. ...22
Table 3.6: Used silica coating references and our methods. 24
Table 4.1: FTIR bands available in literature. 32
Table 4.2: Our FTIR results for synthesized nanopartic. 33
Table A.1: Fe_3O_4 magnetic nanoparticles and silica coated and aminated magnetic nanoparticles given codes. 50
Table A.2: $SrFe_{12}O_{19}$ magnetic nanoparticles and silica coated and aminated magnetic nanoparticles given codes.....55
Table A.3: $BaFe_{12}O_{19}$ magnetic nanoparticles and silica coated and aminated magnetic nanoparticles given codes.....59
Table A.4: $MgFe_2O_4$ magnetic nanoparticles and silica coated and aminated magnetic nanoparticles given codes.....64
Table A.5: $MnFe_2O_4$ magnetic nanoparticles and silica coated and aminated magnetic nanoparticles given codes.....71
Table B.1: Fe_3O_4 Nanoparticles core sized measured in SEM equipment. 77
Table B.2: $SrFe_{12}O_{19}$ Nanoparticles core sized measured in SEM equipment. ...79
Table B.3: $BaFe_{12}O_{19}$ Nanoparticles core sized measured in SEM equipment. 80
Table B.4: $MgFe_2O_4$ Nanoparticles core sized measured in SEM equipment. 82
Table B.5: $MnFe_2O_4$ Nanoparticles core sized measured in SEM equipment. 83
Table C.1: Fe_3O_4 Magneticle nanoparticles core synthesizing conditions and their size and saturation magnetization 85
Table C.2: $SrFe_{12}O_{19}$ magneticle nanoparticles core synthesizing conditions and their size and saturation magnetization. 90
Table C.3: $BaFe_{12}O_{19}$ magneticle nanoparticles core synthesizing conditions and their size and saturation magnetization. 93
Table C.4: $MgFe_2O_4$ magneticle nanoparticles core synthesizing conditions and their size and saturation magnetization. 98
Table C.5: $MnFe_2O_4$ magneticle nanoparticles core synthesizing conditions and their size and saturation magnetization. 105

LIST OF FIGURES

Page

Figure 1.1: Magnetic dipoles and behavior in the presence and absence of an external magnetic field [7]. 3
Figure 1.2: Hystersis loop of magnetic nanoparticles [7]. 4
Figure 1.3: Illustration of the two components of the magnetic relaxation of a magnetic nanoparticles [3]. 6
Figure 1.4: Effect of solution pH on sizes of Fe_3O_4 nanoparticles [28]. 12
Figure 1.5: Effect of reaction temperature on size of Fe_3O_4 nanoparticles [28]. 12
Figure 1.6: Effect of the stirring rate on sizes of Fe_3O_4 nanoparticles [28]. 13
Figure 1.7: XRD patterns of as-prepared Fe_3O_4 MNPs [42]. 13
Figure 1.8: Saturation magnetization (Ms) as a function of magnetite particles size [42]. 13
Figure 1.9: (a) Magnetic nanoparticle core (b) Silica coated (c) Aminated (d) Gold decoration (e) Gold shell coating [67]. 14
Figure 2.1: Bruker optics ALPHA-Transmittance FTIR spectrometer. 17
Figure 2.2: Vibrating sample magnometer (VSM). 18
Figure 2.3: Vacuum pump a) stand alone b) connected to the drying space. 18
Figure 3.1: Core synthesizing process first step by mixing water, $FeCl_3.6H_2O$ and $FeCl_2.4H_2O$ 22
Figure 3.2: Adding NaOH and stirring for 3 hours a) all device b) close view. 23
Figure 3.3: a) Decanding magnetic nanoparticles b) washing them till reaching a solution with the pH 7 c) final pH of solution. 23
Figure 3.4: Our general plan in synthesizing. 24
Figure 3.5: Prepared nanoparticles. 25
Figure 3.6: Prepared cores of the nanoparticles 25
Figure 3.7: Silica coated nanoparticles 25
Figure 3.8: Aminated nanoparticles. 25
Figure 3.9: Drying magnetic nanoparticles in water bath in 80ºC. 26
Figure 3.10: Putting samples in the vacuum space for the final complete drying. 26
Figure 3.11: Equipments used magnetic nanoparticle powder making. 26
Figure 3.12: Dried Nanoparticles a) in dicer b) after making powder. 27
Figure 3.13: Final prepared samples. 27
Figure 3.14: Instruments used for making capsules. 27
Figure 3.15: a) Making capsules from foil b) final product. 28
Figure 3.16: Calibrating the weighing device regarding the empty container foil a) weight of the foil b) close view. 28
Figure 3.17: a) Filling nanoparticle powder into the capsule b) closing the capsule c) final sample. 28
Figure 3.18: Dried droplets of nanoparticles core solution a) close view b) box view. 29

Figure A.1: FTIR analysis results of FO-1 samples (a) core, (b) silica coated, (c) aminated. 51
Figure A.2: FTIR analysis results of FO-2 samples (a) core, (b) silica coated, (c) aminated. 51
Figure A.3: FTIR analysis results of FO-3 samples (a) core, (b) silica coated, (c) aminated. 52
Figure A.4: FTIR analysis results of FO-4 samples (a) core, (b) silica coated, (c) aminated. 52
Figure A.5: FTIR analysis results of FO-5 samples (a) core, (b) silica coated, (c) aminated. 53
Figure A.6: FTIR analysis results of FO-6 samples (a) core, (b) silica coated, (c) aminated. 53
Figure A.7: FTIR analysis results of FO-7 samples (a) core, (b) silica coated, (c) aminated. 54
Figure A.8: FTIR analysis results of FO-8 samples (a) core, (b) silica coated, (c) aminated. 54
Figure A.9: FTIR analysis results of FO-9 samples (a) core, (b) silica coated, (c) aminated. 55
Figure A.10: FTIR analysis results of SF-1 samples (a) core, (b) silica coated, (c) aminated. 56
Figure A.11: FTIR analysis results of SF-2 samples (a) core, (b) silica coated, (c) aminated. 56
Figure A.12: FTIR analysis results of SF-3 samples (a) core, (b) silica coated, (c) aminated. 57
Figure A.13: FTIR analysis results of SF-4 samples (a) core, (b) silica coated, (c) aminated. 57
Figure A.14: FTIR analysis results of SF-5 samples (a) core, (b) silica coated, (c) aminated. 58
Figure A. 15: FTIR analysis results of SF-6 samples (a) core, (b) silica coated, (c) aminated. 58
Figure A.16: FTIR analysis results of BF-1 samples (a) core, (b) silica coated, (c) aminated. 60
Figure A.17: FTIR analysis results of BF-2 samples (a) core, (b) silica coated, (c) aminated. 60
Figure A.18: FTIR analysis results of BF-3 samples (a) core, (b) silica coated, (c) aminated. 61
Figure A.19: FTIR analysis results of BF-4 samples (a) core, (b) silica coated, (c) aminated. 61
Figure A.20: FTIR analysis results of BF-5 samples (a) core, (b) silica coated, (c) aminated. 62
Figure A.21:FTIR analysis results of BF-6 samples (a) core, (b) silica coated, (c) aminated. 62
Figure A.22: FTIR analysis results of BF-7 samples (a) core, (b) silica coated, (c) aminated. 63
Figure A.23: FTIR analysis results of BF-8 samples (a) core, (b) silica coated, (c) aminated. 63
Figure A.24: FTIR analysis results of BF-9 samples (a) core, (b) silica coated, (c) aminated. 64
Figure A.25: FTIR analysis results of MgF-1 samples (a) core, (b) silica coated, (c) aminated. 65

Figure A.26: FTIR analysis results of MgF-2 samples (a) core, (b) silica coated, (c) aminated. 66
Figure A.27: FTIR analysis results of MgF-3 samples (a) core, (b) silica coated, (c) aminated. 66
Figure A.28: FTIR analysis results of MgF-4 samples (a) core, (b) silica coated, (c) aminated. 67
Figure A.29: FTIR analysis results of MgF-5 samples (a) core, (b) silica coated, (c) aminated. 67
Figure A.30: FTIR analysis results of MgF-6 samples (a) core, (b) silica coated, (c) aminated. 68
Figure A.31: FTIR analysis results of MgF-7 samples (a) core, (b) silica coated, (c) aminated. 68
Figure A.32: FTIR analysis results of MgF-8 samples (a) core, (b) silica coated, (c) aminated. 69
Figure A.33: FTIR analysis results of MgF-9 samples (a) core, (b) silica coated, (c) aminated. 69
Figure A.34: FTIR analysis results of MgF-10 samples (a) core, (b) silica coated, (c) aminated. 70
Figure A.35: FTIR analysis results of MgF-11 samples (a) core, (b) silica coated, (c) aminated. 70
Figure A.36: FTIR analysis results of MgF-12 samples (a) core, (b) silica coated, (c) aminated. 71
Figure A.37: FTIR analysis results of MnF-1 samples (a) core, (b) silica coated, (c) aminated. 72
Figure A.38: FTIR analysis results of MnF-2 samples (a) core, (b) silica coated, (c) aminated. 73
Figure A.39: FTIR analysis results of MnF-3 samples (a) core, (b) silica coated, (c) aminated. 73
Figure A.40: FTIR analysis results of MnF-4 samples (a) core, (b) silica coated, (c) aminated. 74
Figure A.41: FTIR analysis results of MnF-2 samples (a) core, (b) silica coated, (c) aminated. 74
Figure A.42: FTIR analysis results of MnF-2 samples (a) core, (b) silica coated, (c) aminated. 75
Figure A.43: FTIR analysis results of MnF-7 samples (a) core, (b) silica coated, (c) aminated. 75
Figure A.44: FTIR analysis results of MnF-8 samples (a) core, (b) silica coated, (c) aminated. 76
Figure B.1: SEM photographs (a) FO-1, (b) FO-2, (c) FO-3, (d) FO-4, (e) FO-5, (f) FO-6, (g) FO-7, (h) FO-8, (i) FO-9.....77
Figure B.2: Fe_3O_4 Nanoparticles core sized measured in SEM equipment. 78
Figure B.3: SEM photographs (a) SF-1, (b) SF-2, (c) SF-3, (d) SF-4, (e) SF-5, (f) SF-6.....78
Figure B.4: $SrFe_{12}O_{19}$ Nanoparticles core sized measured in SEM equipment...79
Figure B.5: SEM photographs (a) BF-1, (b) BF-2, (c) BF-3, (d) BF-4, (e) BF-5, (f) BF-6, (g) BF-7, (h) BF-8, (i) BF-9.....80
Figure B.6: $BaFe_{12}O_{19}$ Nanoparticles core sized measured in SEM equipment. ..81

Figure B.7: SEM photographs (a) MgF-1, (b) MgF-2, (c) MgF-3, (d) MgF-4, (e) MgF-5, (f) MgF-6, (g) MgF-7, (h) MgF-8, (i) MgF-9, (j) MgF-10, (k) MgF-11, (l) MgF-12. 81
Figure B.8: $MgFe_2O_4$ Nanoparticles core sized measured in SEM equipment. ... 82
Figure B.9: SEM phptpgraphs (a) MnF-1, (b) MnF-2, (c) MnF-3, (d) MnF-4, (e) MnF-5, (f) MnF-6, (g) MnF-7, (h) MnF-8. 83
Figure B.10: $MnFe_2O_4$ Nanoparticles core sized measured in SEM equipment.. 84
Figure C.1: FO-1, FO-1-S and FO-1-S-A VSM results. 85
Figure C.2: FO-2, FO-2-S and FO-2-S-A VSM results. 86
Figure C.3: FO-3, FO-3-S and FO-3-S-A VSM results. 86
Figure C.4: FO-4, FO-4-S and FO-4-S-A VSM results. 87
Figure C.5: FO-5, FO-5-S and FO-5-S-A VSM results. 87
Figure C.6: FO-6, FO-6-S and FO-6-S-A VSM results. 88
Figure C.7: FO-7, FO-7-S and FO-7-S-A VSM results 88
Figure C.8: FO-8, FO-8-S and FO-8-S-A VSM results. 89
Figure C.9: FO-9, FO-9-S and FO-9-S-A VSM results. 89
Figure C.10: SF-1, SF-1-S and SF-1-S-A VSM results. 90
Figure C.11: SF-2, SF-2-S and SF-2-S-A VSM results. 91
Figure C.12: SF-3, SF-3-S and SF-3-S-A VSM results. 91
Figure C.13: SF-4, SF-4-S and SF-4-S-A VSM results. 92
Figure C.14: SF-5, SF-5-S and SF-5-S-A VSM results. 92
Figure C.15: SF-6, SF-6-S and SF-6-S-A VSM results. 93
Figure C.16: BF-1, BF-1-S and BF-1-S-A VSM results. 94
Figure C.17: BF-2, BF-2-S and BF-2-S-A VSM results. 94
Figure C.18: BF-3, BF-3-S and BF-3-S-A VSM results. 95
Figure C.19: BF-4, BF-4-S and BF-4-S-A VSM results. 95
Figure C.20: BF-5, BF-5-S and BF-5-S-A VSM results. 96
Figure C.21: BF-6, BF-6-S and BF-6-S-A VSM results. 96
Figure C.22: BF-7, BF-7-S and BF-7-S-A VSM results. 97
Figure C.23: BF-8, BF-8-S and BF-8-S-A VSM results. 97
Figure C.24: BF-9, BF-9-S and BF-9-S-A VSM results. 98
Figure C.25: MgF-1, MgF-1-S and MgF-1-S-A VSM results. 99
Figure C.26: MgF-2, MgF-2-S and MgF-2-S-A VSM results. 99
Figure C.27: MgF-3, MgF-3-S and MgF-3-S-A VSM results. 100
Figure C.28: MgF-4, MgF-4-S and MgF-4-S-A VSM results. 100
Figure C.29: MgF-5, MgF-5-S and MgF-5-S-A VSM results. 101
Figure C.30: MgF-6, MgF-6-S and MgF-6-S-A VSM results. 101
Figure C.31: MgF-7, MgF-7-S and MgF-7-S-A VSM results. 102
Figure C.32: MgF-8, MgF-8-S and MgF-8-S-A VSM results. 102
Figure C.33: MgF-9, MgF-9-S and MgF-9-S-A VSM results. 103
Figure C.34: MgF-10, MgF-10-S and MgF-10-S-A VSM results. 103
Figure C.35: MgF-11, MgF-11-S and MgF-11-S-A VSM results. 104
Figure C.36: MgF-12, MgF-12-S and MgF-12-S-A VSM results. 104
Figure C.37: MnF-1, MnF-1-S and MnF-1-S-A VSM results. 105
Figure C.38: MnF-2, MnF-2-S and MnF-2-S-A VSM results. 106
Figure C.39: MnF-3, MnF-3-S and MnF-3-S-A VSM results. 106
Figure C.40: MnF-4, MnF-4-S and MnF-4-S-A VSM results. 107
Figure C.41: MnF-5, MnF-5-S and MnF-5-S-A VSM results. 107
Figure C.42: MnF-6, MnF-6-S and MnF-6-S-A VSM results. 108
Figure C.43: MnF-7, MnF-7-S and MnF-7-S-A VSM results. 108

Figure C.44: MnF-8, MnF-8-S and MnF-8-S-A VSM results.....109
Figure C.45: Comparison of magnetization of all kinds of magnetic nanoparticles with 12 to 13 nm. 109

SYNTHESIZE AND CHARACTERIZATION OF MULTI-COMPONENT MAGNETIC NANO PARTICLES

SUMMARY

Magnetic nanoparticles are a major class of nonscale materials. Because of their unique properties and ability to function at the cellular and molecular level they have a potential to provide significant improvements in healthcare. They are actively investigated as magnetic resonance imaging contrast agents and carriers for targeted drug delivery.

Accorging to some researches cancer is the third leading cause of death in developed countries. The traditional treatments for cancer are surgery, radiation and chemotherepy each bears the risk of killing healthy cells and fatally damaging healthy tissues along with the infected region. The new techniques being researched aims to target only the infected site with molecular drugs and nanoparticles are considered as the carriers.

At the core of nanotherapeutic agent design is the determination of materials and tecniques to make the nanoparticles biocompatible. For this pupose firstly nanoparticles are coated with oleic acid to prevent oxidization. The next step is to prevent agglomeration and this is provided by silica coating. After that nanoparticles are prepared for gold coating with amination and coated with gold so that nanoparticles become nontoxic. The last step is polymer coating to make nanoparticles organic.

In this project five different magnetic nanoparticles have been synthesized in room temperature. Fe_3O_4, $MgFe_2O_4$, $MnFe_2O_4$, $SrFe_{12}O_{19}$ and $BaFe_{12}O_{19}$ samples have been synthesized in different sizes while magnestic core sizez have been choosen in a way that they are in a size range to be biocompatable for magnetic nanoparticle hyperthermia. Different core sizes have been achieved by changing pH and added water ratio while using precipitation method. Three different pH values and three different concentrations have been used.

After synthezing magnetic nanoparticle cores a specific amount of the nanoparticles has been coated with silica by Stöber method and a specific amount of silica coated samples has been ammunated. As a side note Fe_3O_4 cores have been coated with oleic acid during the core synthesizing process to prevent oxidization.

FTIR analyses of the produced samples have shown Fe-O, Fe-O-Fe, Mg-O, Mn-O, Sr-O, Ba-O, Mg-Fe, Mn-Fe, Sr-Fe and Ba-Fe bonds which confirm the nanoparticles have been produced correctly; Fe-COOO, H-C-H and C-O bonds which shows the existence of oleic acid coating; Si-O, Si-O-Si and Fe-O-Si bonds which sign silica coating and O-H and N-H bonds which confirm amination.

In SEM analysis the structures and particle sizes are investigated. Effects of pH and concentration on particle sizes are determined.

ÇOK BİLEŞENLİ MANYETİK NANO PARÇACIK SENTEZİ VE KARAKTERİZASYONU

ÖZET

Manyetik nanoparçacıklar nano ölçekli malzemelerin mevcut klinik tanı ve tedavi tekniklerinde devrim yaratabilecek potansiele sahip önemli bir sınıfıdır. Manyetik nanoparçacıklar özgün özellikleri ve hücresel ve molekülsel düzeydeki biyolojik etkileşimlerde işlevsel olabilme kabiliyetleri sebebiyle yeni nesil manyetik rezonans görüntüleme (MRI) kontrats maddesi ve hedeflenen ilaç sisteminin taşıyıcıları olarak aktif şekilde incelenmektedirler.

Bu alandaki ilk çalışmalar birkaç on yıl geçmişe tarihlenebilse de yakın geçmişte nanoteknolojiye olan ilgideki artış manyetik nanoparçacık araştırmalarının alanını ve derinliğini önemli derecede genişletmiştir. Kanser, kardiyovasküler rahatsızlıklar ve nörolojik rahatsızlıklar gibi hastalıkların tespit, tanı ve tedavisinde geniş yelpazeli uygulamalarıyle manyetik nanoparçacıklar yakında geleceğin sağlık ihtiyaçlarını karşılamada önemli bir rol oynayabilirler.

Kanser ölüm sebepleri arasında gelişmiş ülkelerde kalp rahatsızlıkları ve inmenin ardından üçüncü Amerika Birleşik Devletleri'nde kalp rahatsızlıklarının ardından ikincidir. Kanser geleneksel olarak ameliyat, radyoterapi ve kemoterapi ile tedavi edilir. Bu yaklaşımların tamamı sağlıklı hücreleri öldürme ve sağlıklı dokulara ölümcül bir şekilde hasar verme riski taşır. Nanoteknolojinin ortaya çıkması ve hızla yükselmesiyle nanomalzemeler küçük moleküler ilaçların ve biyolojik ajanların taşınmasına yardım ederek yeni fırsatlar sunmaktadır. Bu tarz maddelerin nanomalzemelerle taşınmasıyla yapılacak tedaviler ilacın hedeflenen yere etki etmesini ve sağlıklı dokuların tedaviden etkilenmesinin sınırlanmasnı sağlayacaktır.

Nanotedavi ajanının tasarlanmasının merkezinde canlı içerisindeki malzeme akışı, izlenebilirlik ve tedavisel işlev konularındaki sıkı gereksinimleri karşılayan son ürünün oluşturulmasında kullanılabilecek malzeme ve tekniklerin belirlenmesi yer alır. Nanotedavi ajanının içeriğindeki malzemeler hedeflenen işlevlerini gerçekleştirebilirken aynı zamanda, bozunma sonucu ortaya çıkacak malzemeler de göz önünde bulundurularak, biyolojik olarak uyumlu olacak şekilde seçilirler. Bahsi geçen malzemeler biyolojik sistemlerle de etkileşeceği için bu süreç karmaşık olabilir.

Nanoparçacıkların biyolojik olarak uyumlu olması amacıyla birtakım kaplama işlemleri uygulanmaktadır. Nanoparçacıkların okside olmaması için oleik asitle kaplama yapılmaktadır. Parçacıkların yığışarak büyümesinin önlenmesi için silika kaplama uygulanmaktadır. Nanoparçacıkların toksik olmayan hale gelmesi için altın kaplama uygulanmakta fakat bunun yapılabilmesi için öncelikle silika kaplamadan sonra amünasyon işlemi gerçekleştirilmektedir. Altın kaplamanın ardından elde edilen nanoparçacığın organik olması için son adım olarak polimer kaplama yapılmaktadır.

Bu çalışmada oda sıcaklığında, farklı boyutlarda medikal olarak kullanılma potansiyeli olan beş farklı manyetik nanoparçacık çökeltme metofuyla sentezlenmiştir. Bunlar Fe_3O_4, $MgFe_2O_4$, $MnFe_2O_4$, $SrFe_{12}O_{19}$ ve $BaFe_{12}O_{19}$'dur. Sentezlenen malzemelerin manyetik çekirdek boyutları manyetik nanoparçacık hipertermisi için biyolojik olarak uyumlu olacak aralıkta bulunacak şekilde seçilmiştir. Farklı çekirdek boyutları pH ve su oranının değiştirilmesiyle elde edilmiştir. Çökeltme metodu uygulanırken üç farklı konsantrayon ve üç farklı pH değeri kullanılmıştır. Böylece dokuz farklı boyutta çekirdek elde edilmeye çalışılmıştır.

İlk olarak her bir tür nanoparçacıktan üçer gram sentezlenmiştir. FTIR analizinin ardından nanoparçacıkların yapısından emin olunduktan sonra herbir nanopartikül türünden, reaksiyon formüllerine göre, katalizör olarak NaOH kullanılarak yirmişer gram sentezlenmiştir. Sentezlenen malzemelere bakıldığında Fe_3O_4 numunelerinin oksitlendiği görülmüştür. Bu nedenle Fe_3O_4 sentezlenirken sentezleme aşamasında oleik asitle kaplama yapılmasına karar verilmiştir. Fe_3O_4 nanoparçacıkları için gram başına uygun olan oleik asit miktarı belirlendikten sonra sentezlemeye oleik asit de dahil edilmiştir. Sonuçta bazı deneysel şartlar başarısız olmuş ve 44 adet çekirdek numunesi elde edilmiştir. Elde edilen numunelerin üçer gramı ayrılmış ve geri kalanları yüzey kaplama için şişelerde depolanmıştır.

Bir sonraki adımda depolanmış olan manyetik nanopartiküller Stöber yöntemi kullanılarak silika ile kaplanmıştır. TEOS miktarı değiştirilerek 4 ile 6 nm arasında kaplama kalınlığı elde edilmiştir.

Silika kaplamadan sonra silika ile kaplanmış olan numunelerin üçer gramı ayrılmış ve geri kalanları altın ve PEG kaplama için amünasyona tabi tutulmuştur. Bu işlemden sonra yine üçer gram numune ayrılmış ve geri kalanlar altın ve PEG kaplama için şişelerde depolanmıştır.

Bu işlemlerin ardından çekirdek, silika kaplı ve amünasyona tabi tutulmuş, farklı boyutlarda, farklı malzemelerden oluşan 132 numune elde edilmiştir. Sonrasında her numuneden birer gram FTIR, VSM ve XRD analizlerinde kullanılmak üzere 8-9 saat su banyosunda tutularak kurutulmuş ve vakum pompaları kullanılarak otuzar dakika vakum ortamında tutulmuştur. SEM ile nanoparçacıkların boyutlarının ölçülmesinde ise numunelerin çözelti halleri kullanılmıştır.

FTIR analizinde dalga boylarına ve bantlara bakılarak malzeme karakteristikleri incelenmiş ve manyetik nanoparçacıkların doğru bir şekilde sentezlendiği görülmüştür. Yine aynı analizlerde silika kaplama ve amünasyon işlemlerinin de doğru bir şekilde yapıldığı gözlemlenmiştir. Bu çalışmada elde edilen nanopartiküller ferro akışkanlar olarak adlandırılmakta ve Fe bantları (Fe-O ve Fe-O-Fe) 500-600 cm^{-1} aralığında olmalıdır. Yapılan FTIR analizlerinde 540 ile 570 cm^{-1} aralığındaki değerler gözlemlenmiştir. Bu değerler Fe-O ve Fe-O-Fe bantlarının varlığını göstermektedir. Bunun dışında elde edilen nanoparçacıkların birbirinden farkını gösteren Mg-O, Mn-O, Sr-O ve Ba-O bantları da analizler esnasında gözlemlenmiştir. $SrFe_{12}O_{19}$ için numunenin Sr-Fe içerdiğini gösteren 400-600 cm^{-1} aralığındaki değerler okunmuştur. Aynı analizlerde Sr-O içeriğini gösteren 1400 cm^{-1} civarındaki değerler de görülmüştür. $BaFe_{12}O_{19}$ ile yapılan analizlerde Ba-Fe bağlarını gösteren 415-500 cm^{-1} aralığındaki değerlerle Ba-O yapılarını gösteren

1625 cm^{-1} civarındaki değerler gözlemlenmiştir. $MgFe_2O_4$ ve $MnFe_2O_4$ için yapılan analizlerde de benzer şekilde başarılı sonuçlar elde edilmiş ve Mg-Fe ve Mn-Fe varlığını gösteren 550-600 cm^{-1} arasındaki değerlerle sırasıyla Mg-O ve Mn-O varlıklarını işaret eden 1600 cm^{-1} ve 1650 cm^{-1} civarındaki değerler okunmuştur.

FTIR analizlerinde ayrıca oleik asit, silika kaplama ve amünasyon belirtileri de görülmüştür. Oleik asit varlığı içerikteki Fe-COOO, H-C-H ve C-O yapılarından anlaşılmaktadır. Bu bağların varlığını gösteren 1400-1600 cm^{-1} aralığındaki değerler, 2920 cm^{-1} civarındaki değerler ve 1050 cm^{-1} civarındaki titreşimler gözlenmiştir. Silika kaplamanın doğruluğunun teyidi Si-O, Si-O-Si ve Fe-O-Si bağlarının varlığının gözlemlenmesiyle yapılmaktadır. Bu bağların varlığı FTIR analizinde Si-O ve Si-O-Si varlığını gösteren 800-1100 cm^{-1} aralığındaki değerlerin ve Fe-O-Si varlığını gösteren 580 cm^{-1} civarındaki değerlerin okunmasıyla gösterilmiştir. Amünasyonun belirtileri ise O-H ve N-H bağlarının varlığını gösteren 1600 cm^{-1} ve 3000 cm^{-1} civarındaki değerlerin okunmasıyla tespit edilmiştir.

SEM ekipmanıyla yapılan analizlerle parçacıkların yapıları ve boyutları incelenmiştir. Biyolojik uyumluluk için gerekli olan çap olarak 30 nm'den küçük parçacık boyutları gözlemlenmiştir. Sonuç olarak Fe_3O_4 için en büyük boyutun pH değeri 13 olduğunda ortaya çıktığı görülmüştür, sentezleme esnasında eklenen suyun azaltılması, yani derişikliğin arttırılması parçacık boyutunu küçültmektedir. Derişikliğe göre parçacık boyutunun değişimi doğrusaldır. $SrFe_{12}O_{19}$ için en büyük boyut kullanılan en düşük pH seviyesi olan 12'de elde edilmiştir. Derişim arttıkça parçacık boyutu düşmektedir. $BaFe_{12}O_{19}$ için pH değeri düştükçe parçacık boyutunun arttığı ve derişim azaldıkça parçacık boyutunun da küçüldüğü görülmüştür. $MgFe_2O_4$ için derişim artışıyla parçacık boyutunun düştüğü görülmüştür. Fakat pH için düzenli bir patern gözlemlenmemiştir. $MnFe_2O_4$ için ise pH ya da derişim ile parçacık boyutu arasında mantıksal bir ilişki kurulamamıştır.

1. INTRODUCTION

Cancer is the third leading cause of death(after heart desease and stroke) in developed countries and the second leading cause of death(after heart diseasse) in the United States. Studies have shown that there were million new cases, 6 million deathes, and 22 million people living with cancer worldwide in the year 2000. These numbers represent an increase of about 22% in incidence and mortality from that of the year 1990. It is projected that the number of new cases of all cancers worldwide will be 12.3 and 15.4 million in the year 2010 and 2020, respectively [1].

Cancers are traditionally treated with surgery, radiation, and chemotherapy. Each of these approaches bears the risk of killing normal cells of fatally damaging healthy tissue. With the emergence and rapid growth of nanotechnology, nanomaterials are providing new opportunities that can assist in the therapeutic index ny driving the therapeutic to the target site and limiting its expwsure to healthy tissue. Among many nanomaterials studied for cancer diagnosis and therapy, superparamagnetic iron oxide nanoparticles(SPIONs) have emerged as one of the most appealing candidates [2]. Due to rapid adcances in nanotechnology, novel synthetic routes to nanoparticles(NPs) with the ability to rigorously control the microstructure of the magnetic core(such as size monodispersity and monodispersity) have beeb discribed. These nanosystems can be made to heat up, which leads to their use as hyperthermia anents, delivering toxic amounts of thermal energy to tumors, or as chemotherapy and radiotherapy enhancement agentsi where a moderate degree of tissue warming results in more effective cell destruction [3,4]. Numerous forms of MNP with various chemical compositions have been proposed and evaluated for biomedical applications to exploit nanoscale magnetic phenomena, such as enhanced magnestic moments and superparamagnetism. Composition, size, morphlogy and sufrace chemistry can now be tailored by various processes to not only improve magnetic properties bot also affect the behavior of nanoparticles in vivo. In its simplest form, a biomedical MNP platform is comprised of an inorganic nanoparticle core and a

biomedical MNP and a biocompatible surface coating that prvides stabilization under physiological conditions [5].

1.1 Purpose of Thesis

In this research 5 different magnetic nanoparticles including Fe_3O_4, $MgFe_2O_4$, $MnFe_2O_4$, $SrFe_{12}O_{19}$ and $BaFe_{12}O_{19}$ nanoparticles have been synthesized using precipitation method in room temperature while all the samples have been silica coated using Stöber method. In the next step all MNPs have been aminated for preparing the nanoparticles for gold coating and PEG coating. All five kinds of magnetic nanoparticles have been synthesized in different sizes in the range which they are biocompatable by changing PH and water ratio in the synthesizing procces while in every step 3 gram of the samples have been separated for analysis. The samples have been analyized using FTIR, SEM, VSM in order to study their size changing behavior by changing PH and water ratio in synthisizing condition and studying different magnetic nanoparticles structure and magnetization behavior for further research and biomedical studies.

1.2 Literature Review

1.2.1 Magnetism

1.2.1.1 Nanomagnetism

The design of MNPs with tailored properties depends of the fundamental concepts of nanomagnetism(i.e., magnetism observed in nanoparticles). A review of what produces magnetization, including the relationship between various extrinsic and intrinsic parameters, will enable us to better evaluate the underlying factors that influence magnetism at the nanoscale. Explanations about the role of atomic and molecular structure upon magnetization are readily available. Based on the response of the intrinsic MNP magnetic dipole and the magnetization in the presence and absence of an applied magnetic field, MNPs are typically classified as:

- Diamagnetics,
- Paramgnetics,
- Ferromagnetic,
- Ferrimagnetic,

- Antiferrimagnetic [6]

Figure 1.1 shows the net magnetic dipole arrangement for each of Diamagnetics, Paramgnetics, Ferromagnetic, Ferrimagnetic and Antiferrimagnetic materials.

Diamagnetics

For diamagnetic materials in the absence of a magnetic field, magnetic dipoles are not present. However upon application of a field, the material produces a magnetic dipole that is oriented opposite to that of the applied field; thus, a material that has strong diamagnetic character is repelled by a magnetic field.

Paramagnetics

For paramagnetic materials, there exist magnetic dipoles as illustrated in Figure 1.1, but these dipoles are aligned only upon application of an external magnetic field. For the balance of the magnetic properties illustrated in Figure 1.1, the magnetization in the absence of an applied field reveals their fundamental character.

Ferromagnetic

Ferromagnetic materials have net magnetic dipole moments in the absence of an external magnetic field.

Ferrimagnetic and antiferrimagnetic

In antiferrimagnetic and ferrimagnetic materials, the atomic level magnetic dipole moments are similar to those of ferromagnetic materials, however, adjacent dipole moments exist that are not oriented in parallel and effectively cancel or reduce, respectively, the impact of neighboring magnetic dipoles within the material in the absence of an applied field.

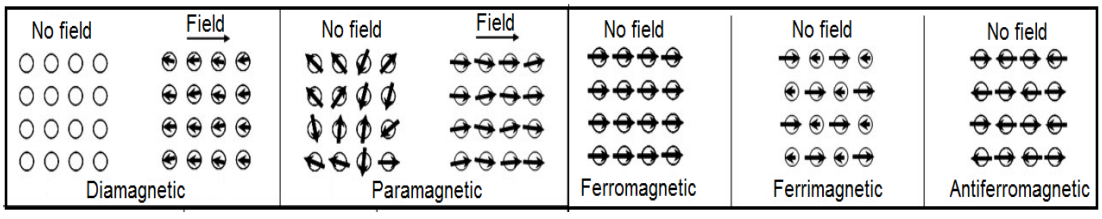

Figure 1.1: Magnetic dipoles and behavior in the presence and absence of an external magnetic field [7].

1.2.1.2 Physics of magnetism

When a magnetic material is placed in a magnetic field of strength H, the individual atomic moments in the material contribute to its overall response; the magnetic moment and induction is given by equations 1.1 and 1.2.

$$M = \chi H \quad \textbf{(1.1)}$$

$$B = \mu_0 (H + M) \quad \textbf{(1.2)}$$

where μ_0 is the permeability in vacuum and M is the magnetic moment per volume. The magnetic materials may be conveniently classified in terms of their volumetric magnetic susceptibility, χ.

1.2.1.3 Hystersis loop

For MNPs, the maximum magnetization possible is called the saturation magnetization, and it arises when all the magnetic dipoles are aligned in an external magnetic field. Figure 1.2 shows a typical magnetization curve for ferromagnetic or ferrimagnetic nanoparticles showing the characteristic positions on the curve associated with *saturation magnetization* (Ms, maximum induced magnetization), *remanent magnetization* (Mr, induced magnetization remaining after an applied field is removed), and *coercivity* (H, the intensity of an external coercive field needed to force the magnetization to zero). In the same figure, in contrast to the hysteresis observed in the case of ferromagnetic nanoparticles (red loop), the response of superparamagnetic nanoparticles to an external field also follows a sigmoidal curve but shows no hysteresis (green line) [7].

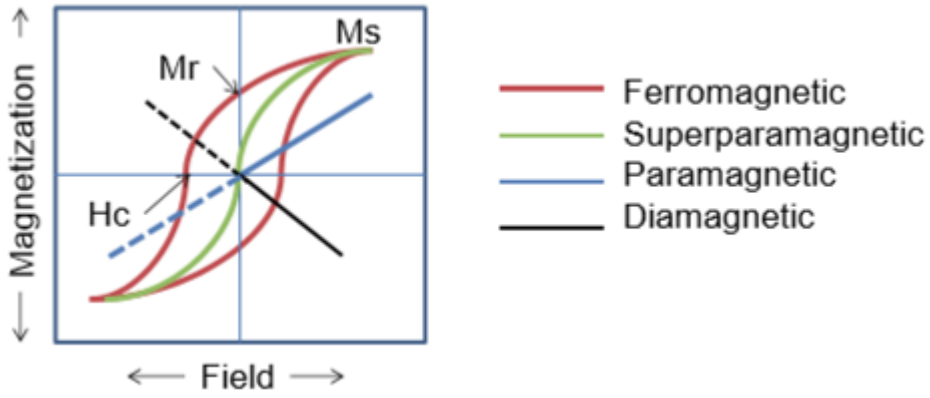

Figure 1.2: Hystersis loop of magnetic nanoparticles [7].

1.2.1.4 Superparamagnetic magnetic nanoparticles

Research in magnetic nanoparticles typically focuses of developing an optimal response for MNPs to an external magnetic field, and the majority of the published research has involved MNPs that are typically classified as either ferromagnetic, ferrimagnetic, or superparamagnetic particles (a special case of ferro- or ferri-magnetic particles). Below certain critical dimensions(that vary with the material parameters), MNPs exhibit magnetic responses reminiscent of those of paramagnetic materials, which is a zero average magnetic moment in the absence of an external field and a rapidly increasing (as compared to paramagnetic materials) magnetic moment under application of an external field in the direction of the field. This phenomenon, observed at temperatures above the so-called blocking temperature arises from the thermal fluctuations within nanoparticles being comparable to or greater than the energy barrier for moment reversal, allowing rapid random flipping of the nanoparticle magnetic moments. In the case where the magnetization of the MNP over the measurement/observation interval is equal to zero in the absence of an external field, such nanoparticles are referred to as superparamagnetic. Superparamagnetism is especially important in applications such as drug delivery of MRI, where the nanoparticles exhibit no magnetic properties upon removal of the external field and therefore have no attraction for each other, eliminating the major driving force for aggregation. More importantly, superparamagnetic nanoparticles allow better control over the application of their magnetic properties because they provide a strong response to an external magnetic field [7-9].

1.2.1.5 Heat dissipation mechanism

In this part, the behaviour and the heating in alternate magnetic field will be presented. Also, the properties of nanoparticles have been shortly discussed. The magnetization of nanoparticles can relax by two different mechanism, the so-called Neel relaxation and the Brownian relaxation. Neel relaxation is caused by the reorientation of the magnetization vector inside the magnetic core against an energy barrier . Brownian relaxation is due to rotational diffusion of the whole particle in the carrier liquid. Figure 1.3 is illustrating the magnetic nanoparticles orientation and their relaxation statuse after application of a Maagnetic field B their [10,11].

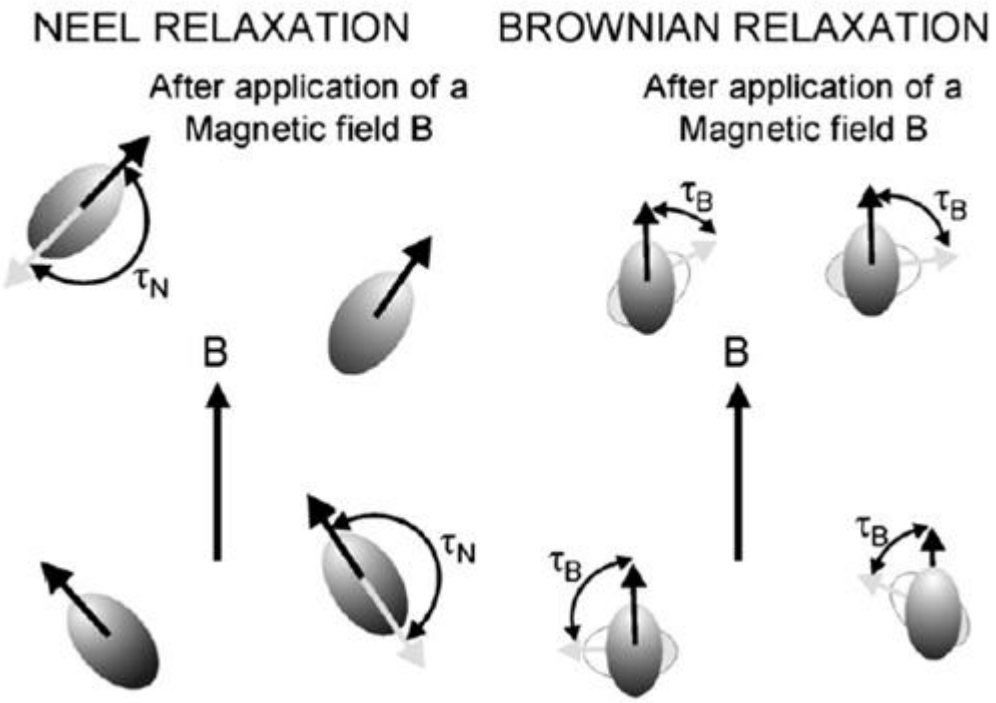

Figure 1.3: Illustration of the two components of the magnetic relaxation of a magnetic nanoparticles [3].

Heat dissipation from magnetic particles is caused by the delay in the relaxation of the magnetic moment through either the rotation within the particle (Neel) or the rotation of the particle itself (Brownian), when they are exposed to an AC magnetic field with magnetic field reversal times shorter than the magnetic relaxation times of the particles.

The Neel (τ_N) and Brownian (τ_B) magnetic relaxation times of a particle are given by the following equations:

$$\tau_N = \tau_0 \exp(\frac{KV_M}{kT}) \quad \textbf{(1.3)}$$

$$\tau_B = \frac{3\eta V_H}{kT} \quad \textbf{(1.4)}$$

$$\tau = \frac{\tau_B \tau_N}{\tau_B + \tau_N} \quad \textbf{(1.5)}$$

where τ_N is the Neel relaxation time, τ_B the Brown relaxation time τ the effective relaxation time, $\tau_0 = 10^{-9} s$, K the anisotropy constant, V_M the volume of particle, k

the Boltzmann constant, T the temperature, Z the viscosity and V_H the hydrodynamic particle volume.

From the above equations, it is clear that the relaxation time relies on the particle diameter. When the particles are exposed to an AC magnetic field with time of magnetic reversals less than the magnetic relaxation times of particles, heat is dissipated due to the delay in the relaxation of the magnetic moment. Thus, the heat dissipation value is calculated using the harmonic average of both relaxations and their relative contributions depending on the particle diameter. The heat dissipation is given by the following equation [11]:

$$P = \mu_0 \chi'' f H_{apply}^2 \quad \textbf{(1.6)}$$

Where P is the heat dissipation value, μ_0 the permeability of free space, χ'' the AC magnetic susceptibility (imaginary part), f the frequency of applied AC magnetic field and H_{apply} the strength of applied AC magnetic field.

1.2.2 Synthesis methods of magnetic nanoparticles

Magnetic nanoparticles have been synthesized with a number of different compositions and phases, including iron oxides, such as Fe_3O_4 and $\gamma - Fe_3O_4$, pure metals, such as Fe and Co, spibel-type ferromagnets such as $MgFe_2O_4$, $MnFe_2O_4$, $SrFe_{12}O_{19}$ and $BaFe_{12}O_{19}$. In the last decades, much research has been devoted to the synthesis of magnetic nanoparticles. Especially during the last few years, many publications have described efficient synthetic routes to shape-controlled, highly stable, and monodisperse magnetic nanoparticles. Several popular methods including co-precipitation, thermal decomposition and/or reduction, micelle synthesis, hydrothermal synthesis, and lasesr pyrolysis techniques can all be directed at the synthesis of highly-quality magnetic nanoparticles [12].

1.2.2.1 Thermal decomposition

Inspired by the synthesis of high-quality semiconductor nanocrystals and oxides in nan-aqueous media by thermal decomposition, similar methods for the synthesis of magnetic particles with control over size and shape have been developed. Monodisperse magnetic nanocrystals with smaller size can essentially be synthesized

through the thermal decompositionof organometalic compounds in high-boiling organic solvents containing stabilizing surfactants. The rapid injection of the reagents, often organometallic compounds, in to hot surfactant solution gas yielded with respect to soprecipitation methods markedly improved samples with good size control, narrow size distribution and good crystallinity of individual and dispersible Fe-based magnetic nanoparticles [4,6,13-15].

1.2.2.2 Microemulsion

A microemulsion can be defined as a thermodynamically stable isotropic dispersion of two immiscible liquids consisting of nanosized domains of one liquid in the other, stabilized by an interfacial film of surface-active molecules. The surfactant molecules provide a confinement effect that limits particle nucleation, growth and agglomeration. In this method, co-precipitation occurs in tiny droplets of water ("water pools") embedded with surfactant molecules and homogenously distributed in an oil phase. [13,16-18,19].

1.2.2.3 Hydrothermal synthesis

Hydrothermal technique is defined as any heterogeneous reaction in the presence of aqueous solvents or mineralizers under highpressure and temperature conditions. Hydrothermal treatment of iron salt could generate iron oxides when the applied conditionsare appropriate [16]. Under hydrothermal conditions a broad range of nanostructured materials can be formed [13].

1.2.2.4 Lases pyrolysis

The laser pyrolysis method involves heating a flowing mixture of gases with a continuous wave carbon dioxide laser, which initiates and sustains a chemical reaction. Above a certain pressure and laser power, a cririca concentration of nuclei is reached in the reaction zone, which leads to homogeneous nucleation of particles that are further tranported to a filter by an inert gas. Three charactristics for this method must be emphasized: (a) the small particle size, (b) the narrow particle size distribution, and (c) the bearly absence of aggregation [14].

1.2.2.5 Riverse Micelle method

Reverse Micelles have been used to synthesize a wide variety of nanoparticles including metallic, bimetallic, metal oxide and semiconducting particles. The general process consists of formulating a water in oil microemulsion from a ternary water/oil/surfactant system. Next, the desired reaction precursor(s), such as a water soluble metal salt for metallic nanoparticles, are dissolved into the aqueous centers of the micelle. A reducing agent, is then added, either by simple injection, or dispersed in analogous reverse micelles and added to the system. When the salt is reduced by the reducing agent, active metal nuclei are formed. The nuclei-containing micelles then collide under Brownian motion and may exchange their contents causing the metal particles to grow. The greater the average number of successful collisions, the larger the particles [20].

1.2.2.6 Co-precipitation

Co-precipitation is a facile and convinient way to synthesize MFe_nO_m (M: Fe, Sr, Ba, Mn, Mg. n=2,12 and m=4,19)magnetic nanoparticles from aqueous Fe^{2+}/F^{3+} salt solution by the addition of a base ubder inert atmosphere at room temperature or at a elevated temperature. The size, shape, and composition of the type of salts used(e.g. chlorides, sulfates, nitrates), the Fe^{2+}/Fe^{3+} ratio, the reaction temperation, the PH value and ionic strength and the concentration of materials in synthesis environment [21-25]. Among the various synthesis procedures of the magnetic nanoparticles (MFe_xO_y), most commonly used solution phase procedure has been the co-precipitation of Fe^{2+} and Fe^{3+} ions and different M materials including (Sr, Ba, Mn and Mg) ions by an alkali, usually NH_4OH or $NaOH$ in an aqueous solution. Although this method is most suitable and convenient for mass production of mahnetic nanoparticles based ferrofluids with desired properties, it requires careful maintenance of Fe^{2+}:Fe^{3+} ions and M ions ratio and the adjustment for Ph value of the solution for the formation of magnetic nanoprticles.In literature there are plenty of studies in synthesising mahnetic nanoparticle core by co-precipitation method for biomedical purposes. Synthesizing magnetite nanoparticles for biomedical applications and hyperthermia has been attained most of the attentions and since nearly most of the synthesizing magnetic nanoparticles include Fe_3O_4 for its good

behavior in the biomedical applications [21,25-31]. About synthesizing $SrFe_{12}O_{19}$, $BaFe_{12}O_{19}$, $MgFe_2O_4$ and $MnFe_2O_4$ magnetic nanoparticles there are few research and experiments by co-precipitation method [32-40]. We see that in all research and experiments authors have changed magnetic nanoparticles size and structure by changing different parameters like PH, material molar ratio, temperature, stirring speed and material concentration in used DI water, used in co-precipitation method. In this project by studying different papers and their results and parameters that have been varied for synthesizing nanoparticles and according some reference and their particle sizes [28, 41-44]. Table 1.1 is a summary of synthesizing magnetic nanoparticles in different sizes which different parameters like pH, stirring speed, temperature or used catalyst are different and as a results nanoparticles size is different from each other under different conditions. Figure 1.4 shows nanoparticles sizes by changing the pH of the reaction system. Figure 1.5 depicts the nanoparticle sizes in different reaction temperature. Figure 1.6 is shows nanoparticles size variation in different stirring rates and Figure 1.7 shows XRD results for Fe_3O_4 in different sizes and Figure 1.8 respresents magnetization change of magnetic nanoparticles in different diameter sizes. We decided to have 5 different type of nanoparticles($SrFe_{12}O_{19}$, $BaFe_{12}O_{19}$, Fe_3O_4, $MgFe_2O_4$ and $MnFe_2O_4$) by changing the PH and concentration of nanoparticles in the DI water environment while our synthesizing condition and results will be explained in Table 1.1.

Table 1.1: Parameters for synthesizing Fe_3O_4 nanoparticles in different sizes using co-precipitation method available in literature.

Author	NPs	Size (nm)	Temperature	PH	Catalyst	Amount (mol)	Addition rate	Total Fe concentration (mol/L)	molar ratio Fe3+/Fe2+
Ref.[41]	Fe_3O_4	11.5	Room temp.	10.34	NaOH	0.08	1 ml/min		0.48
Ref.[41]	Fe_3O_4	11.2	Room temp.	11.94	NaOH	0.085	1 ml/min		0.48
Ref.[41]	Fe_3O_4	11	Room temp.	12.08	NaOH	0.09	1 ml/min		0.45
Ref.[41]	Fe_3O_4	10.9	Room temp.	12.2	NaOH	0.095	1 ml/min		0.46

Table 1.1 (continued): Parameters for synthesizing Fe_3O_4 nanoparticles in different sizes using co-precipitation method available in literature.

Author	NPs	Size (nm)	Temperature	PH	Catalyst	Amount (mol)	Addition rate	Total Fe concentration (mol/L)	molar ratio Fe3+/Fe2+
Ref.[41]	Fe_3O_4	10.7	Room temp.	12.6	NaOH	0.01	1 ml/min	-	0.43
Ref.[41]	Fe_3O_4	10.2	Room temp.	9.4	NaOH	0.08	Fast addition	-	0.49
Ref.[41]	Fe_3O_4	9.1	Room temp.	10.7	NaOH	0.09	Fast addition	-	0.44
Ref.[41]	Fe_3O_4	8.2	Room temp.	11.8	NaOH	0.1	Fast addition	-	0.43
Ref.[41]	Fe_3O_4	7.1	Room temp.		KOH	0.09	Fast addition	-	0.42
Ref.[41]	Fe_3O_4	6.5	Room temp.		TEAOH	0.09	Fast addition	-	0.41
Ref.[43]	Fe_3O_4	1.3	Room temp.	14	NaOH	0.9	-	-	-
Ref.[43]	Fe_3O_4	1.7	Room temp.	14	NaOH	1	-	-	-
Ref.[43]	Fe_3O_4	2.9	Room temp.	14	NaOH	1.1	-	-	-
Ref.[43]	Fe_3O_4	3	Room temp.	14	NaOH	1.5	-	-	-
Ref.[43]	Fe_3O_4	5.5	Room temp.	12.5	NaOH	1.5	-	-	-
Ref.[43]	Fe_3O_4	6	Room temp.	11.54	NaOH	1.5	-	-	-
Ref.[44]	Fe_3O_4	8	-		NH4Cl	-	-	-	-
Ref.[42]	Fe_3O_4	-	40° C	10	NaOH	-	-	0.15	-
Ref.[42]	Fe_3O_4	-	80° C	10	NaOH	-	-	0.15	-
Ref.[42]	Fe_3O_4	-	80° C	10	NaOH	-	-	0.86	-
Ref.[42]	Fe_3O_4	-	80° C	10	NaOH	-	-	0.86	-

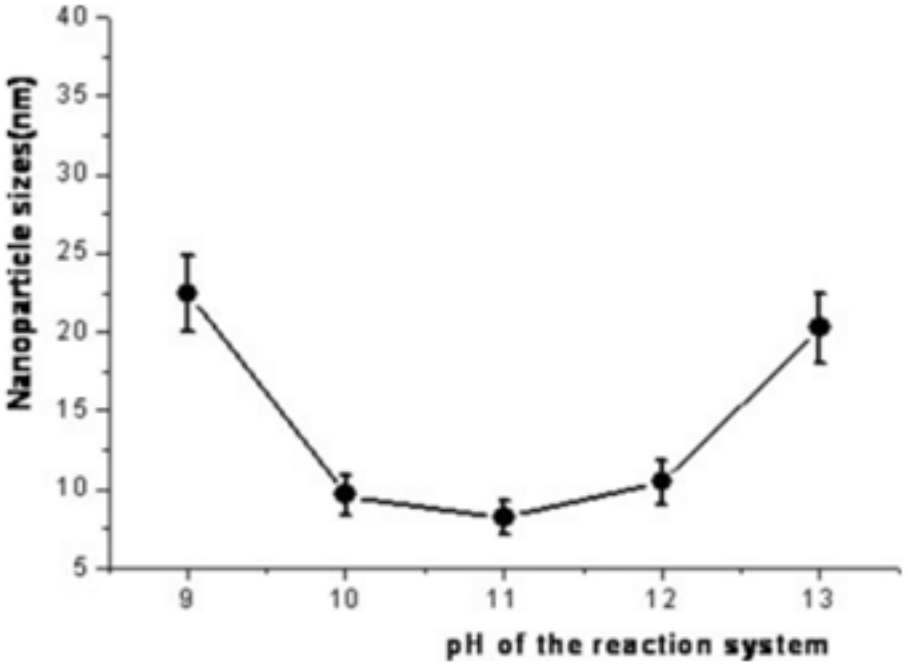

Figure 1.4: Effect of solution pH on sizes of Fe_3O_4 nanoparticles [28].

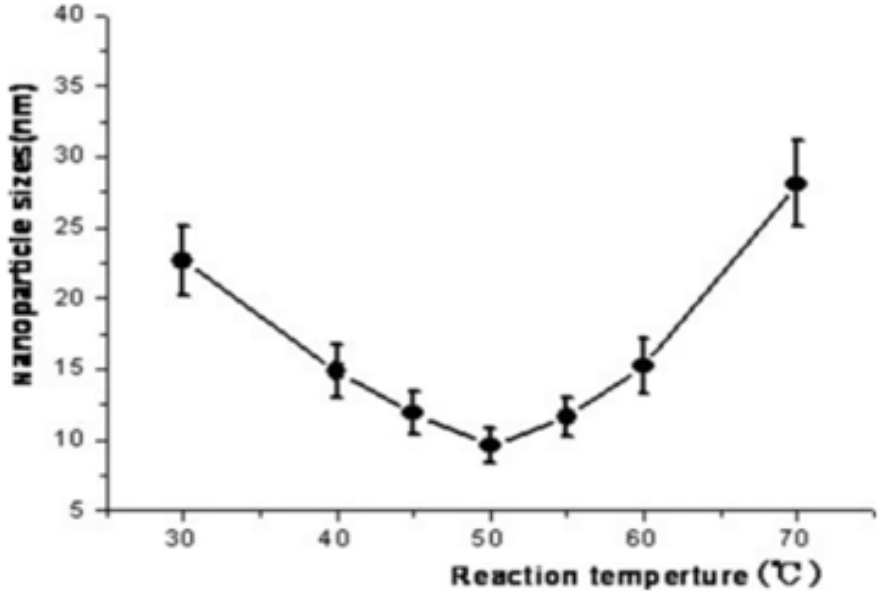

Figure 1.5: Effect of reaction temperature on size of Fe_3O_4 nanoparticles [28].

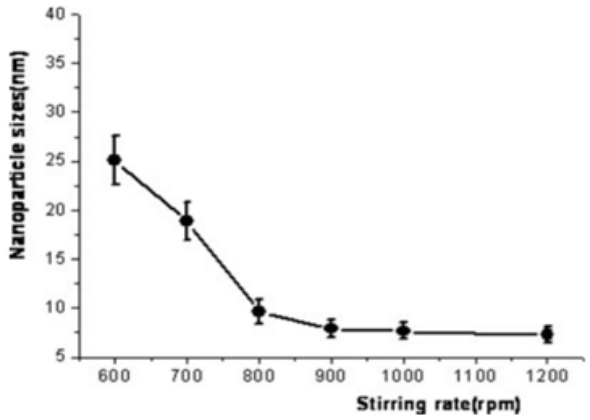

Figure 1.6: Effect of the stirring rate on sizes of Fe_3O_4 nanoparticles [28].

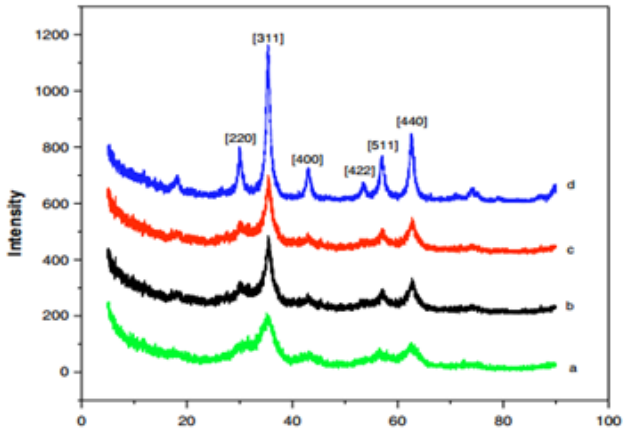

Figure 1.7: XRD patterns of as-prepared Fe_3O_4 MNPs [42].

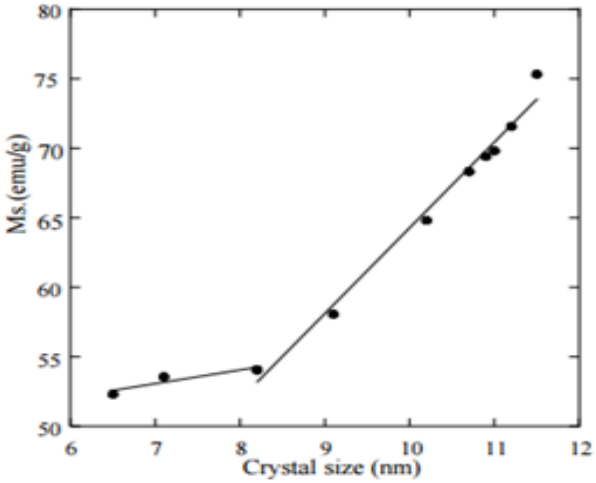

Figure 1.8: Saturation magnetization (Ms) as a function of magnetite particles size [42].

1.2.3 Surface functionalization of magnetic nanoparticles

Surface modification of magnetic nanoparticles is often necessary in order to achieve ferrofluidic stability, solubility in a certain solvent environment or in order to introduce molecular entities on the surface serving either as sites for further functionalization or as molecular probes in biotechnological applications. Immobilization of biomolecules onto the surface of magnetic nanoparticles is a process commonly denoted bioarticles functionalization. There exist numerous publications on biofunctionalization of magnetic nanoparticles in the scientific literature and by that also a large number of coupling chemistries [45]. In general surface modification for cancer therapy application includes oleic acid coating [46,47] for preventing oxidation of magnetite nanoparticles and silica coating[48-62] for preventing agglomiration and amination[63-68] for preparing them for gold coating [63-67,69-76] for making them intoxic for body organs and polymer coating [68,77-86] for making them biocompatable for attaching to body organs and cells. Figure 1.9 is represents magnetic nanoparticles core synthesis and in the following its surface coatings which includes silica coating, amination and gold decoration and changing it to gold shell coating.

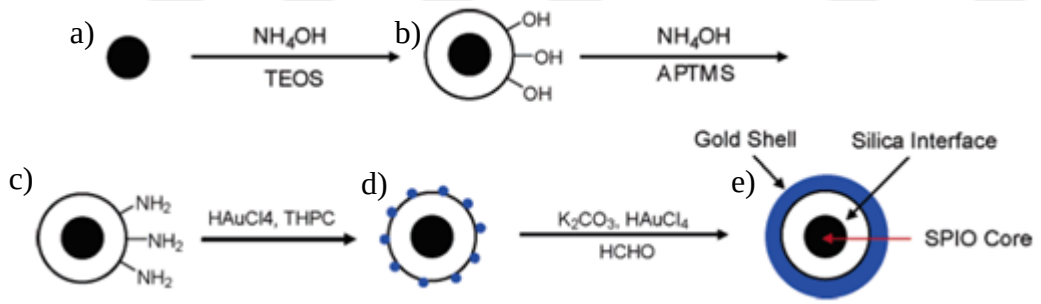

Figure 1.9: (a) Magnetic nanoparticle core (b) Silica coated (c) Aminated (d) Gold decoration (e) Gold shell coating [67].

2. MATERIALS AND EQUIPMENTS

The following chapter presents chemical reagents and devices used for the nanoparticle synthesis, the nanoparticle characterization and the heating experiments.

2.1 Chemical Reagents

Hereafter all used reagents are summed up with details of their chemical formula, purity, company and country of manufacture and possible abbreviations in **Error! eference source not found.**.1. All chemical were used without further purification or treatment.

Table 2.1: Materials used for synthesizing nanoparticle cores, silica coating and amination.

Trade name	Chemical formula	Purity [%]	Company / Country of Manufacture
Magnetic core fabrication of Fe_3O_4- and $SrFe_{12}O_{19}$-nanoparticles			
Iron (II) chloride tetrahydrate	$FeCl_2 \cdot 4H_2O$	99	Merck, Germany
Iron (III) chloride hexahydrate	$FeCl_3 \cdot 6H_2O$	99	Merck, Germany
Strontium (II) nitrate (dry)	$Sr(NO_3)_2$	99	Kimetsan, Turkey
Barium nitrate (dry)	Ba(NO3)2	O	Merck, Germany
Magnesium nitratehedrahydrate(dry)	$Mg(NO_3)_2.6H_2O$	-	Merck, Germany
Manganese (II) nitrate (dry)	$Mn(NO_3)_2.4H_2O$	-	Merck, Germany

Table 2.1 (continued): Materials used for synthesizing nanoparticle cores, silica coating and amination.

Trade name	Chemical formula	Purity [%]	Company / Country of Manufacture
Manganese (II) nitrate (dry)	$Mn(NO_3)_2.4H_2O$	-	Merck, Germany
Sodium hydroxide	NaOH	97	Merck, Germany
Oleic acid	$C_{18}H_{34}O_2$	98	ZAG, Turkey
N-hexane	C_6H_{14}	95	Merck, Germany
De-ionized water	De-ionized water generated via evaporation. Evaporator was purchased from Nüve.		
Silica coating and amination			
Tetraethyl orthosilicate	$C_8H_{20}O_4Si$	98	Sigma-Aldrich, Germany
3-Aminopropyltrimethoxy-silane	$H_2N(CH_2)_3Si(OCH_3)_3$	-	Flurochem, U.K.
Ammonia solution	NH_4OH	25 wt. %	Merck, Germany
2-propanol	C_3H_8O	99,5	Merck, Germany

2.2 Devices for Nanoparticle Characterization

In the following the function and specification of used devices for the nanoparticle characterization (FTIR, VSM, SEM and vacuum pump) are discussed.

2.2.1 Bruker optics ALPHA-Transmittance FTIR spectrometer

The principle of Fourier transform infrared spectroscopy bases on the specific absorption of electromagnetic waves of chemical groups like alcohol, amine or carboxyl groups. It is commonly used to verify successful surface modifications. Figure 2.1 is our used Bruker optics ALPHA-Transmittance FTIR spectrometer in labaratory which we have measured our samples FTIR using this instrument.

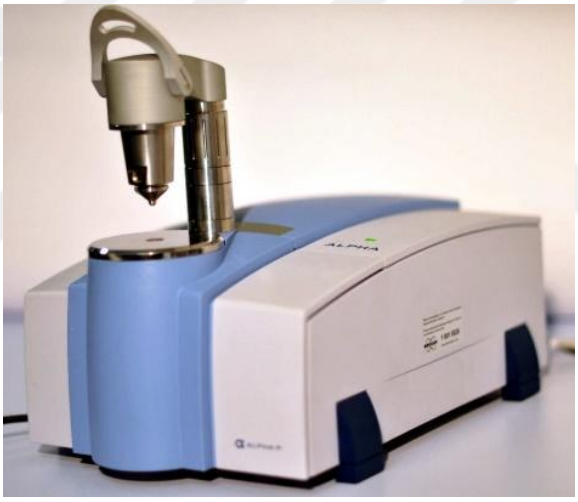

Figure 2.1: Bruker optics ALPHA-Transmittance FTIR spectrometer.

2.2.2 Vibrating sample magnetometer (VSM)

The VSM measurements were performed at the Physics Department of Istanbul Technical University. A homemade device was utilized, which is visualized in Figure 2.2 where our samples camsules are being positioned inside the sample holder one by one .

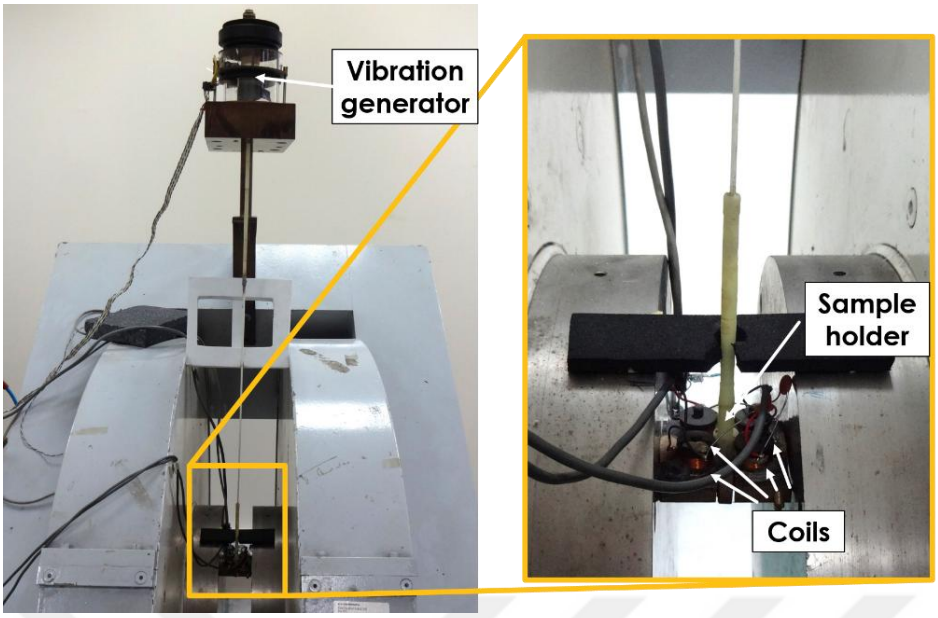

Figure 2.2: Vibrating sample magnometer (VSM).

Figure 2.3 shows the pump which we used for making the vacuum situations inside the white dish where we put our samples after drying in the water bath inside it and the pump is sucking the last probable water remaining in the samples by making a vacuum situation inside the dish.

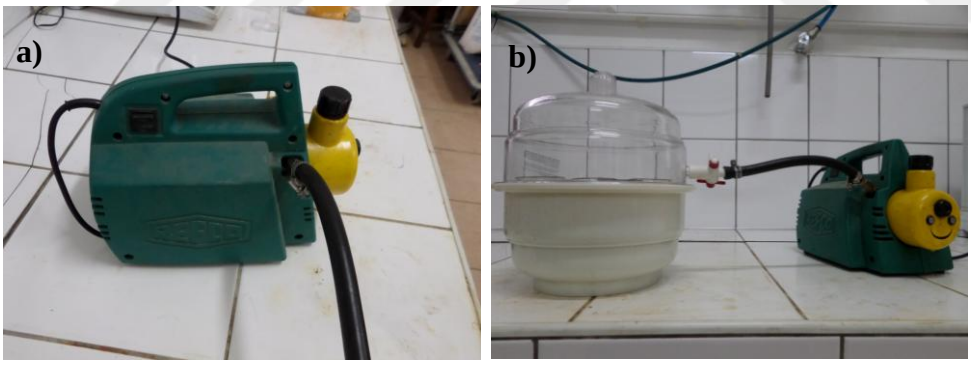

Figure 2.3: Vacuum pump a) stand alone b) connected to the drying space.

3. METHODS

In our work we used co-precipitation method in order to synthetize magnetic nanoparticle cores. Fe_3O_4 magnetic nanoparticles were oleic acid coated in order to prevent oxidation. In the next step all of the magnetic nanoparticles were silica coated using Stöber method in order to prevent nanoparticles agglomeration and make them biocompatible. In the final step of our work particles were aminated making magnetic nanoparticles ready for gold coating and PEG coating for future works.

The mentioned surface coatings make magnetic nanoparticles ready to enter into human organs for biomedical applications like hypertermia which is our main goal.

3.1 Core Synthesizing

In this project we synthesised 5 different magnetic nanoprticles including Fe_3O_4, $MgFe_2O_4$, $MnFe_2O_4$, $SrFe_{12}O_{19}$ and $BaFe_{12}O_{19}$ in different sizes by precipitation method and changing the PH of the solution via changing the amount of the alkalin(NaOH) and changing the concentration of synthesizing solution by changing the amount of the used DI water for synthesizing 20gr of each sample. Table

In our work we used the formulation of the reaction for choosing the amount of the materials for synthesizing each kind of the nanoparticle. Equations 3.1-3.5. In this method Fe_3Cl_6.OH, Fe_2Cl_4.OH and half of the used water in hole process was mixed together under 300rpm for 30minutes (Figure 3.1) and then NaOH solved in the other half of the DI water and simultaniously with $Sr(NO_3)_2$ or $Ba(NO_3)_2$ or $Mg(NO_3)_2.6H_2O$ or $Mn(NO_3)_2.4H_2O$ was added to the solution depending on the required kind of nanoparticle and was stirred for another 3 hours (Figure 3.2). And then decanded using magnets,measuring the PH of the solution and then washing till their 7 PH (Figure 3.3).

During Precipitation for synthesizing nanoparticles these chemical reactions are occuring:

For Synthesizing Iron Oxide:

$2\ FeCl_3\ .6H_2O + FeCl_2.4H_2O + 8\ NaOH$

$$\rightarrow \quad Fe_3O_4 + 16H_2O + 8\ NaCl + 2O_2 \qquad \textbf{(3.1)}$$

For Synthesizing Barium Ferrite:

$2Ba(NO_3)_2 + 8\ FeCl_2.4H_2O + 16\ FeCl_3.6H_2O + 64NaOH$

$$\rightarrow \quad 2BaFe_{12}O_{19}\ (s) + 160\ H_2O + 64\ NaCl + 3O_2 + 2N_2 \qquad \textbf{(3.2)}$$

For Synthesizing Strontium Ferrite:

$2Sr(NO_3)_2 + 8\ FeCl_2.4H_2O + 16FeCl_3 + 64\ NaOH$

$$\rightarrow \quad 2SrFe_{12}O_{19}\ (s) + 160\ H_2O + 64\ NaCl + 3O_2 + 2N_2 \qquad \textbf{(3.3)}$$

For Synthesizing Magnesium Ferrite:

$2Mg(NO_3)_2.6H_2O + 2\ FeCl_3.6H_2O + 2FeCl_2.4H_2O + 20NaOH$

$$\rightarrow 2MgFe_2O_4\ (s) + 42H_2O + 20\ NaCl + 7O_2 + 2N_2 \qquad \textbf{(3.4)}$$

For Synthesizing Manganese Ferrite:

$4Mn(NO_3)_2.4H_2O + 4FeCl_3.6H_2O + 4FeCl_2.4H_2O + 20\ NaOH$

$$\rightarrow 4MnFe_2O4\ (s) + 66H_2O + 20\ NaCl + O_2 + 4N_2 \qquad \textbf{(3.5)}$$

Table 3.1: Materials and parameters for synthesizing Fe_3O_4 nanoparticles.

Code	$FeCl_3.6H_2O$ (gram)	$FeCl_2.4H_2O$ (gram)	NaOH (gram)	Concentration of Fe3O4/DIwater (mol/L)	pH
FO-1	46.7	17.6	40	9.64	13
FO-2	46.7	17.6	50	5.78	13
FO-3	46.7	17.6	50	3.85	13
FO-4	46.7	17.6	25	9.64	5-6
FO-5	46.7	17.6	30	5.78	12.5
FO-6	46.7	17.6	35	3.85	12.5
FO-7	46.7	17.6	27	9.64	12.5
FO-8	46.7	17.6	28	5.78	10.5
FO-9	46.7	17.6	28	3.85	12

Table 3.2: Materials and parameters for synthesizing $SrFe_{12}O_{19}$ nanoparticles.

Code	$FeCl_3.6H_2O$ (gram)	$FeCl_2.4H_2O$ (gram)	$Sr(NO_3)_2$	NaOH (gram)	Concentration of Sr12O19/DI water (mol/L)	pH	Success
SF	40	14.8	4	20	53.08	-	-
SF-1	40	14.8	4	40	26.54	13	+
SF-2	40	14.8	4	45	26.54	14	+
SF	40	14.8	4	20	53.08	-	-
SF-3	40	14.8	4	30	17.7	14	+
SF-4	40	14.8	4	30	17.7	13	+
SF-5	40	14.8	4	26	26.54	12	+
SF-6	40	14.8	4	27	17.7	12	+
SF	40	14.8	4	15	26.54	-	-

Table 3.3: Materials and parameters for synthesizing $BaFe_{12}O_{19}$ nanoparticles.

Code	$FeCl_3.6H_2O$ (gram)	$FeCl_2.4H_2O$ (gram)	$Ba(NO_3)_2$	NaOH (gram)	Concentration of BaFe12O19/DI water (mol/L)	pH	Success
BF-1	38.9	14.3	4.7	35	27.78	13	+
BF-2	38.9	14.3	4.7	50	27.78	14	+
BF	38.9	14.3	4.7	20	55.57	-	-
BF-3	38.9	14.3	4.7	45	18.52	13	+
BF-4	38.9	14.3	4.7	60	18.52	14	+
BF-5	38.9	14.3	4.7	28	18.52	12	+
BF-6	38.9	14.3	4.7	28	46.31	13	+
BF-7	38.9	14.3	4.7	27.2	27.78	11	+
BF-8	38.9	14.3	4.7	40.8	18.52	13	+
BF-9	38.9	14.3	4.7	30	46.31	12	+

Table 3.4: Materials and parameters for synthesizing $MgFe_2O_4$ nanoparticles.

Code	$FeCl_3.6H_2O$ (gram)	$FeCl_2.4H_2O$ (gram)	$Mg(NO_3)_2.6H_2O$	NaOH (gram)	Concentration of MgFe2O4/DI water (mol/L)	pH
MgF-1	27.03	19.882	25.64	40	4.99	13
MgF-2	27.03	19.882	25.64	40	3.33	13
MgF-3	27.03	19.882	25.64	23	8.33	6
MgF-4	27.03	19.882	25.64	30	3.33	12
MgF-5	27.03	19.882	25.64	30	4.99	12
MgF-6	27.03	19.882	25.64	20	3.33	6
MgF-7	27.03	19.882	25.64	25	5	6
MgF-8	27.03	19.882	25.64	35	8.33	6
MgF-9	27.03	19.882	25.64	20	5	6
MgF-10	27.03	19.882	25.64	30	3.33	13
MgF-11	27.03	19.882	25.64	27	5	10
MgF-12	27.03	19.882	25.64	26	3.33	9

Table 3.5: Materials and parameters for synthesizing $MnFe_2O_4$ nanoparticles.

Code	$FeCl_3.6H_2O$ (gram)	$FeCl_2.4H_2O$ (gram)	$Mn(NO_3)_2.4H_2O$	NaOH (gram)	Concentration of Sr12O19/ DI water (mol/L)	pH	Success
Mn-1	23.44	17.24	21.6	30	5.76	13	+
Mn-2	23.44	17.24	21.6	25	5.76	12	+
Mn-3	23.44	17.24	21.6	30	3.84	12	+
Mn-4	23.44	17.24	21.6	40	3.84	13	+
Mn-5	23.44	17.24	21.6	20	5.76	6	+
Mn	23.44	17.24	21.6	20	3.84	-	-
Mn-6	23.44	17.24	21.6	25	9.6	12	+
Mn-7	23.44	17.24	21.6	30	9.6	13	+
Mn-8	23.44	17.24	21.6	20	9.6	6	+

Figure 3.1: Core synthesizing process first step by mixing water, $FeCl_3.6H_2O$ and $FeCl_2.4H_2O$.

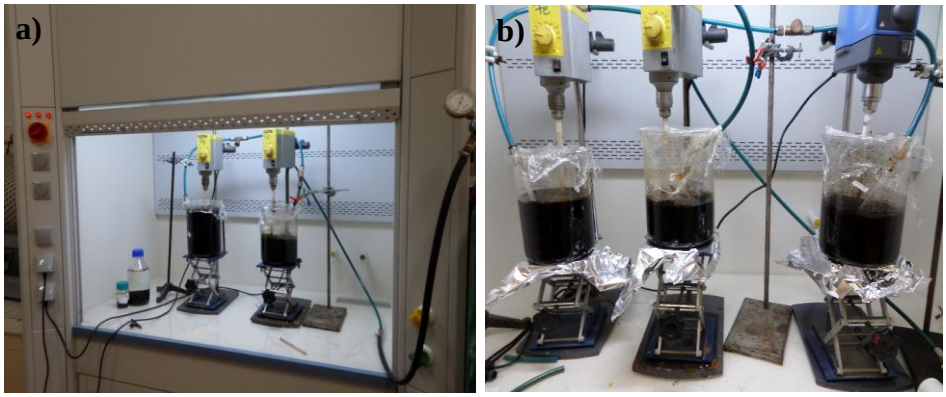

Figure 3.2: Adding NaOH and stirring for 3 hours a) all device b) close view.

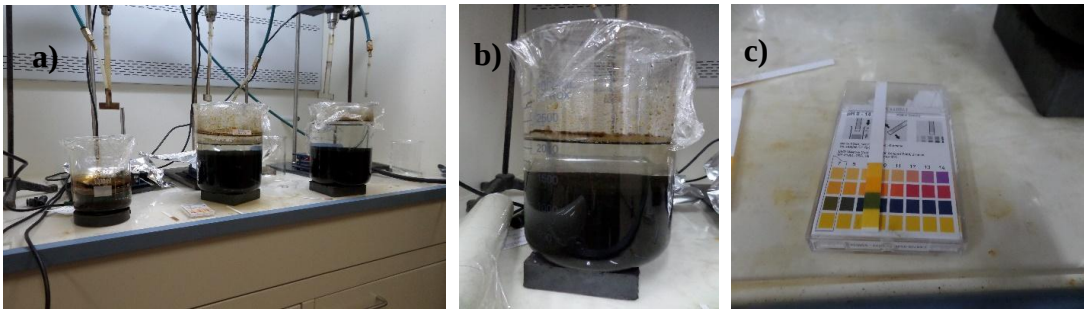

Figure 3.3: a) Decanding magnetic nanoparticles b) washing them till reaching a solution with the pH 7 c) final pH of solution.

3.2 Magnetic Nanoparticles Surface Coating

3.2.1 Oleic acid coating

In this project before starting to synthesizing nanoparticles in large amount nanoparticles were synthisized in little amount of 3gr to study their behavior and as in the firs step synthesized one sample as a core from each magneticnanoparticles we noticed just Fe_3O_4 oxideses after synthesis and $SrFe_{12}O_{19}$, $BaFe_{12}O_{19}$, $MgFe_2O_4$ and $MnFe_2O_4$ are stale and don't be oxidiesed. So in order to stop Fe_3O_4 magnetic nanoparticles from oxidization they became oleic acid coating that oleic acid was mixed to the solution after 2 hours when NaOH and the third material was added to Fe^{3+} and Fe^{2+} mixture and and after testing different amount of oleic-acid we decided to add 0.l ml of oleic-acid for synthesising 1gr of nanoparticles.

3.2.2 Silica coating and amination of the magnetic nanoparticles

In the third step nanoparticles were silica coated using Stober method. After going thorough the available literarures in this field as I mentioned befor we choosed several literatures and as the amount of the TEOS and Amonia and kind of Alcohol effedts the silica coating thickness and its structer and particles agglomiration we used references in chosing the amount of TEOS and kind of alcohol(ethanol25%) and amount of the amonia as have been represented in Table 3.6. First water, nanoparticles and ethanol were mixed together under 300rpm for 30minutes and after that Amonia and TEOS were added to the solution and were stirred for another 3hours then calculated amount of the solution containing 3gr of nanoparticles were seprated as a silica coated nanoparticles and were decanded and washed for 5

times. The other remained nanoparticles were aminated as after adding APTES the solution were stirred under 300rpm for another 6hours and then were decanded and washed 5 times.

Table 3.6: Used silica coating references and our methods.

Method	Thickness (nm)	NP core (nm)	TEOS	Solvent	Water (ml)	Amonia (ml)	Temperature
E. Ghasemi 2012	8	11	0.75 g	0.75 ml EtOH	5	0.75	40°C
Michael 2014	2	-	1.43 ml	286 ml (2-ProOH2)	60	8.58	Room Temp.
M.Kuzminskaa 2015	2	-	0.15 ml	284.7 ml (IsoproOH)	56.9	10.67	Room Temp.
YH Deng 2005	-	-	0.5 ml	80 EtOH	20	1.5	Room Temp.
Values in this project	-	-	0.5 ml	284.7ml EtOH	56.9	10.67	Room Temp.
New values in this project (successful)	4-6	-	0.5 ml	133ml EtOH	33	10.67	Room Temp.
Other values in this project (unsuccessful)	-	-	0.5 ml	133 ml EtOH	33	4	Room Temp.

Figure 3.4 shows general plan for our magnetic synthesis and their future surface coatings. Figure 3.5 to 3.8 are the images of prepared samples which in every bottle there is 3 gram of magnetic nanoparticles core, 3gram silica coated and 3 gram of aminated for each of 44 core samples which in total there are 132 samples.

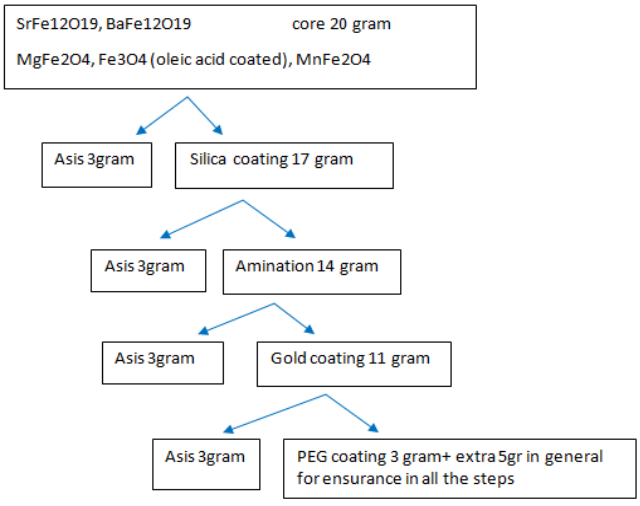

Figure 3.4: Our general plan in synthesizing.

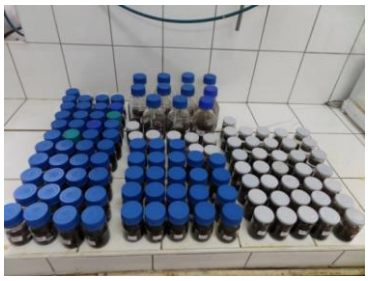

Figure 3.5: Prepared nanoparticles.

Figure 3.6: Prepared cores of the nanoparticles

Figure 3.7: Silica coated nanoparticles

Figure 3.8: Aminated nanoparticles.

3.2.3 Nanoparticle powder preparation for FTIR and VSM measurements

We dried 1 gram of each sample about 30 ml of nanoparticle solution in the water bath uneder 70-90$^{\circ}C$ temperature for about 10 hours in the 50ml baker (Figure 3.9) and then we put samples in the ambient place for evaporating the remained water and

then milled with a mortar (Figure 3.11). Our final powder magnetic nanoparticles have been shown in Figure 3.12 and Figure 3.13.

Figure 3.9: Drying magnetic nanoparticles in water bath in 80ºC.

Figure 3.10: Putting samples in the vacuum space for the final complete drying.

Figure 3.11: Equipments used magnetic nanoparticle powder making.

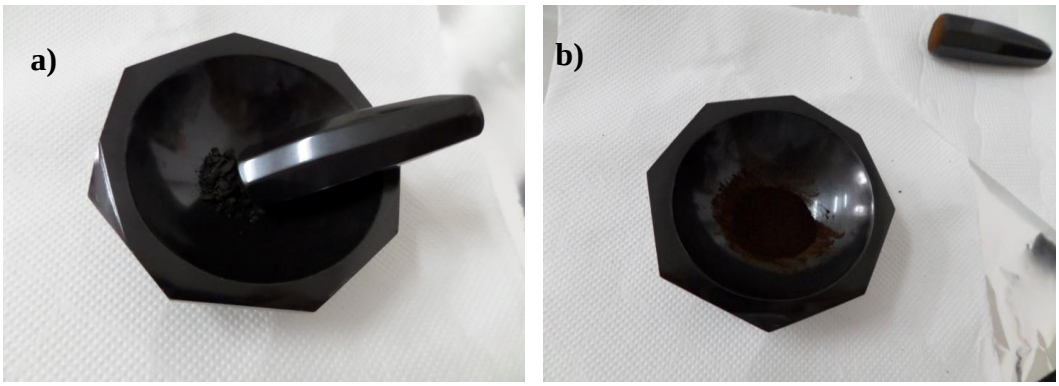

Figure 3.12: Dried Nanoparticles a) in dicer b) after making powder.

Figure 3.13: Final prepared samples.

3.2.4 Making capsules out of nanoparticles for VSM

Magnetic Nanoparticles of each samples were prepared for VSM measurments by making capsules which the weight of the embeded nanoparticles in each capsule made of foil should be more than 20 mg. Figure 3.14. Figure 3.15 is the process we have made capsules out of foil and after weighing them and calibrating Figure 3.16 capsules have been filled with nanoparticle powders Figure 3.17.

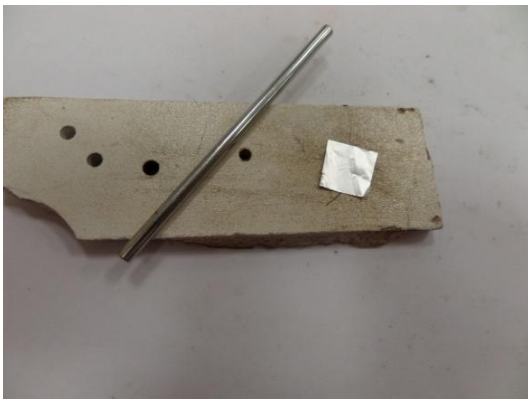

Figure 3.14: Instruments used for making capsules.

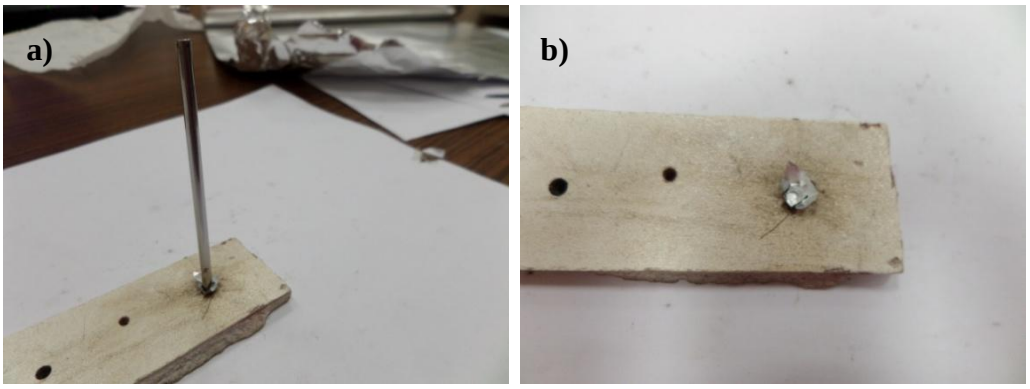

Figure 3.15: a) Making capsules from foil b) final product.

Figure 3.16: Calibrating the weighing device regarding the empty container foil a) weight of the foil b) close view.

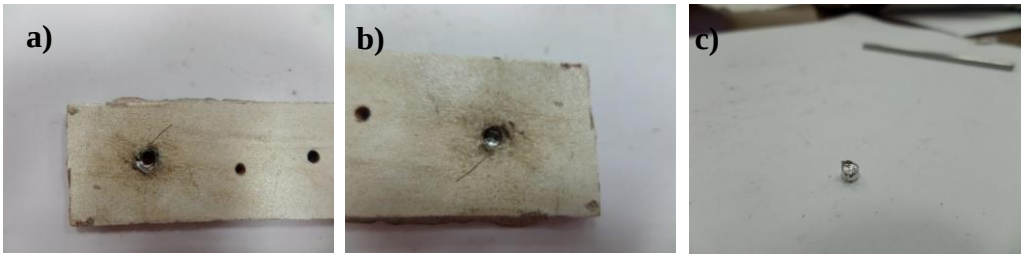

Figure 3.17: a) Filling nanoparticle powder into the capsule b) closing the capsule c) final sample.

3.2.5 Sample preparation for SEM measurements

For measuring the magnetic core size and observing samples structure droplets of Magnetic nonoparticles solution were dried on silicon wafer as we can see in Figure 3.18.

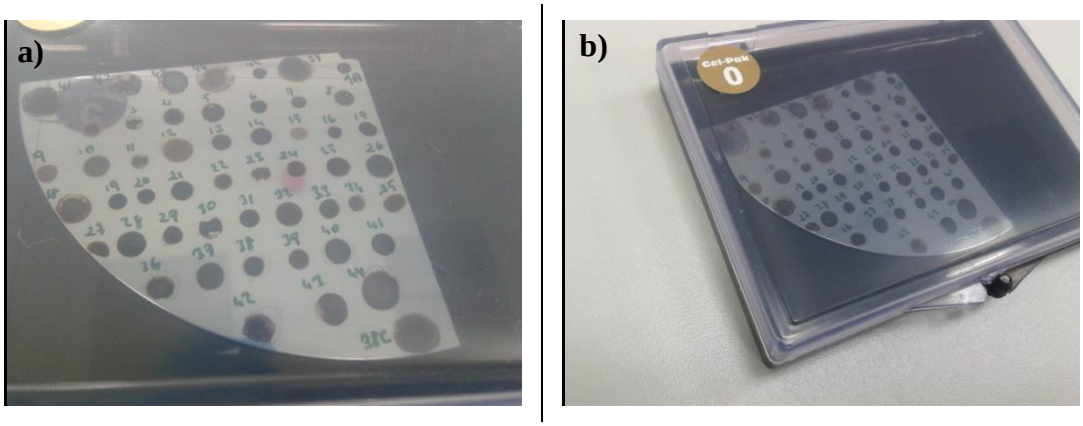

Figure 3.18: Dried droplets of nanoparticles core solution a) close view b) box view.

4. RESULTS AND DISCUSSION

In our synthesizing magnetic nanoparticles in different pH and concentrations some of the samples with low concentrations which have been achived by reducing the DI used water (1000 ml DI water for synthesizing 20 gram magnetic nanoparticles) were not successful so the water amount have been change to 1200 ml water in order to synthesize magnetic nanoparticles in high concentration. In addition as reducing the amount of NaOH for low pH there is a limitation for amount of pH. In another word, when amount of NaOH was reduced in order to reach to 8 or 9 complete precipitation did not occur and all the materials could not participate in precipitation reaction and in these situations which have been called **Failed** (Negative sign in success column) in Table 3.2, Table 3.3 and Table 3.5 solution pH reached to 4-5. Generally speaking reaction pH for Fe_3O_4 were 13, 12.5, 10,5 and 5.5 and for $SrFe_{12}O_{19}$ were 14, 13 and 12, for $BaFe_{12}O_{19}$ were 14, 13, 12 and 11, for $MgFe_2O_4$ were 13, 12, 6 and for $MnFe_2O_4$ were 13,12 and 6.

Tables A.1 to A.5 are representing the magnetic nanoparticles and silica coated magnetic nanoparticles and aminated magnetic nanoparticles codes; given for each of them in order to clarify the results and for better understanding. And after representing the related codes FTIR results have been presented in Figures A.1 to A.44 and in the following SEM results for magnetic nanoparticles core and their dimension have been presented and at the end VSM results have been included results have been discussed.

As we have different nanoparticles (Fe_3O_4, $SrFe_{12}O_{19}$, $BaFe_{12}O_{19}$, $MgFe_2O_4$ and $MnFe_2O_4$) in different synthesizing conditions all of the samples in FTIR have been analyzed in order to study their structure and to make sure that nanoparticles have been coated by Tetraethyl orthosilicate and (3-Aminopropyl)triethoxysilane. As we have summarized in Table 4.1 every material has a specific vibration peak like a finger print and by using FTIR we can identify the structure of materials. In our magnetic nanoparticles as they are referred as ferrofluids Fe vibration bands (Fe-O, and Fe-O-Fe) are in the range between 500-650cm^{-1} [87-91]. As we can see the

numbers between 540-570 in all of our samples demonstrating the presence of Fe-O and Fe-O-Fe bands in our magnetic nanoparticles. In addition we represent vibration of another bands in our samples showing the Mg-O, Mn-O , Sr-O, Ba-O, Sr-Fe, Ba-Fe, Mg-Fe and Mn-Fe representing the differences between magnetic nanoparticles as in the SrFe12O19 nanoparticles vibration bands between 400-600 cm^{-1} [92,93,94] represent the Sr-Fe and around 1400 cm^{-1} represent Sr-O bands in the materials. And weak bands in 662, 586,554 and 440 cm^{-1} [2] can be seen in Stransiom Fereit nanoparticles. Vibration bands of Ba-Fe in $BaFe_{12}O_{19}$ nanoparticles are in the range of 415-500 cm^{-1} [95,96] and Mg-Fe vibration bands are expected between 580 cm^{-1} and 600 cm^{-1} and Mg-O vibration bands are around 1600 cm^{-1} [97,98,99]. Furthermore, Mn-Fe and Mn-O vibration bands can be seen in 550 and 1650 cm^{-1} [100,101]. And oleic acid coating, silica coating and amination of magnetic nanoparticles FTIR analysis represent a vibration arond 950-1700 as their details have been shown in table 4.1 referring to previous researches. And as our samples number are not small and we have 5 kind of magnetic nanoparticles as mentioned previously we tried to summarize our FTIR results in table 4.2.

Table 4.1: FTIR bands available in literature.

Chemical group/bond	Characteristic vibration band [cm^{-1}]	Literature source
	Fe_3O_4-nanoparticles	
Fe-O	563,4; 540,2; 581; 582; 586	[87]; [88]; [89]; [90];
Fe-O-Fe	568	[91]
	$SrFe_{12}O_{19}$-nanoparticles	
Sr-O	524, 625,	[92]
Sr-Fe	400-600	[94]
	BaFe12O19-nanoparticles	
Ba-Fe	415,572,529, 490,580	[95]
Ba-O	1624	[96]
	MgFe2O4-nanoparticles	
MgO	1016, 1627	[97], [98]
Mg-Fe	582,473, 697560	[96]; [97]; [98]
	MnFe2O4-nanoparticles	
Mn-O	1382, 1458, 1638	[98]
Mn-Fe	697, 700-1100	[98]; [99]
Mn-OH	1641,1428,1237	

Table 4.1 (continued): FTIR bands available in literature.

Chemical group/bond	Characteristic vibration band [cm^{-1}]	Literature source
Oleic acid coating on Fe NPs		
Fe-COO	1389,2, 1628,4	[87]
υ(COO-)	1541; 1538	[100]; [101]
	1639; 1438	[100]; [101]
H-C-H	2922, 2921	[100]; [101]
	2852; 2850	[100]; [101]
C-O	1050	[100]; [101]
Porous silica coating		
Fe-O-Si	583	[91]
Si-O	1093; 1070, 1100	[89]; [90]
Si-O-Si	802,6	[87]
	1095,9	[87]
SiO_4	800	[89]
Hydroxyl groups attached at the surface		
O-H	1630, 3400	[89]; [90]
	3500 – 3600, 3500 – 3200	[102]
Amin groups attached at the surface		
N-H (primary amines)	3500 – 3100	[102]
	1640 – 1550; 1650-1580	[102]; [103]
	3400-3300 and 3330-3250	[103]

Table 4.2: Our FTIR results for synthesized nanopartic.

Fe_3O_4 nanoparticles	
Fe-O	
Fe-O-Fe	540-570
$SrFe_{12}O_{19}$ nanoparticles	
Sr-Fe	480
Sr-O	
$BaFe_{12}O_{19}$ nanoparticles	
Ba-O	490-500-600
Ba-Fe	490
$MgFe_2O_4$ nanoparticles	
Mg-O	1016.1630
Mg-Fe	550-580
$MnFe_2O_4$ nanoparticles	
Mn-O	1350-1480
Mn-Fe	800-900

Table 4.2 (continued): Our FTIR results for synthesized nanopartic.

Oleic acid coating	
Fe-COO	1330-1650
C-O	2900-3200
Silica Coating	
Si-O	900-1100
Si-O-Si	
Amination	
NH_3	1590-1650
O-H	2990-3200

In the SEM equipment we observed the structure of particles and measured their sizes which all were less than 30 nm in diametere as we were accpected for their biocompatibility purpose and in our samples we obserwed that in synthesizing Fe_3O_4 nanoparticles as PH 13 is the the largest, largest diameters have been achieved and as the amount of synthesig added water decreases mean, the concentration increases the nanoparticles size decreases and their behavior is linear . $SrFe_{12}O_{19}$nanoparticles largest sizes can be seen in the lowest PH condition which was 12 and as concentration increases their size is decreasing. In $BaFe_{12}O_{19}$ nanoparticles as decreases nanoparticle size increases and as concentration increases their size increases. In $MgFe_2O_4$ as concentration increases particles size decreases but there is no regular pattern between PH and particle size in our samples. And in $MnFe_2O_4$ nanoparticles no logical relation between PH and concentration and nanoparticle size have been seen. Generally speaking, exccept in Barium Fereit, in Figure B.6 as concentration decreases nanoparticles diameter size increases which it is visversa in Barium Ferreit and as reaction concentration decreases particle size decreases. And as maximum nanoparticle diameter size have been achieved in largest PH in Fe_3O_4 and $SrFe_{12}O_{19}$ nanoparticles synthesis reactions and maximum nanoparticle size for b$BaFe_{12}O_{19}$ and $MgFe_2O_4$ has been achieved in smallest reaction pH. But in order to our results we can not speake for sure that the minimum nanoparticles size have been in smallest or largest pH. From structure view seen in the SAM images, magnetic nanoparticles in concentration that 1200 ml water have been used do not have good structures and it seems that some other reactions have happened and some of materials have could not participate in reaction. And the nanoparticles which 2000

and 3000 ml DI water have been used for synthesizing 20 gram of each magnetic nanoparticles have much better structure and we can see a clear image of nanoparticles in the SAM results.

The magnetic properties were measured at room temperature (Figures C.1 to C.45) As we can see, the magnetization curve is to be without hysteresis, the coercivity field and remnant magnetization cannot be found from the curve. It confirms that magnetic nanoparticles are characteristic of superparamagnetic properties. From the magnetization curve, we can also see that the saturation magnetization (Ms) of all the magnetic nanoparticles increase when the sizes of magnetite increase, which can be attributed to the increase of weight and volume of magnetite nanoparticles. Also as it was ecpected that with silica coating and amination magnetic propertize decrease it is evident that in some samples due to magnetic nanoparticles surface coated and increase in their weight their saturation magnetization have increased.

From the Fe_3O_4 magnetic nenoparticles magnetization curve Figure C.1 to Figure C.9, it is apparent that aminated nanoparticles saturation magnetizations is higher than silica coated and cores which have been Oleic-acid coated for preventing oxidation. Explanation for this experiment results most probably is that during amination of silica coated and oleic acid coated of Fe_3O_4 magnetic nanoparticles previous coated layers have been removed from surface of magnetic nanoparticles and in FTIR results in silica coated and aminated oleic acid bonds are so weak or there is no band related to oleic-acid bands in aminated nanoparticles. In addition some of aminated $MgFe_2O_4$ and $MnFe_2O_4$ nanparticles have higher saturation magnetization than silica coated ones which is again can be explained by removal of silica coated layer during amination. Furthermore, increase of the weight and volume of magnetic nanoparticles after amination can effect the saturation magnetization of nanoparticles.

From the results we see that nanoparticles with larger size have higher saturation magnetization but since there is a big range of nanoparticle size with different size in different pH and concentration it seems difficult to conclude about nanoparticles size and magnetization power and as all 5 kind of magnetic nanoparticles with 12 nm size magnetization have been compared in Figure C.45. It is evident that Strantium Fereit has the highest Magnetization power under the applied field and Manganese Fereit is

the second nanoparticles in magnetization power and the third powerful magnetic nanoparticle is Magnetite stronger than Barium Fereit and the last kind of nanoparticles in magnetization power are Mangesium Fereit.

5. FUTURE WORK

As in this project different magnetic nanoparticles and their FTIR analyses for each sample and silica coated and aminated nanoparticles have been produced and nanoparticles size and their structure have been analyzed in future works researchers can use the optimized samples in size and structure to continue their studies and these results can be a good resource for the future researchers who are working on synthesizing Fe_3O_4, $SrFe_{12}O_{19}$, $BaFe_{12}O_{19}$, $MgFe_2O_4$ and $MnFe_2O_4$ magnetic nanoparticles. In addition all of the magnetic synthesized magnetic nanoparticles have been silica coated and aminated for preparing these nanoparticles for gold coating and PEG coating in order to be biocompatible for their application in cancer therapy and as there is a limit for magnetic nanoparticles between 30-60 nm nanoparticles for successful magnetic nanoparticles hyperthermia. These nanoparticles sizes and structure analysis in FTIR and SAM can be a ready resource for future coating and studies. Furthermore VSM results measured for any of magnetic nanoparticles in different sizes can open a new window for their magnetization intensity under magnetic field and their heating performance.

REFERENCES

[1] **Cai, W., Gao, T., Hong, H., & Sun, J.** (2008). Applications of gold nanoparticles in cancer nanotechnology. *Nanotechnology, Science and Applications, 1*, 17–32.

[2] **Kievit, F. M., & Zhang, M.** (2011). Surface Engineering of Iron Oxide Nanoparticlesfor Targeted Cancer Therapy. *Accounts of Chemical Research, 9,* 9-99.

[3] **Laurent, S., Dutz, S., Häfeli, U. O., & Mahmoudi, M.** (2011). Magnetic fluid hyperthermia: Focus on superparamagnetic iron oxide nanoparticles. *Advances in Colloid and Interface Science, 166,* 8-23.

[4] **Roca1, A. G., Morales, M. P., Grady, K. O., & Serna, C. J.** (2006) Structural and magnetic properties of uniform magnetite nanoparticles prepared by high temperature decomposition of organic precursors. *Nanotechnology, 17*,2783–2788.

[5] **Sun, C., Lee, J. S. H., & Zhang, M.** (2008). Magnetic nanoparticles in MR imaging and drug delivery. *Advanced Drug Delivery Reviews, 60,* 1252–1265.

[6] **Marinin, A.** (2012). *Synthesis and characterization of superparamagnetic iron oxide nanoparticles coated with silica.* (Master thesis). Royal Institute of Technology, Stockholm.

[7] **Kolhatkar, A. G., Jamison, A. C., Litvinov, D., Willson, R. C., & Lee, T. R.** (2013). Tuning the Magnetic Properties of Nanoparticles. *International Journal of Molecular Sciences, 14*, 15977-16009.

[8] **Obaidat, I. M., Issa, B., & Haik, Y.** (2015). Magnetic Properties of Magnetic Nanoparticles for Efficient Hyperthermia. *Journal of nanomaterials, 5*, 63-89.

[9] **Dennis, C. L. & Ivkov, R.** (2013). Physics of heat generation using magnetic nanoparticles for hyperthermia. *International Journal of Hyperthermia*, 29(8), 715–729.

[10] **Köktitz, R., Weitschies, W., Trahms, L., & Semmler, W.** (1999). Investigation of Brownian and NeHel relaxation in magnetic fluids. *Journal of Magnetism and Magnetic Materials, 201,* 102-104.

[11] **Suto, M., Hirota, Y., Hiroaki, M., Fujit, A., Kasuya, R., Tohji, K., & Jeyadevan, B.** (2009). Heat dissipation mechanism of magnetite nanoparticles in magnetic fluid hyperthermia. *Journal of Magnetism and Magnetic Materials, 321*, 1493–1496.

[12] **Lu, A., Salabas, E. L., & Schüth, F.,** (2007). Magnetic Nanoparticles: Synthesis, Protection, Functionalization, and Application. *Magnetic Nanoparticles,* 46, 1222 – 1244.

[13] **Wendt, M., & Ergun, C.**, (2014). *Magnetic heating of smart nanoparticles embedded in agar – influence of magnetic core and surfacedemodifications on the*

heating performance. (Master Thesis). Department of Mechanical Engineering, Istanbul Technical University, Istanbul.

[14] **Tartaj, P., Morales, M. P., Gonzalez-Carreno, T., Veintemillas-Verdaguer, S., & Serna, C. J.** (2005). Advances in magnetic nanoparticles for biotechnology applications. *Journal of Magnetism and Magnetic Materials, 290–291*, 28–34.

[15] **Frey, N. A., Peng, S., Cheng, K., & Sun, Sh.** (2009). Magnetic nanoparticles: synthesis, functionalization, and applications in bioimaging and magnetic energy storage. *National Institute of Health, Public Access, 38(9)*, 2532–2542.

[16] **Mohapatra, M., & Anand, S.** (2010). Synthesis and applications of nano-structured iron oxides/hydroxides– a review. *International Journal of Engineering, Science and Technology, 2(8)*, 127-146.

[17] **Drmota, A. Drofenik,M. Koselj, J. and Žnidaršič, A.** Edited by Dr. Najjar, R. (2012). Microemulsion Method for Synthesis of Magnetic Oxide Nanoparticles. *Microemulsions - An Introduction to Properties and Applications*, Chapter 10.

[18] **Santra, S., Tapec, R., Theodoropoulou, N., Dobson, J., Hebard, A.i & Tan, W.** (2001). Synthesis and Characterization of Silica-Coated Iron Oxide Nanoparticles in Microemulsion: The Effect of Nonionic Surfactants. *American Chemical Society 17*, 2900-2906.

[19] **Ding, H. L., Zhang, Y. X., Wang, S., Xu, J. M., Xu, S. C., & Li, G. H**. (2012). Fe3O4@SiO2 Core/Shell Nanoparticles: The silica soating regulations with a single core for different core sizes and shell thicknesses. *American Chemical Society, 24*, 4572−4580.

[20] **Barber, K.** (2005) *Size Controlled Reverse Micelle Synthesis of Metallic Cobalt Nanoparticles.* (Master thesis) Faculty of the Graduate College, Oklahoma State University, Oklahoma.

[21] **Kim, K. H., Kim. M. J., Choa, Y. H. Kim, D. H., & Yu, J. H,** (2008). Synthesis and Magnetic Properties of Surface Coated Magnetite Superparamagentic Nanoparticles. *IEEE Transacations on Magnetics, 44(11),* 2940-2943.

[22] **Gnanaprakash, G., Mahadevan, S., Jayakumar, T., Kalyanasundaram, P., Philip, J., & Raj, B.** (2007). Effect of initial pH and temperature of iron salt solutions on formation of magnetite nanoparticles. *Materials Chemistry and Physics, 103*, 168–175.

[23] **Figuerola, A., Corato, R. D., Manna, L., & Pellegrino, T.** (2010). From iron oxide nanoparticles towards advanced iron-based inorganic materials designed for biomedical applications. *Pharmacological Research, 62*, 126–143.

[24] **Hong, R. Y., Li, J. H., Zhang, S. Z., Li, H. Z., Zheng, Y., Ding, J., & We, D. G.** (2009). Preparation and characterization of silica-coated Fe3O4 nanoparticles used as precursor of ferrofluids. *Applied Surface Science, 255*, 3485–3492

[25] **Kim, D. K., Zhang, Y., Voit, W., Rao, K. V., & Muhammed, M.** (2001). Synthesis and characterization of surfactant-coated superparamagnetic monodispersed iron oxide nanoparticles. *Journal of Magnetism and Magnetic Materials, 225*, 30-36.

[26] **Sun, S. & Zeng, H.** (2002). Size-controlled cynthesis of magnetite nanoparticles. *Journal of the American Chemical Society, 124,* 8204-8205.

[27] **Kim, K. H., Kim, M. J., Choa, Y. H., Ki, D. H., & Yu, J. H**. (2008). (2008). Synthesis and Magnetic Properties of Surface Coated Magnetite Superparamagentic Nanoparticles. *IEEE Transacations on Magnetics, 44(11),* 2940-2943.

[28] **Sun, J., Zhou, S. Hou,P., Yang, Y., Weng, J., Li, X., & Li, M.** (2006). Synthesis and characterization of biocompatible Fe3O4 nanoparticles. *Journal of Biomedical Materials Research Part A.*

[29] **Hariani, P. L., Faizal, M., Marsi, R., & Setiabudidaya, D.** (2013). Synthesis and properties of Fe3O4 nanoparticles by co-precipitation method to removal procion dye. *International Journal of Environmental Science and Development, 4(3),* 336-340.

[30] **Kang, Y. S., Risbud, S., Rabolt, J. F., & Stroeve, P.,** (1996). Synthesis and characterization of nanometer-size Fe3O4 and Fe2O3 particles. *Chemistry of Materials, 8(9),* 2209-2211.

[31] **Petcharoena, K. & Sirivat, A.** (2012). Synthesis and characterization of magnetite nanoparticles via the chemical co-precipitation method. *Journal of Materials Science and Engineering, 177,* 421– 427.

[32] **Zhang, L., & Li, Z.,** (2009). Synthesis and characterization of SrFe12O19/CoFe2O4 nanocomposites with core-shell structure. *Journal of Alloys and Compounds, 469,* 422–426.

[33] **Drmota, A., Žnidaršič, A., & Košak, A.,** (2010). Synthesis of strontium hexaferrite nanoparticles prepared using co-precipitation method and microemulsion processing, *Journal of Physics: Conference Series, 200*.

[34] **Hessien, M. M., Rashad, M. M., & El-Barawy, K.** (2007). Controlling the composition and magnetic properties of strontium hexaferrite synthesized by co-precipitation method. *Journal of Magnetism and Magnetic Materials, 320*: 336–343.

[35] **Palla, B. J., Shah, D. O., Garcia-Casillas, P., & Matutes-Aquino, J.** (1999). Preparation of nanoparticles of barium ferrite from precipitation in microemulsions. *Journal of Nanoparticle Research, 1*, 215–221.

[36] **GoodarzNaseri, M., BinSaion, E., AbbastabarAhangar, H., Hashim, M., & Shaari, A. H.** (2011). Synthesis and characterization of manganese ferrite nanoparticles by thermal treatment method. *Journal of Magnetism and Magnetic Materials, 323,* 1745–1749.

[37] **Chen, Q., Rondinone, A. J., Chakoumakos, B. C., & Zhang, Z. J.** (1999). Synthesis of superparamagnetic MgFe2O4 nanoparticles by coprecipitation. *Journal of Magnetism and Magnetic Materials, 194,* 1-7.

[38] **Sheykhan, M., Mohammadnejad, H., Akbari, J., & Heydari, A.,** (2012) Superparamagnetic magnesium ferrite nanoparticles: a magnetically reusable and clean heterogeneous catalyst. *Tetrahedron Letters, 53*, 2959–2964.

[39] **Pereira, C., Pereira, A., Fernandes, C., Rocha, M., Mendes, R., FernándezGarcía, M. P., Guedes, A., Tavares, P. B., Grenèche, J. M., Araújo, J. P., & Freire, C.** (2012). Superparamagnetic MFe2O4 (M = Fe, Co, Mn)

nanoparticles: Tuning the particle size and magnetic properties through a novel one-step coprecipitation route. *Journal of American Chemistry Society, 24,* 1496−1504.

[40] **Sun, S., Zeng, H., Robinson, D. R., Raoux, S., Rice, P. M., Wang, S. X., & Li, G.** (2003). Monodisperse MFe2O4 (M) Fe, Co, Mn) nanoparticles. *Journal of the American Chemical Society, 126*, 273-279.

[41] **Mascolo, M. C., Pei, Y., and Ring, T. A.,** (2013). Room temperature co-precipitation synthesis of magnetite nanoparticles in a large pH window with different bases. *Journal of Materials, 6,* 5549-5567.

[42] **Weia, Y., Hanb, B., Hua, X., Linc, Y., Wangd, X., & Denga, X.** (2011). Synthesis of Fe3O4 nanoparticles and their magnetic properties. *Chinese Materials Conference,. 27*, 632 – 637.

[43] **Kim, D. K., Zhang, Y., Voit, W., Rao, K.V., Muhammed, M.,** (2001). Synthesis and characterization of surfactant-coated superparamagnetic monodispersed iron oxide nanoparticles. *Journal of Magnetism and Magnetic Materials, 225*, 30-36.

[44] **Shen, Y. F., Tang, J., Nie, Z. H., Wang, Y. D., Ren, Y., & Zuo, L.,** (2009). Preparation and application of magnetic Fe3O4 nanoparticles for wastewater purification. *Journal of Separation and Purification Technology, 68*, 12–319.

[45] **Svedlindh, P., Gunnarsson, K., Strömberg, & M., Oscarsson, S.** *Bionanomagnetism, Chapter XXX*.

[46] **Chen, C. L., Zhang, H., Ye, Q., Hsieh, W. Y., Hitchens, T. K., Shen, H. H., Liu, L., Wu, Y., J. Foley, L. M., Wang, S. J., & Ho, C.** (2011). A new nano-sized iron oxide particle with high sensitivity for cellular magnetic resonance imaging. *Journal of Molecular Imaging and Society for Molecular Imaging, 13*, 825-839.

[47] **Omer, M., Haider, S., & Park, S. Y.** (2011). A novel route for the preparation of thermally sensitive core-shell magnetic nanoparticles. *Journal of Polymer, 52.* 91-97.

[48] **Guerrero-Martinez, B. A., Perez-Juste, J., & Liz-Marzan, L. M.** (2010). Recent progress on silica coating of nanoparticles and related nanomaterials. *Journal of Advanced Materials, 22*, 1182–1195.

[49] **Ammar, M., Mazaleyrat, F., Bonnet, J. P., Audebert, P., Brosseau, A., Wang, G., & Champion, Y.** *Synthesis and characterization of coreshell structure silicacoated Fe29.5Ni70.5 nanoparticles*.

[50] **Johnson, N. J. J., Sangeetha, N. M., Boyer, J. C., & Veggel, F. C. J. M.,** (2010). Facile ligand-exchange with polyvinylpyrrolidone and subsequent silica coating of hydrophobic upconverting b- NaYF4:Yb3+/Er3+ nanoparticles. *Journal of the Royal Society of Chemistry, 2*, 771–777.

[51] **Jana, N. R., Earhart, C., & Ying, J. Y.** (2007). Synthesis of water-soluble and functionalized nanoparticles by silica coating. *Journal of American Chemical Society, 19(21),* 5074-5082.

[52] **Ji, X., Shao, R., Elliott, A. M., Stafford, R. J., Esparza-Coss, E., Bankson, J. A., Liang, G., Luo, Z. P., Park, K., Markert, J. T., & Li, C.** (2007). Bifunctional gold nanoshells with a superparamagnetic iron oxide-silica core suitable for both MR

imaging and photothermal therapy. *The Journal of Physical Chemistry, 111,* 6245-6251.

[53] **Deng, Y. H., Wang, C. C., Hu, J. H., Yang, W. L., & Fu, S. K**. (2005). Investigation of formation of silica-coated magnetite nanoparticles via sol–gel approach. *Journal of Colloids and Surfaces A, 262*, 87–93.

[54] **Dick, K., Dhanasekaran, T., Zhang, Z., & Meisel, D.,** (2002). Size-dependent melting of silica-encapsulated gold nanoparticles. J*ournal of American Chemistry Society, 124(10),* 2312-2317.

[55] **Yi, D. K., Selvan, S. T., Lee, S. S., Papaefthymiou, G. C., Kundaliya, D. & Ying, J. Y.** (2005). Silica-coated nanocomposites of magnetic nanoparticles and quantum dots. *Journal of American Chemistry Society, 127*, 4990-4991.

[56] **Kobayashi, Y., Horie, M., Konno, M., Rodriguez-Gonzalez, B., & Liz-Marzan, L. M.** (2003). Preparation and properties of silica-coated cobalt nanoparticles. *The Journal of Physical Chemistry B., 107*, 7420-7425.

[57] **Kobayashi, Y., Katakami, H., Mine, E., Nagao, D., Konno, M., & Liz-Marzán, L. M.** (2005). Silica coating of silver nanoparticles using a modified Stöber method. *Journal of Colloid and Interface Science,283,* 392–396.

[58] **Santra, S. Tapec, R. Theodoropoulou, N. Dobson, J. Hebard, A. and Tan, W.** (2001). Synthesis and Characterization of Silica-Coated Iron Oxide Nanoparticles in Microemulsion: The Effect of Nonionic Surfactants. Journal of American Chemistry Society. No. *17. pp:* 2900-2906.

[59] **Lopez, C. F., Mateo, C. M., Alvarez-Puebla, R. A., Perez-Juste, J., Pastoriza-Santos, I., & Liz-Marzan, L. M.** (2009). Highly controlled silica coating of PEG-capped metal nanoparticles and preparation of SERS-encoded particles. *Journal of Langmuir, 25(24),* 13894–13899.

[60] **Lu, Y., Yin, Y., Mayers, B. T., & Xia, Y.** (2001). Modifying the surface properties of superparamagnetic iron oxide nanoparticles through a sol-gel approach. *Journal of Nano Letters, 2(3),* 183-186.

[61] **Ghasemia, E., Ghaharia, M., Mehranpoor, N., & Mirhabibi, A**. (2012). Silica coated magnetite nanoparticles: effects of TEOS concentration**.** *Proceedings of the 4th International Conference on Nanostructures (ICNS4).*

[62] **Ibrahim, I. A. M., Zikry, A.A.F., & Sharaf, M. A.** (2010). Preparation of spherical silica nanoparticles: Stober silica. *Journal of American Science, 6(11),* 985-989.

[63] **Lin, J.** (2001). Gold-coated iron (Fe@Au) nanoparticles: synthesis, characterization, and magnetic field-induced aelf-assembly. *Journal of Solid State Chemistry, 159,* 26-31 .

[64] **Otoufi, M. K., Shahtahmasebebi, N., Kompany, A., & Goharshadi, E.** (2014). A systematic growth of gold nanoseeds on silica for silica@gold core-shell nanoparticles and investigation of optical properties. *International Journal of Nano Dimension, 5(6),*525-531.

[65] **Khosroshahi, M. E., & Nourbakhsh, M. S.** (2010). Preparation and characterization of self assembled gold nanoparticles on amino functionalized SiO2

dielectric core. *International Journal of Chemical, Molecular, Nuclear, Materials and Metallurgical Engineering, 4(4),* 264-267.

[66] **Kouassi, G. K., & Irudayaraj, J**. (2006). Magnetic and gold-coated magnetic nanoparticles as a DNA sensor. *Journal of American Chemical Society, 10,* 3234-3241.

[67] **Ji, X., Shao, R., Elliott, A. M., Stafford, R. J., EsparzaCoss, E., Bankson, J. A., Liang, G., Luo, Z. P., Park, K., Markert, J. T., & Li, C.** (2007). Bifunctional gold nanoshells with a superparamagnetic iron oxide-silica core suitable for both MR imaging and photothermal therapy. *Journal of American Chemical Society, 111,* 6245-6251.

[68] **Yamauraa, M., Camiloa, R. L., Sampaiob, L. C., Macedoc, M. A., Nakamurad, M., & Toma, H. E.** (2004) Preparation and characterization of (3-aminopropyl) triethoxysilane-coated magnetite nanoparticles. *Journal of Magnetism and Magnetic Materials, 279,* 210–217.

[69] **Chen, M., Yamamuro, S., Farrell, D., and Majetich, S. A.** (2003). Gold-coated iron nanoparticles for biomedical applications. *Journal of Applied Physics, 93*, 7551-7553.

[70] **Pal, S., Morales, M., Mukherjee, P., & Srikanth, H.** (2009) Synthesis and magnetic properties of gold coated iron oxide nanoparticles. *Journal of Applied Physics, 105*, 07B504.

[71] **Madhuri, M., Kundu, S., Ghosh, S. K., Panigrahi, S., Sau, T. K., Yusuf, S. M., & Pal, T.** (2005). Magnetite nanoparticles with tunable gold or silver shell. *Journal of Colloid and Interface Science, 286,* 187–194.

[72] **Salehizadeh, H., Hekmatian, E., Sadeghi, M., & Kennedy, K.,** (2012). Synthesis and characterization of core-shell Fe3O4-gold-chitosan nanostructure. *Journal of Nanobiotechnology, 10(3).*

[73] **Lo, C. K., Xiao, D., & Choi, M. M. F.** (2007). Homocysteine-protected gold-coated magnetic nanoparticles: synthesis and characterisation. *Journal of Materials Chemistry, 17,* 2418–2427.

[74] **Rahman, M. T., Krishnamurthy, P. G., Parthiban, P., Jain, A., Park, C. P., Kim, D. P., & Khan, S. A.** (2013). Dynamically tunable nanoparticle engineering enabled by short contact-time microfluidic synthesis with a reactive gas. *Journal of Electronic Supplementary Material.*

[75] **Cho, S. J., Idrobo, J. C., Olamit, J., Liu, K., Browning, N. D., & Kauzlarich, S. M.** Growth mechanisms and oxidation-resistance of gold-coated iron nanoparticles.

[76] **Park, S. E., Park, M. Y., Han, P. K., & Lee, S. W.** (2006) The effect of pH-adjusted gold colloids on the formation of gold clusters over APTMS-coated silica cores. *Journal of Korean Chemical Society, 27(9),* 1341-1345.

[77] **Chen, C. L., Zhang, H., Ye, Q., Hsieh, W. Y., Hitchens, T. K., Shen, H. H., Liu, L., Wu, Y. J., Foley, L. M., Wang, S. J., & Ho, C.** (2011). A new nano-sized iron oxide particle with high sensitivity for cellular magnetic resonance imaging. *Journal of Molecular Imagingand Biology, 13*, 825Y839.

[78] **Hodenius, M., Hieronymus, T., Zenke, M., Becker, C., Elling, L., Bornemann, J., Wong, J. E., Richtering, W., Himmelreich, U., & Cuyper, M.,** (2012). Magnetically triggered clustering of biotinylated iron oxide nanoparticles in the presence of streptavidinylated enzymes. *Journal of Nanotechnology, 23,* 9.

[79] **Qu, J. B., Shao, H. H., Jing, G. L., & Huang, F.,** (2013). PEG-chitosan-coated iron oxide nanoparticles with high saturated magnetization as carriers of 10 hydroxycamptothecin: Preparation, characterization and cytotoxicity studies. *Journal of Colloids and Surfaces B, 102,* 37– 44

[80] **Fenga, B., Hong, R.Y., Wanga, L.S., Guoc, L., Lib, H.Z., Dingd, J., Zhenge, Y., & Wei, D.G.** (2008). Synthesis of Fe3O4/APTES/PEG diacid functionalized magnetic nanoparticles for MR imaging. *Journal of Colloids and Surfaces A, 328,* 52–59

[81] **Zhang, Y., Kohler, N., & Zhang, M.** (2002). Surface modification of superparamagnetic magnetite nanoparticles and their intracellular uptake. *Journal of Biomaterials, 23,* 1553–1561.

[82] **Chen, T. J., Cheng, T. H., Hung, Y. C., Lin, K.T., Liu, G. C., & Wang, Y. M.,** (2007). Targeted folic acid-PEG nanoparticles for noninvasive imaging of folate receptor by MRI. *Wiley InterScience,* 165-175.

[83] **Park, J. Y., Daksha, P., Lee, G. H., Woo, S., & Chang, Y.** (2008). Highly water-dispersible PEG surface modified ultra small superparamagnetic iron oxide nanoparticles useful for target-specific biomedical applications. *Journal of Nanotechnology, 19.*

[84] **Herve, K., Douziech-Eyrolles, L., Munnier, E., Cohen-Jonathan, S., Souce, M., Marchais, H., Limelette, P., Warmont, F., Saboungi, M. L., Dubois, P., & Chourpa, I.** (2008). The development of stable aqueous suspensions of PEGylated SPIONs for biomedical applications. *Journal of Nanotechnology*, 19.

[85] **Sun, C., Veiseh, O., Gunn, J., Fang, C., Hansen, S., Lee, D., Sze, R., Richard G., Ellenbogen, J. O., & Zhang, M.** (2008). In vivo MRI detection of gliomas by chlorotoxin-conjugated superparamagnetic nanoprobes. *Small Journal, 3,* 372 – 379.

[86] **Xie, B. J., Xu, C., Kohler, N., Hou, Y., & Sun, S.** *(2007).* Controlled PEGylation of Monodisperse Fe3O4 Nanoparticles for Reduced Non-Specific Uptake by Macrophage Cells. *Journal of Advanced Materials, 19,* 3163–3166.

[87] **Hong, R. Y. Li, J.-H. S.-Z. Zhang, H.-Z. Li, Y. Zheng, J.-M. Ding & D.-G. Wei,** (2009) Preparation and characterization of silica-coated Fe3O4 nanoparticles used as precursor of ferrofluids, *Applied Surface Science, 255*, 3485-3492.

[88] **Hong, R. Y., Zhang, S. Z., Di, G. Q., Li, H. Z., Zheng, H. Z. Ding, J., & Wei, D. G.** (2008). Preparation, charaterization and application of Fe3O4/ZnO core/shell magnetic nanoparticles, *Materials Research Bulletin, 42*, 2457-2468..

[89] **Chen, L., Xu, Z., Dai, H., & Zhang, S.,** (2010). Facile synthesis and magnetic properties of monodisperse Fe3O4/silica nanocomposite microshperes with embedded structures via a direct solution-based route, *Journal of Alloys and Composites, 497*, 221-227.

[90] **Hu, H., Wang, Z., & Pan, L.** (2010). Synthesis of monodisperse Fe3O4@silica core-shell microspheres and their application for removal of heavy ions from water, *Journal of Alloys and Compounds, 492*, 656-661..

[91] **Chen, F. H., Gao, Q., & Ni, J. Z.** (2008) The grafting and release behavior of doxorubincin from Fe3O4@SiO2 core-shell structure nanoparticles via an acid cleaving amide bond: The potential for magnetic targeting drug delivery, *Nanotechnology, 19*, 1-9.

[92] **Arellano-Tanori, O., Rojas-Hernandez, A., Gomez-Fuentes, R., Ochoa-Landin, R., Berman-Mendoza, D., Mendivil-Reynoso, T, Ramirez-Rodriguez, L. P. and Castillo, S. J.** (2014) Novel synthesis of SrSe by reduction of selenium itno rongalite solutions, *Journal of Ovonic Research, 12*, 55-59.

[93] **Primc, D., Drofenik, M., & Makovec, D.** (2011) Low-Temperature Hydrothermal Synthesis of Ultrafine Strontium Hexaferrite Nanoparticles, *Journal of Inorganic Chemistry*, 3802–3809.

[94] **Meng, X., Zhu, Y., Xu, S., & Liu, T.** (2016). Facile synthesis of shell-core polyaniline/SrFe12O19, *Journal of Royal Society of Chemistry*, 4946-4949

[95] **Durmus, Z., Durmus, A., & Kavas, H.** (2015) Synthesis and characterization of structural and magneticproperties of graphene/hard ferrite nanocomposites as microwave-absorbing material, *Journal of Material Science*, *50*, 1201–1213.

[96] **Meng, Y. Y., He, M. H., Zeng, Q., Jiao, D. L., Shukla, S., Ramanujan, R. V., & Liu, Z. W.** (2014) Synthesis of barium ferrite ultrafine powders by a sol–gel combustion method using glycine gels, *Journal of Alloys and Compounds*, 220–225.

[97] **Khot, V. M., Salunkhe, A. B., Thorat, N. D., Ningthoujam, R. S., & Pawar, S. H.** (2013) Induction heating studies of dextran coated MgFe2O4 nanoparticles for magnetic hyperthermia, *Journal of Dalton Transactions*, 1249–1258.

[98] **Bangale, S. V., Patil, D. R., & Bamane, S. R.** (2011) Preparation and electrical properties of nanocrystalline MgFe2O4 oxide by combustion route. *Archives of Applied Science Research, 3*, 506-513.

[99] **Xu, Y., Sherwood, J., Qin, Y., Hollerc, R. A., & Bao, Y.** (2015) A general approach to the synthesis and detailed characterization of magnetic ferrite nanocubes, *Journal of Royal Society of Chemistry, 7*, 12641–12649.

[100] **Hosseini, S. H. & Asadnia, A.** (2012) Synthesis, Characterization, and Microwave-Absorbing Properties of Polypyrrole/MnFe2O4 Nanocomposite , *Journal of Nanomaterials, Article ID 198973*.

[101] **Zhang, L., He, R., & Gu, H. C.,** (2006) Oleic acid coating on the monodisperse magnetic nanoparticles. *Applied Surface Science*, no. article in press, 2006.

[102] **Mahdavi, M., Ahmad, M. B., Haron, M. J., Namvar, F., Nadi, B. Rahman, M. Z., & Amin, J.** (2013) Synthesis, surface modification and characterization of biocompatimble magnetic iron oxide nanoparticles for biomedical applications, *Molecules*, 7533-7548.

[103] **Lambert, J. B**. *Introduction to organic spectroscopy*, New York: Macmillan, 1987.

APPENDICES

APPENDIX A: FTIR Results

APPENDIX B: SEM Results

APPENDIX C: VSEM Results

APPENDIX A

Table A.1: Fe_3O_4 magnetic nanoparticles and silica coated and aminated magnetic nanoparticles given codes.

Material	Condition	Code
	Core	FO-1
Fe_3O_4	Silica coated	FO-1-S
	Aminated	FO-1-S-A
	Core	FO-2
Fe_3O_4	Silica coated	FO-2-S
	Aminated	FO-2-S-A
	Core	FO-3
Fe_3O_4	Silica coated	FO-3-S
	Aminated	FO-3-S-A
	Core	FO-4
Fe_3O_4	Silica coated	FO-4-S
	Aminated	FO-4-S-A
	Core	FO-5
Fe_3O_4	Silica coated	FO-5-S
	Aminated	FO-5-S-A
	Core	FO-6
Fe_3O_4	Silica coated	FO-6-S
	Aminated	FO-6-S-A
	Core	FO-7
Fe_3O_4	Silica coated	FO-7-S
	Aminated	FO-7-S-A
	Core	FO-8
Fe_3O_4	Silica coated	FO-8-S
	Aminated	FO-8-S-A
	Core	FO-9
Fe_3O_4	Silica coated	FO-9-S
	Aminated	FO-9-S-A

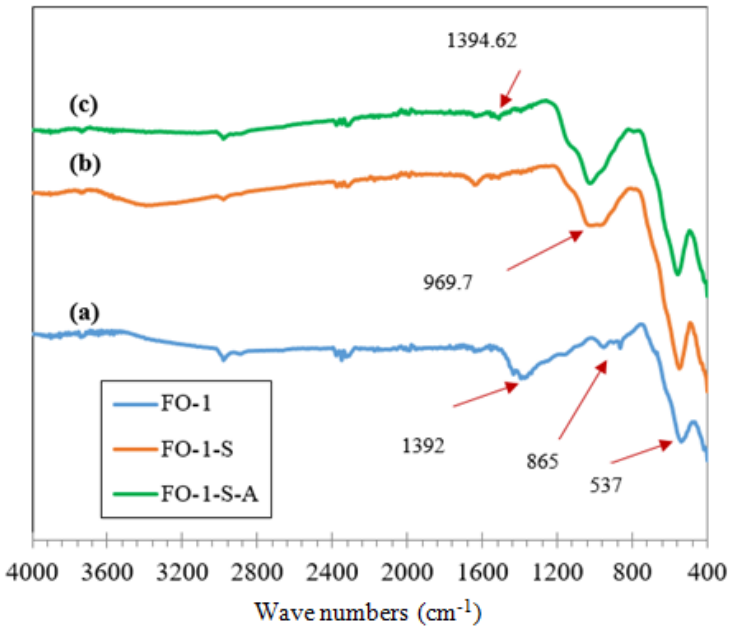

Figure A.1: FTIR analysis results of FO-1 samples (a) core, (b) silica coated, (c) aminated.

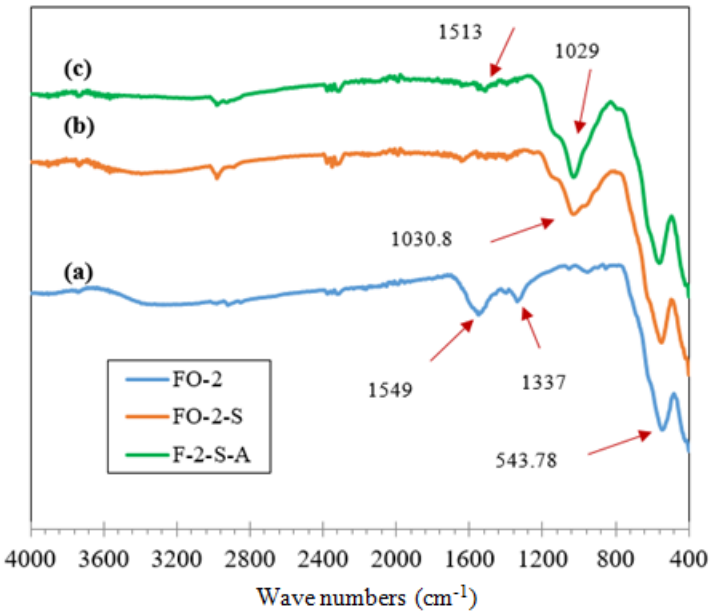

Figure A.2: FTIR analysis results of FO-2 samples (a) core, (b) silica coated, (c) aminated.

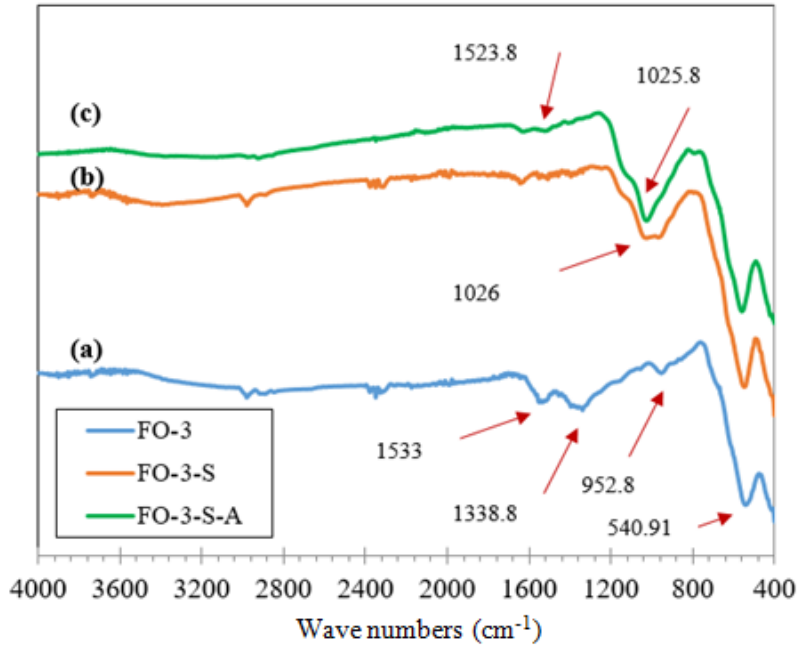

Figure A.3: FTIR analysis results of FO-3 samples (a) core, (b) silica coated, (c) aminated.

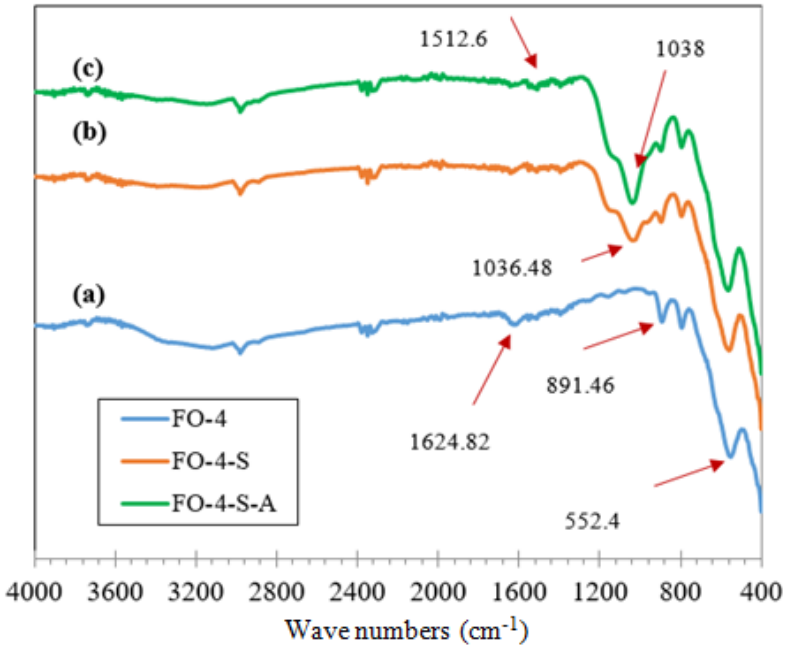

Figure A.4: FTIR analysis results of FO-4 samples (a) core, (b) silica coated, (c) aminated.

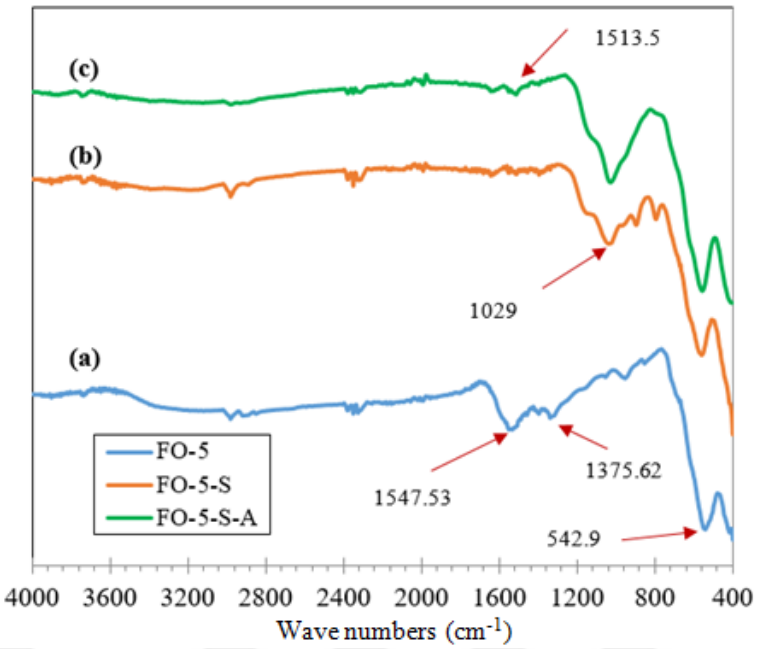

Figure A.5: FTIR analysis results of FO-5 samples (a) core, (b) silica coated, (c) aminated.

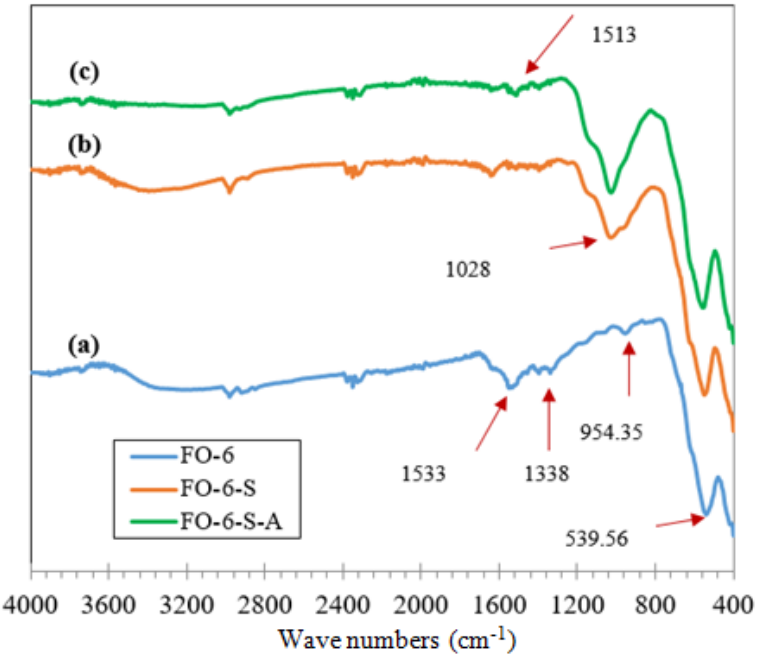

Figure A.6: FTIR analysis results of FO-6 samples (a) core, (b) silica coated, (c) aminated.

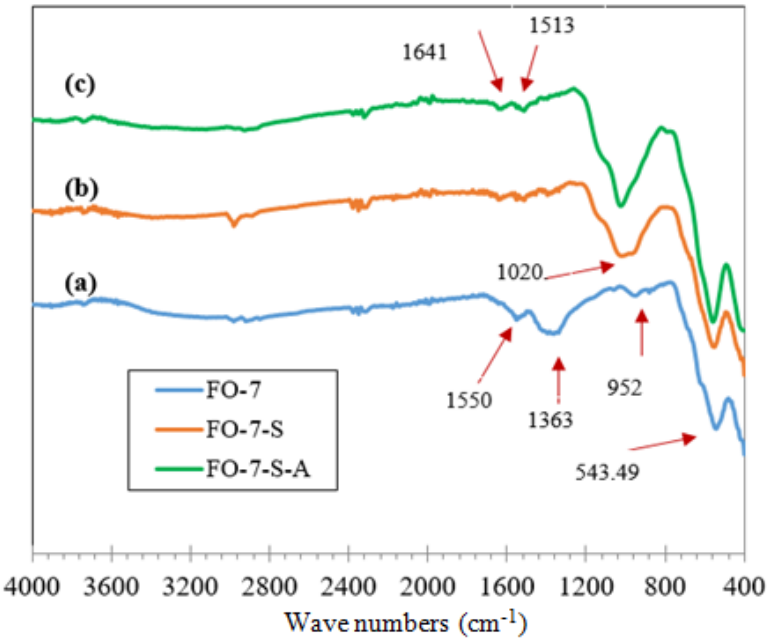

Figure A.7: FTIR analysis results of FO-7 samples (a) core, (b) silica coated, (c) aminated.

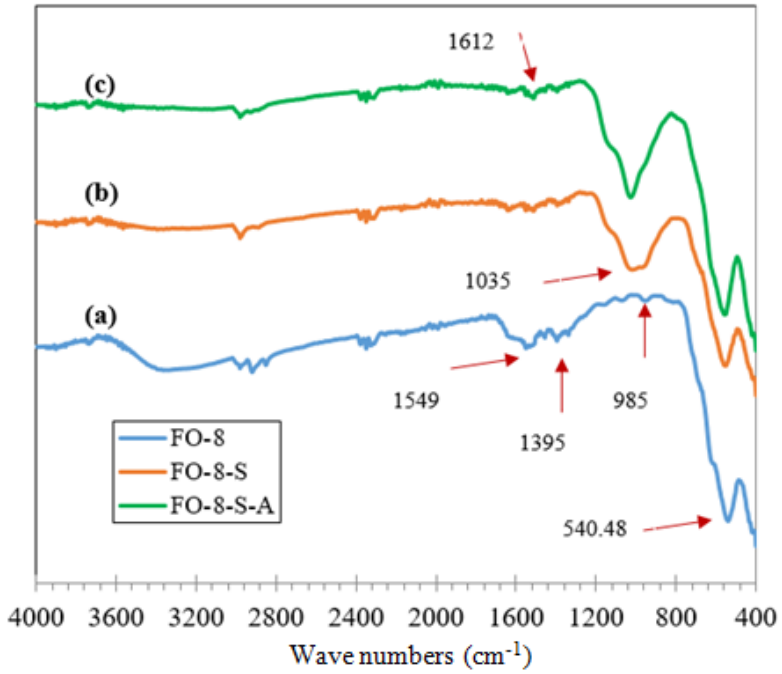

Figure A.8: FTIR analysis results of FO-8 samples (a) core, (b) silica coated, (c) aminated.

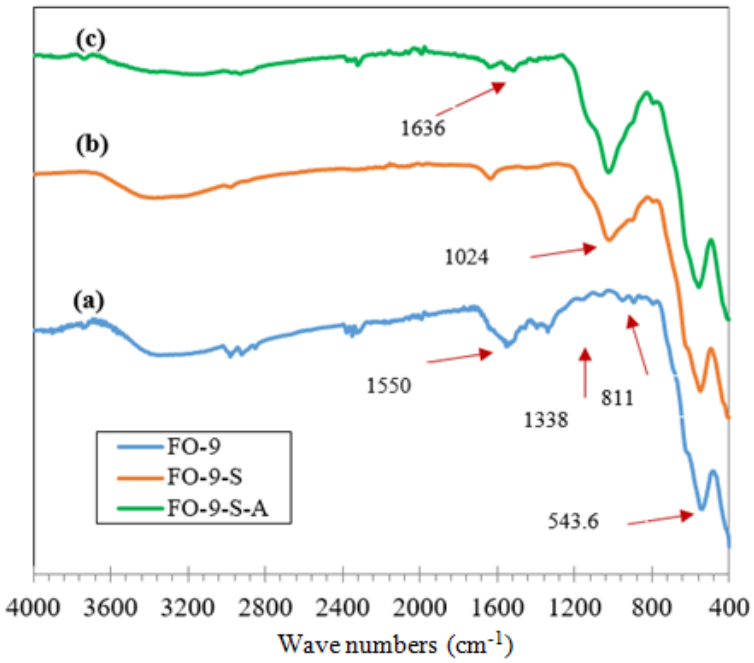

Figure A.9: FTIR analysis results of FO-9 samples (a) core, (b) silica coated, (c) aminated.

Table A.2: $SrFe_{12}O_{19}$ magnetic nanoparticles and silica coated and aminated magnetic nanoparticles given codes.

Material	Condition	Code
SrFe12O19	Core	SF-1
	Silica coated	SF-2-S
	Aminated	SF-2-S-A
SrFe12O20	Core	SF-2
	Silica coated	SF-2-S
	Aminated	SF-2-S-A
SrFe12O21	Core	SF-3
	Silica coated	SF-3-S
	Aminated	SF-3-S-A
SrFe12O22	Core	SF-4
	Silica coated	SF-4-S
	Aminated	SF-4-S-A
SrFe12O23	Core	SF-5
	Silica coated	SF-5-S
	Aminated	SF-5-S-A
SrFe12O24	Core	SF-6
	Silica coated	SF-6-S
	Aminated	SF-6-S-A

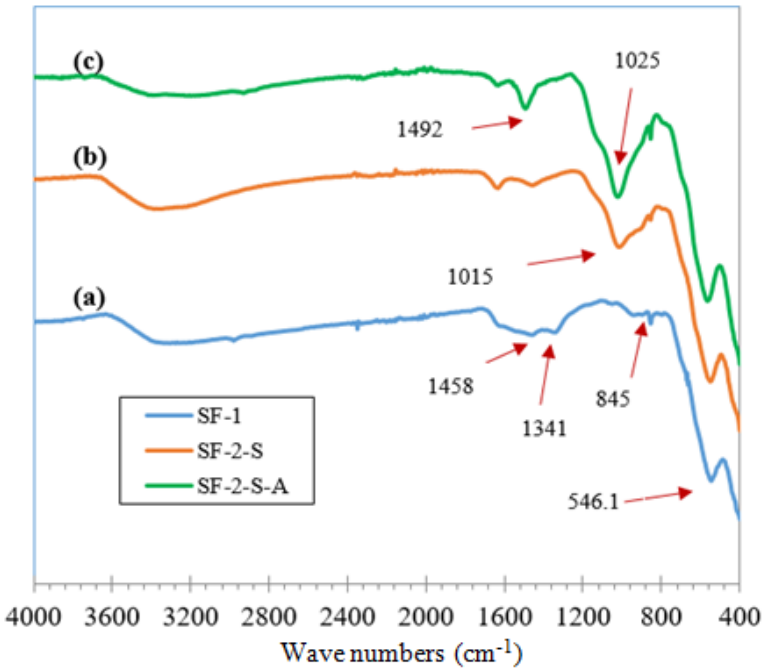

Figure A.10: FTIR analysis results of SF-1 samples (a) core, (b) silica coated, (c) aminated.

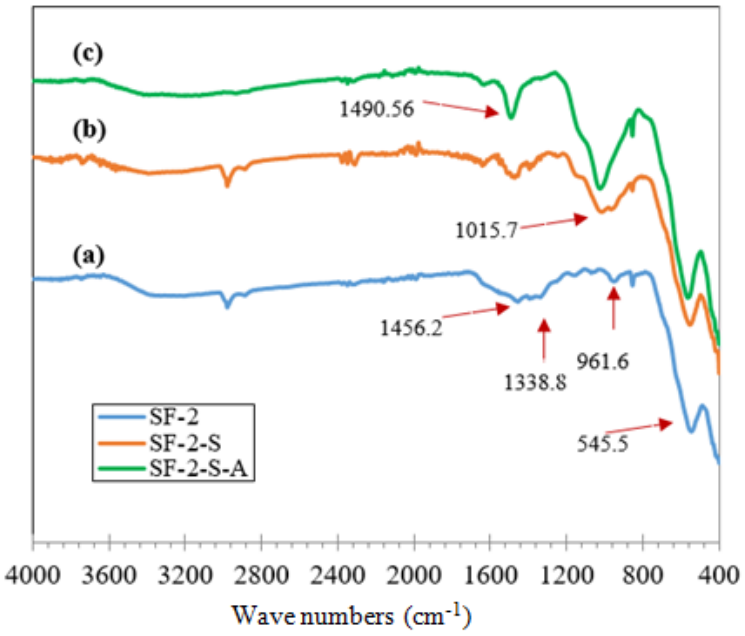

Figure A.11: FTIR analysis results of SF-2 samples (a) core, (b) silica coated, (c) aminated.

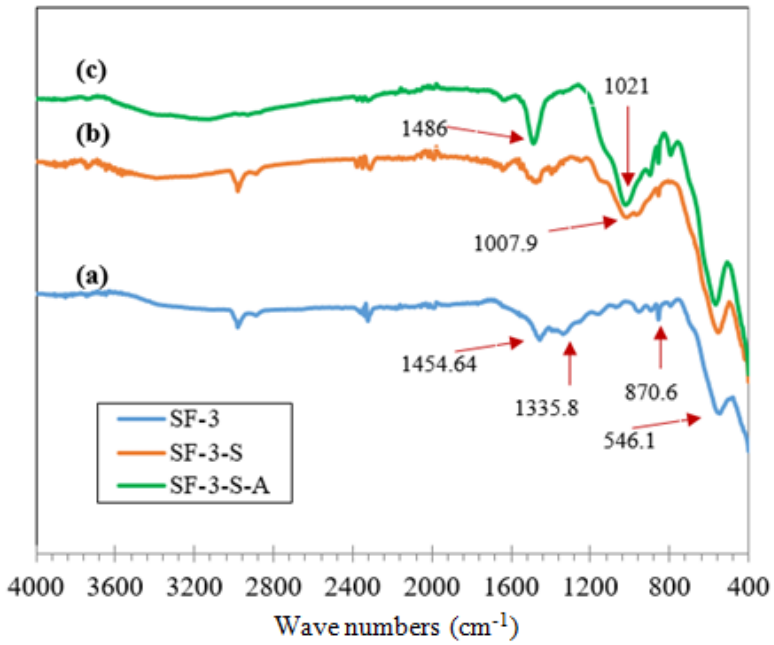

Figure A.12: FTIR analysis results of SF-3 samples (a) core, (b) silica coated, (c) aminated.

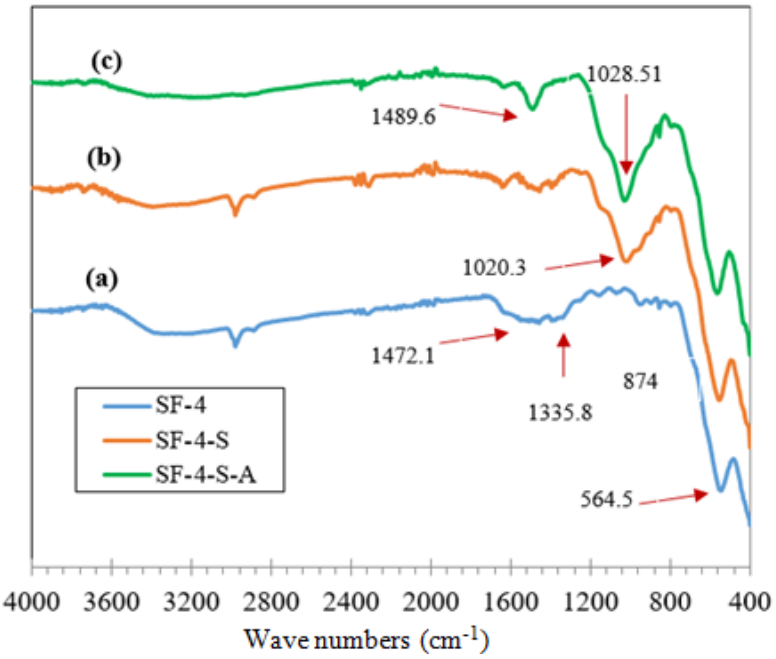

Figure A.13: FTIR analysis results of SF-4 samples (a) core, (b) silica coated, (c) aminated.

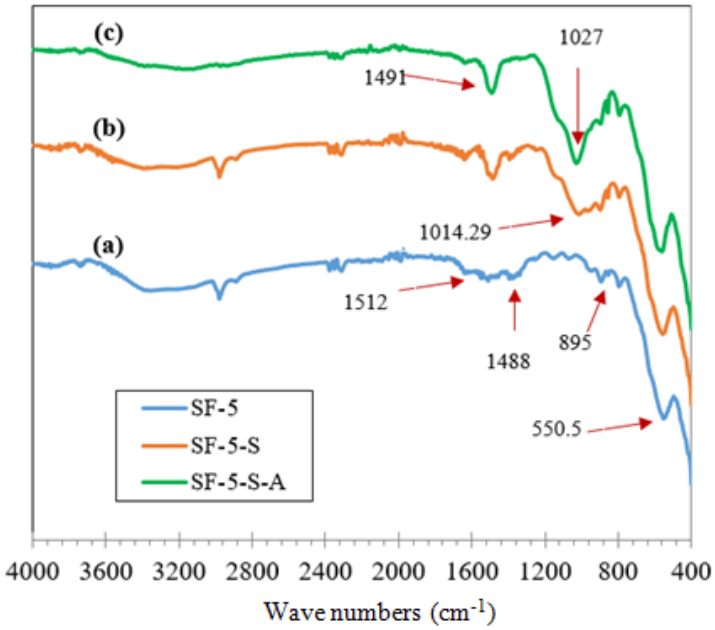

Figure A.14: FTIR analysis results of SF-5 samples (a) core, (b) silica coated, (c) aminated.

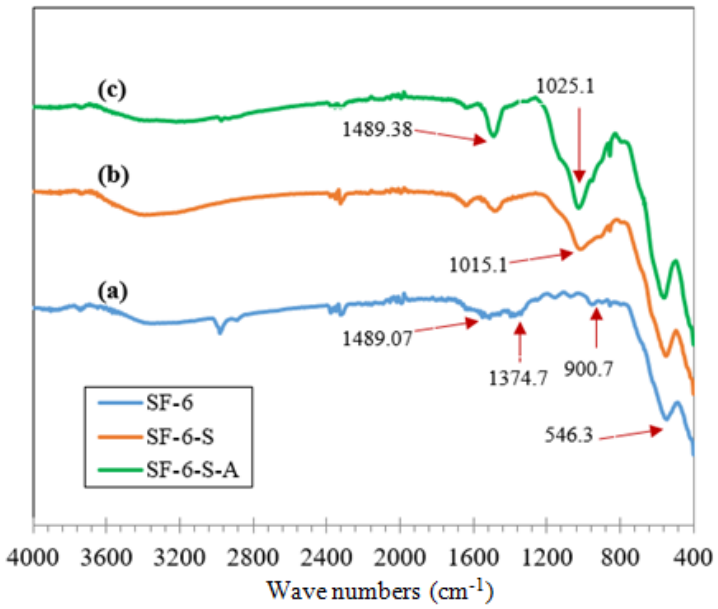

Figure A. 15: FTIR analysis results of SF-6 samples (a) core, (b) silica coated, (c) aminated.

Table A.3: $BaFe_{12}O_{19}$ magnetic nanoparticles and silica coated and aminated magnetic nanoparticles given codes.

Material	Condition	Code
$BaFe_{12}O_{19}$	Core	BF-1
	Silica coated	BF-1-S
	Aminated	BF-1-S-A
$BaFe_{12}O_{19}$	Core	BF-2
	Silica coated	BF-2-S
	Aminated	BF-2-S-A
$BaFe_{12}O_{19}$	Core	BF-3
	Silica coated	BF-3-S
	Aminated	BF-3-S-A
$BaFe_{12}O_{19}$	Core	BF-4
	Silica coated	BF-4-S
	Aminated	BF-4-S-A
$BaFe_{12}O_{19}$	Core	BF-5
	Silica coated	BF-5-S
	Aminated	BF-5-S-A
$BaFe_{12}O_{19}$	Core	BF-6
	Silica coated	BF-6-S
	Aminated	BF-6-S-A
$BaFe_{12}O_{19}$	Core	BF-7
	Silica coated	BF-7-S
	Aminated	BF-7-S-A
$BaFe_{12}O_{19}$	Core	BF-8
	Silica coated	BF-8-S
	Aminated	BF-8-S-A
$BaFe_{12}O_{19}$	Core	BF-9
	Silica coated	BF-9-S
	Aminated	BF-9-S-A

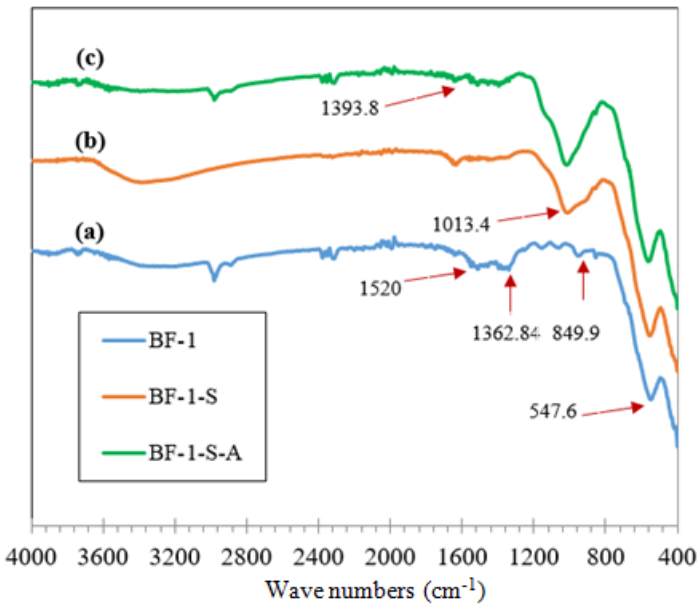

Figure A.16: FTIR analysis results of BF-1 samples (a) core, (b) silica coated, (c) aminated.

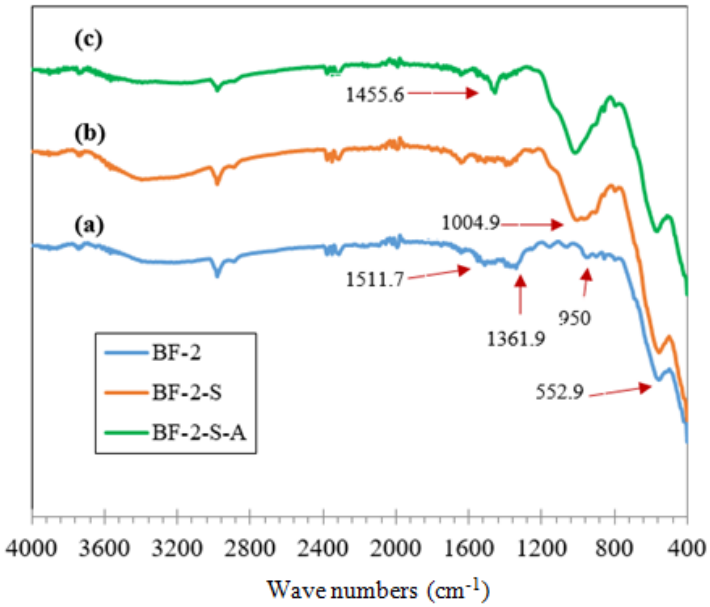

Figure A.17: FTIR analysis results of BF-2 samples (a) core, (b) silica coated, (c) aminated.

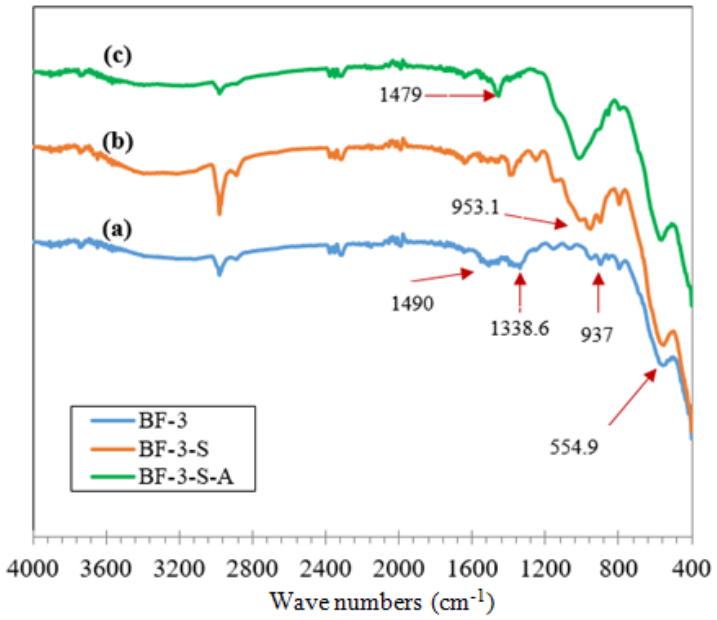

Figure A.18: FTIR analysis results of BF-3 samples (a) core, (b) silica coated, (c) aminated.

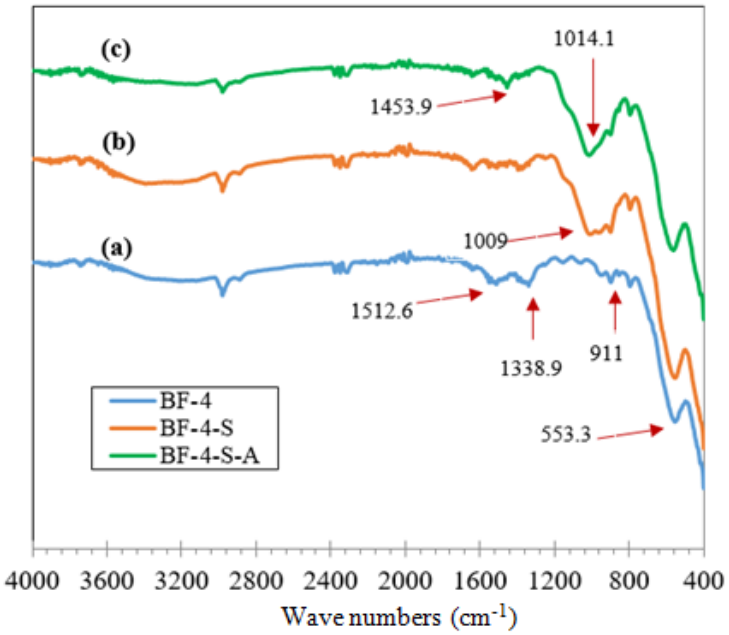

Figure A.19: FTIR analysis results of BF-4 samples (a) core, (b) silica coated, (c) aminated.

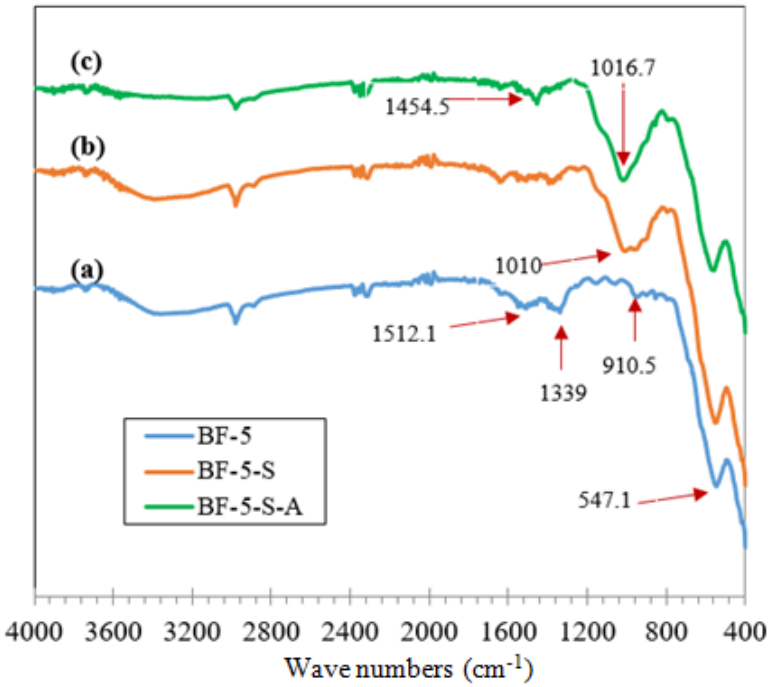

Figure A.20: FTIR analysis results of BF-5 samples (a) core, (b) silica coated, (c) aminated.

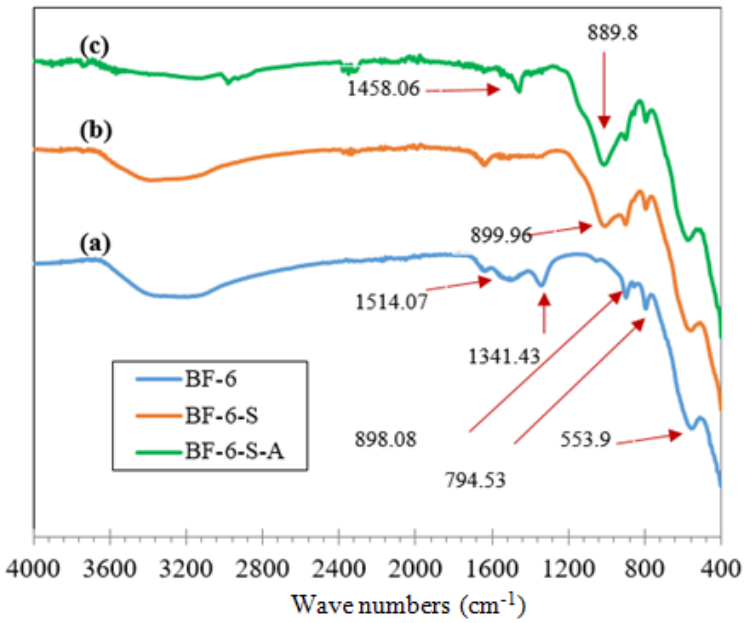

Figure A.21:FTIR analysis results of BF-6 samples (a) core, (b) silica coated, (c) aminated.

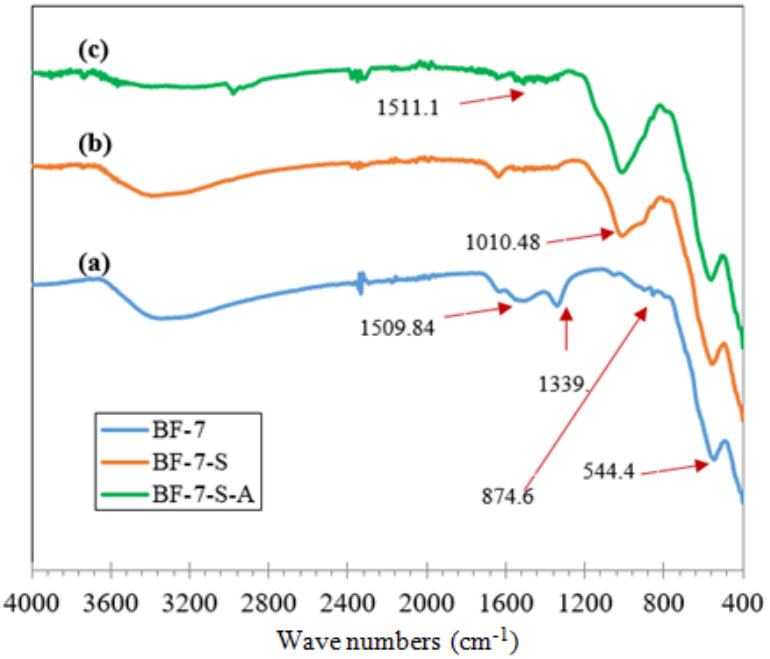

Figure A.22: FTIR analysis results of BF-7 samples (a) core, (b) silica coated, (c) aminated.

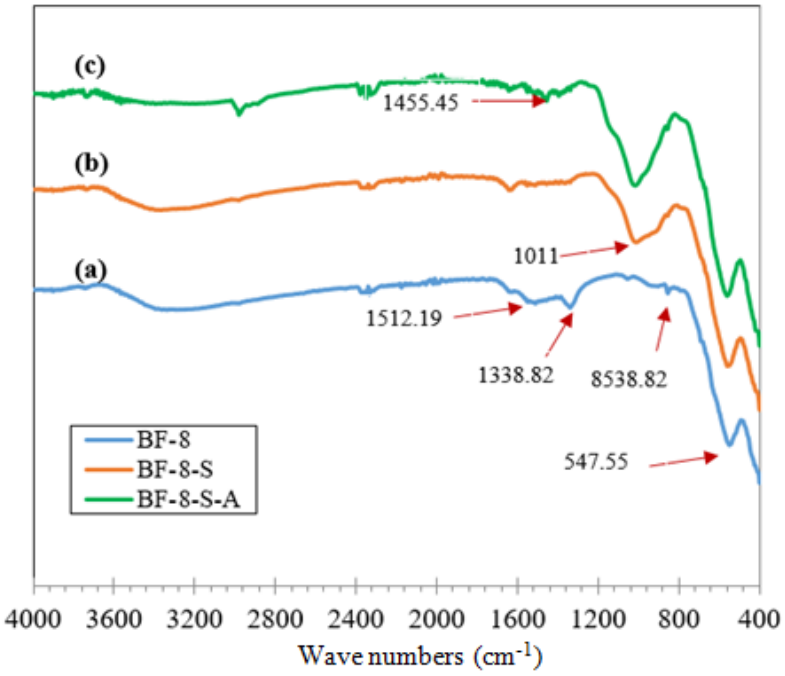

Figure A.23: FTIR analysis results of BF-8 samples (a) core, (b) silica coated, (c) aminated.

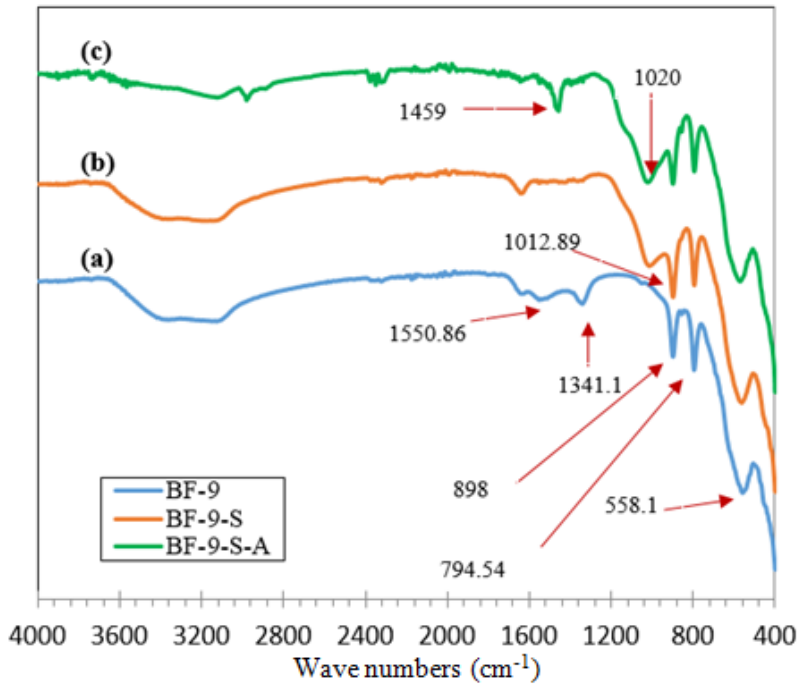

Figure A.24: FTIR analysis results of BF-9 samples (a) core, (b) silica coated, (c) aminated.

Table A.4: $MgFe_2O_4$ magnetic nanoparticles and silica coated and aminated magnetic nanoparticles given codes.

Material	Condition	Code
	Core	MgF-1
$MgFe_2O_4$	Silica coated	MgF-1-S
	Aminated	MgF-1-S-A
	Core	MgF-2
$MgFe_2O_4$	Silica coated	MgF-2-S
	Aminated	MgF-2-S-A
	Core	MgF-3
$MgFe_2O_4$	Silica coated	MgF-3-S
	Aminated	MgF-3-S-A
	Core	MgF-4
$MgFe_2O_4$	Silica coated	MgF-4-S
	Aminated	MgF-4-S-A
	Core	MgF-5
$MgFe_2O_4$	Silica coated	MgF-5-S
	Aminated	MgF-5-S-A
	Core	MgF-6
$MgFe_2O_4$	Silica coated	MgF-6-S
	Aminated	MgF-6-S-A

Table A.4 (continued): $MgFe_2O_4$ magnetic nanoparticles and silica coated and aminated magnetic nanoparticles given codes.

Material	Condition	Code
	Core	MgF-7
$MgFe_2O_4$	Silica coated	MgF-7-S
	Aminated	MgF-7-S-A
	Core	MgF-8
$MgFe_2O_4$	Silica coated	MgF-8-S
	Aminated	MgF-8-S-A
	Core	MgF-9
MgFe2O4	Silica coated	MgF-9-S
	Aminated	MgF-9-S-A
	Core	MgF-10
$MgFe_2O_4$	Silica coated	MgF-10-S
	Aminated	MgF-10-S-A
	Core	MgF-11
$MgFe_2O_4$	Silica coated	MgF-11-S
	Aminated	MgF-11-S-A
	Core	MgF-12
$MgFe_2O_4$	Silica coated	MgF-12-S
	Aminated	MgF-12-S-A

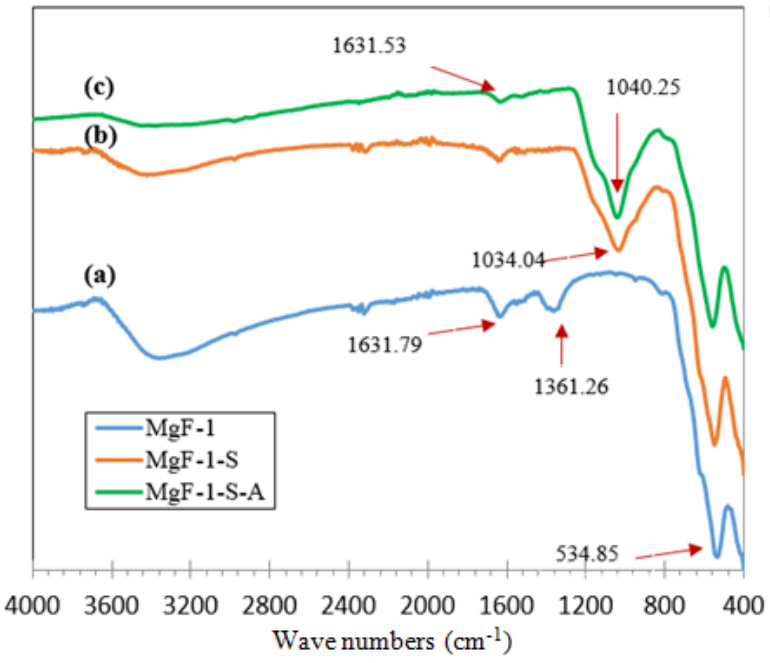

Figure A.25: FTIR analysis results of MgF-1 samples (a) core, (b) silica coated, (c) aminated.

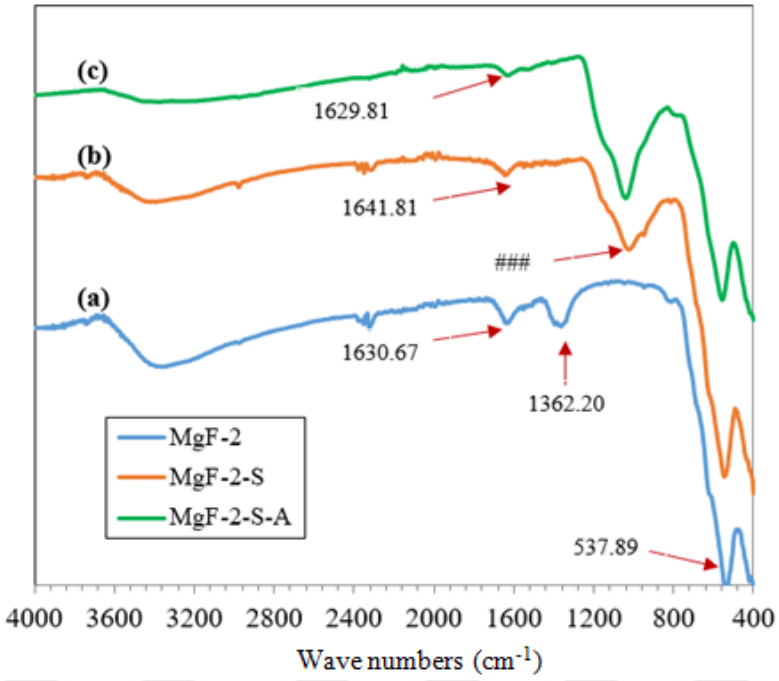

Figure A.26: FTIR analysis results of MgF-2 samples (a) core, (b) silica coated, (c) aminated.

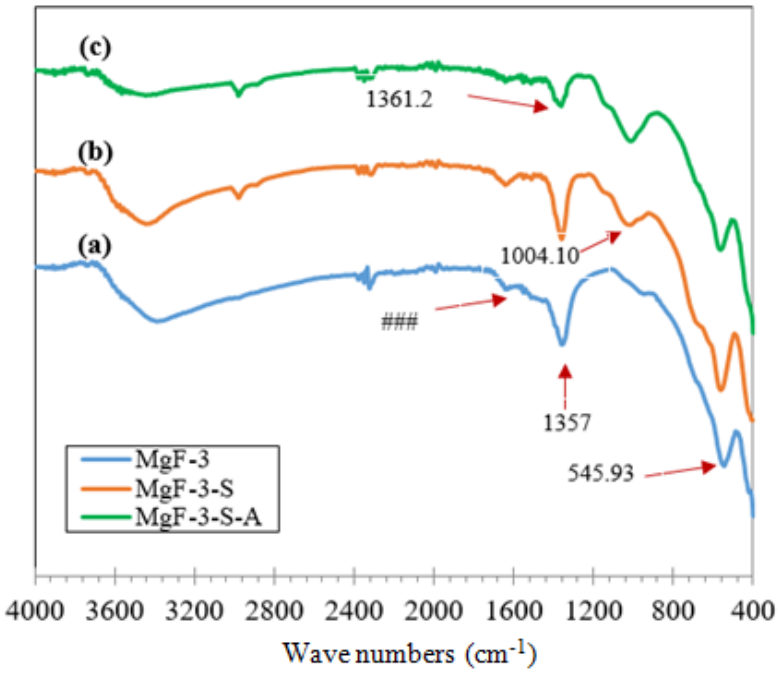

Figure A.27: FTIR analysis results of MgF-3 samples (a) core, (b) silica coated, (c) aminated.

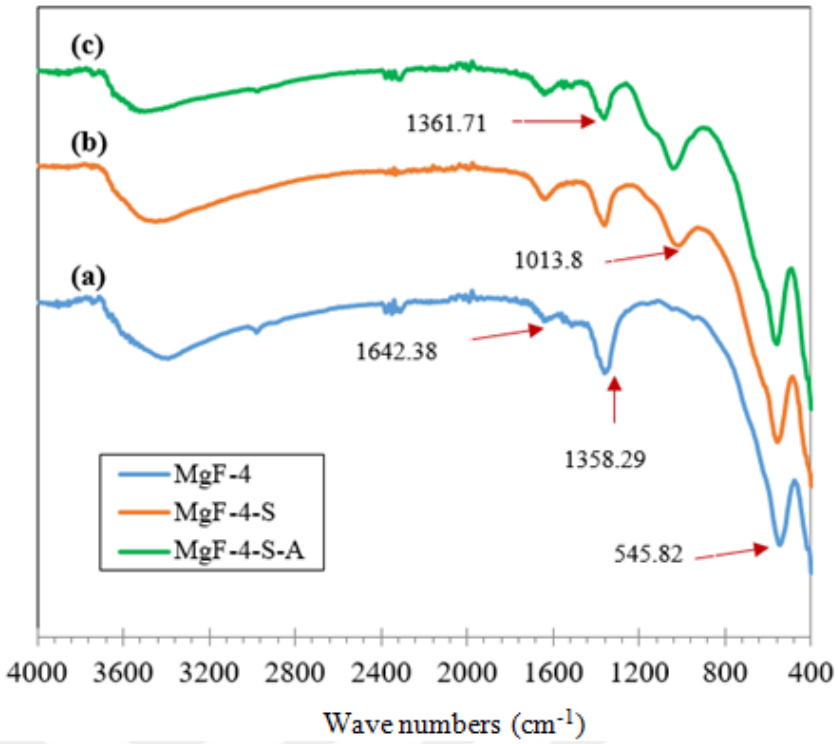

Figure A.28: FTIR analysis results of MgF-4 samples (a) core, (b) silica coated, (c) aminated.

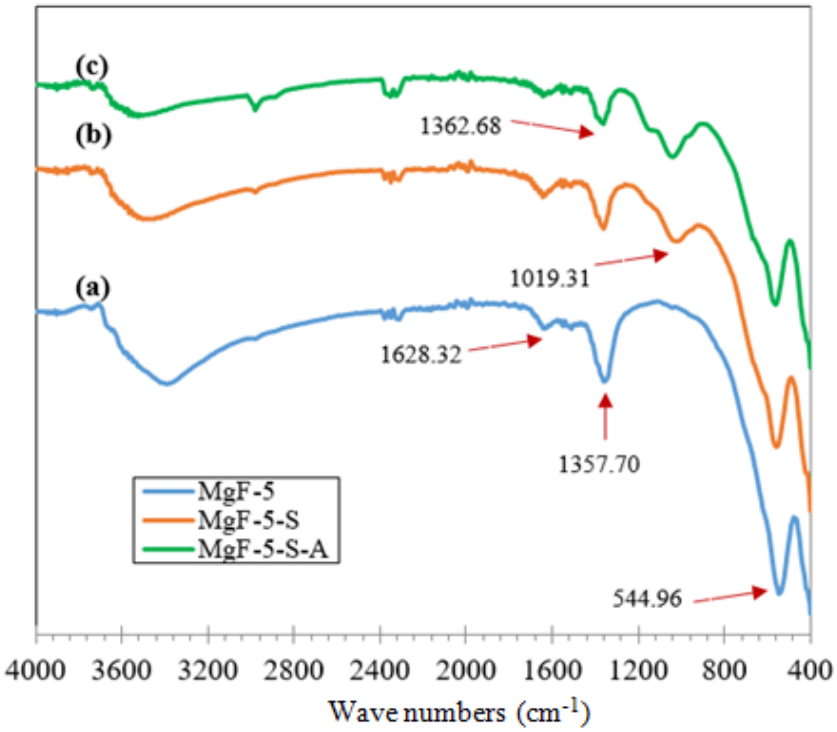

Figure A.29: FTIR analysis results of MgF-5 samples (a) core, (b) silica coated, (c) aminated.

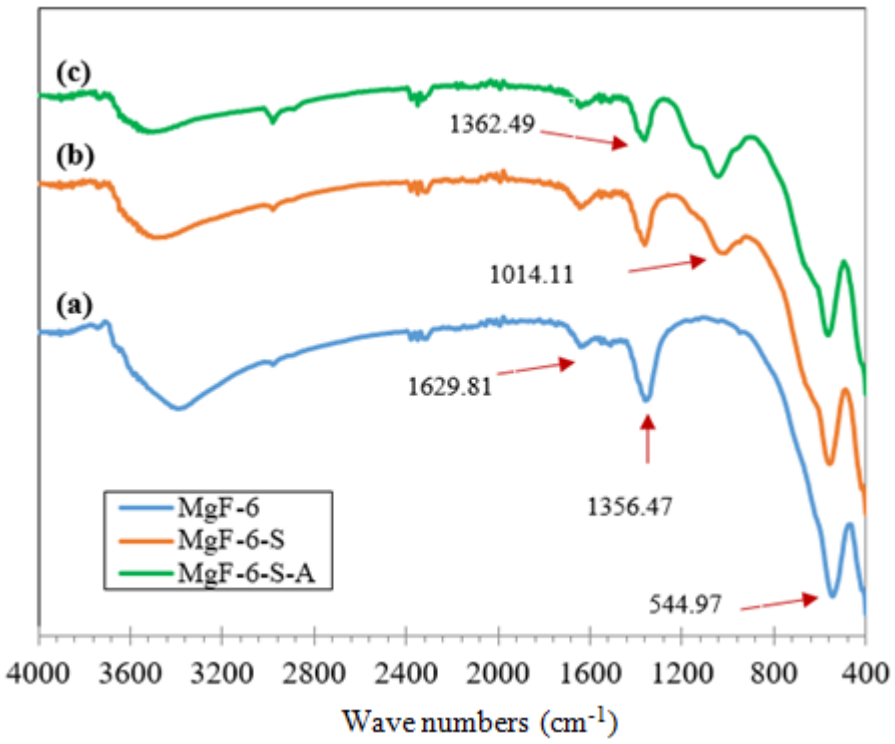

Figure A.30: FTIR analysis results of MgF-6 samples (a) core, (b) silica coated, (c) aminated.

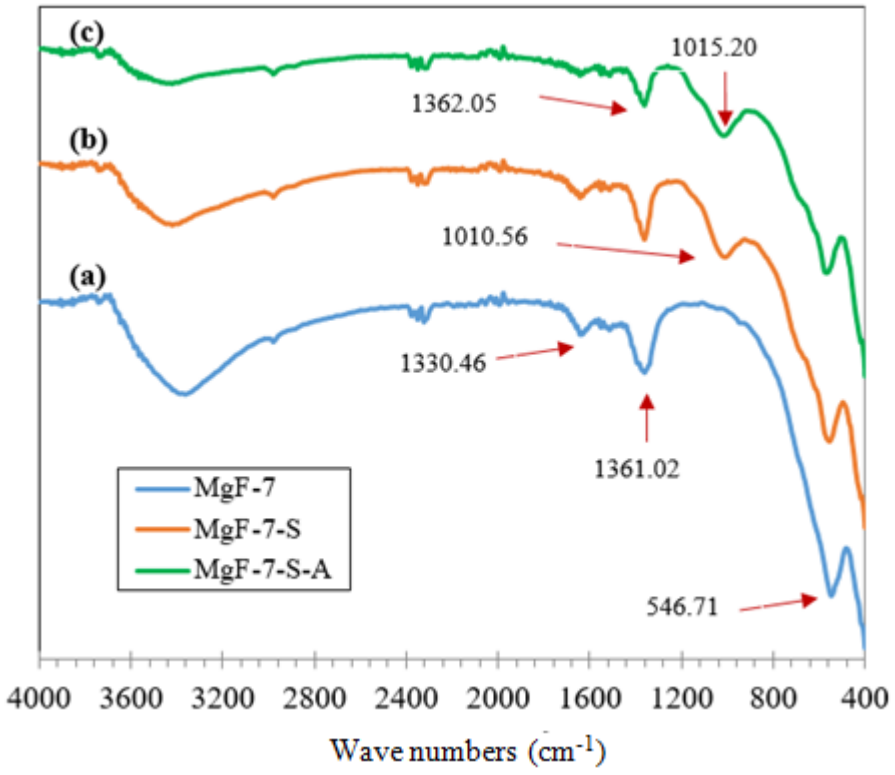

Figure A.31: FTIR analysis results of MgF-7 samples (a) core, (b) silica coated, (c) aminated.

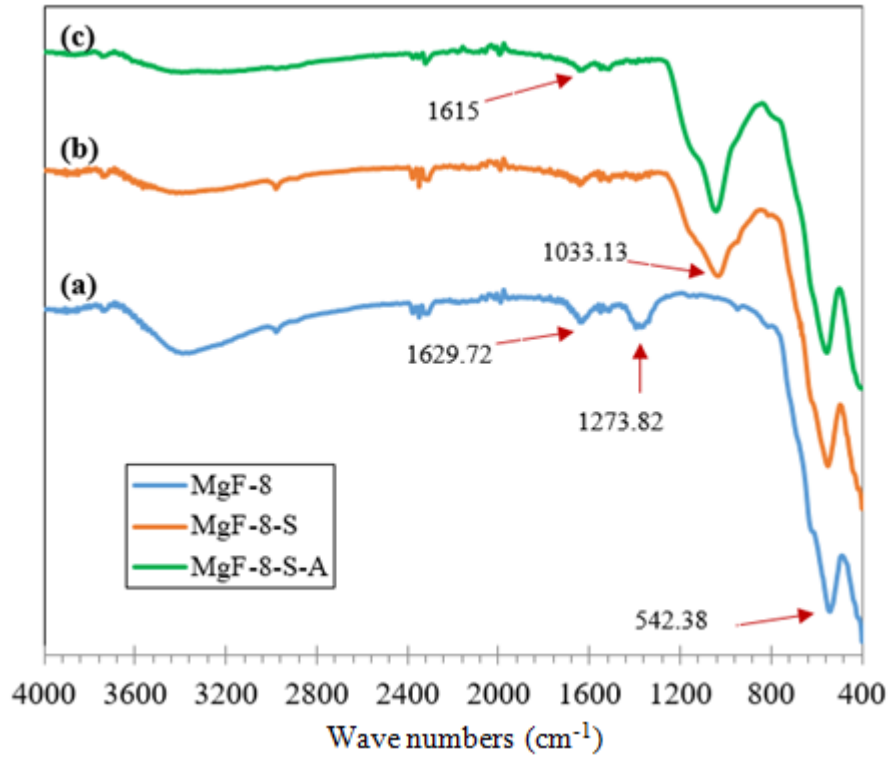

Figure A.32: FTIR analysis results of MgF-8 samples (a) core, (b) silica coated, (c) aminated.

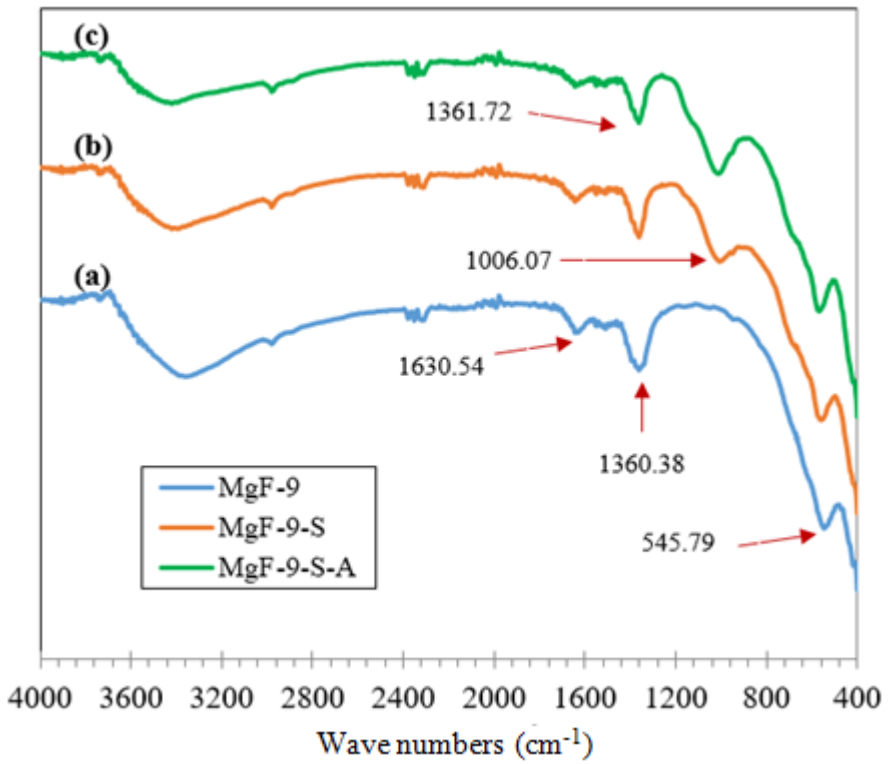

Figure A.33: FTIR analysis results of MgF-9 samples (a) core, (b) silica coated, (c) aminated.

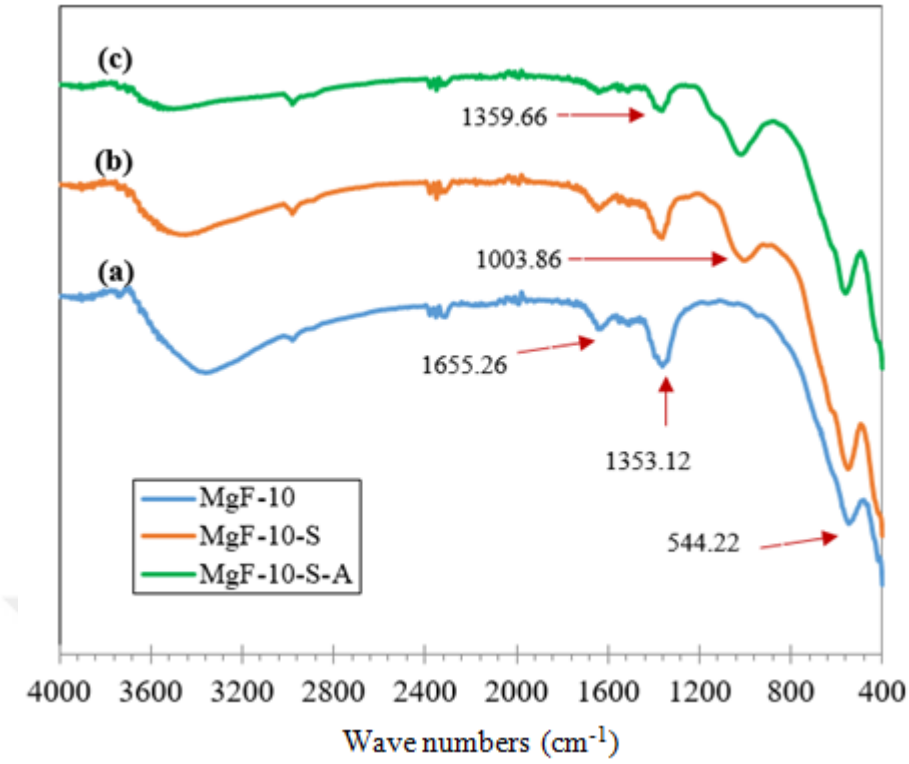

Figure A.34: FTIR analysis results of MgF-10 samples (a) core, (b) silica coated, (c) aminated.

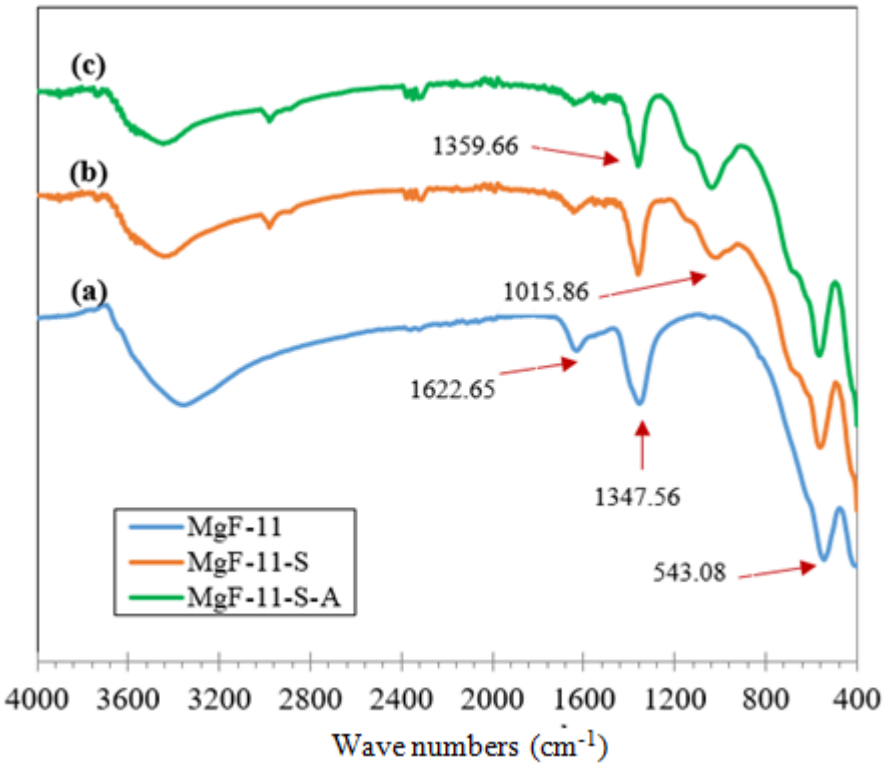

Figure A.35: FTIR analysis results of MgF-11 samples (a) core, (b) silica coated, (c) aminated.

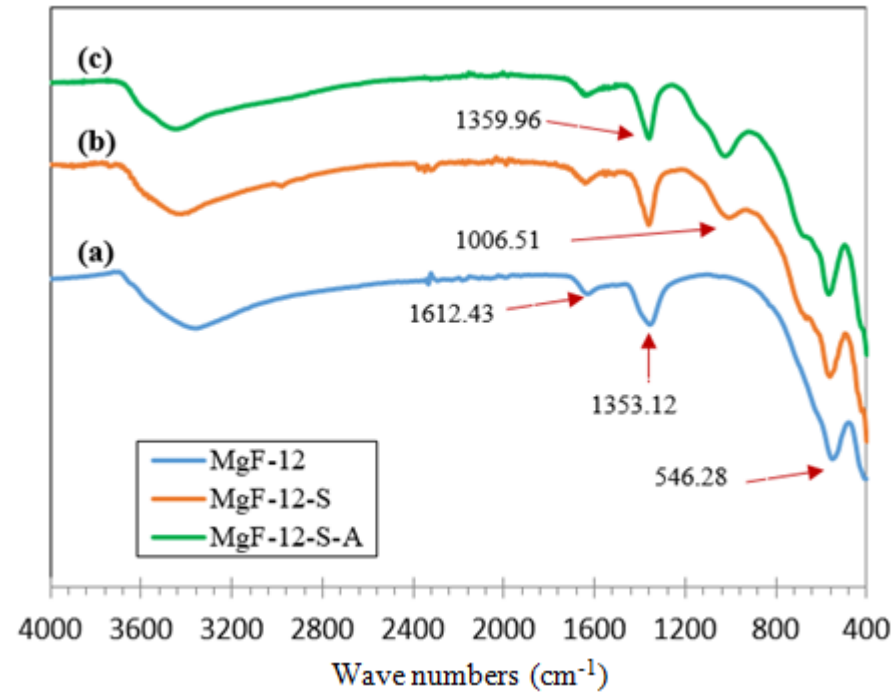

Figure A.36: FTIR analysis results of MgF-12 samples (a) core, (b) silica coated, (c) aminated.

Table A.5: $MnFe_2O_4$ magnetic nanoparticles and silica coated and aminated magnetic nanoparticles given codes.

Material	Condition	Code
$MnFe_2O_4$	Core	MnF-1
	Silica coated	MnF-1-S
	Aminated	MnF-1-S-A
$MnFe_2O_4$	Core	MnF-2
	Silica coated	MnF-2-S
	Aminated	MnF-2-S-A
$MnFe_2O_4$	Core	MnF-3
	Silica coated	MnF-3-S
	Aminated	MnF-3-S-A
$MnFe_2O_4$	Core	MnF-4
	Silica coated	MnF-4-S
	Aminated	MnF-4-S-A

Table A.5 (continued): MnFe2O4 magnetic nanoparticles and silica coated and aminated magnetic nanoparticles given codes.

Material	Condition	Code
$MnFe_2O_4$	Core	MnF-5
	Silica coated	MnF-5-S
	Aminated	MnF-5-S-A
$MnFe_2O_4$	Core	MnF-6
	Silica coated	MnF-6-S
	Aminated	MnF-6-S-A
$MnFe_2O_4$	Core	MnF-7
	Silica coated	MnF-7-S
	Aminated	MnF-7-S-A
$MnFe_2O_4$	Core	MnF-8
	Silica coated	MnF-8-S
	Aminated	MnF-8-S-A

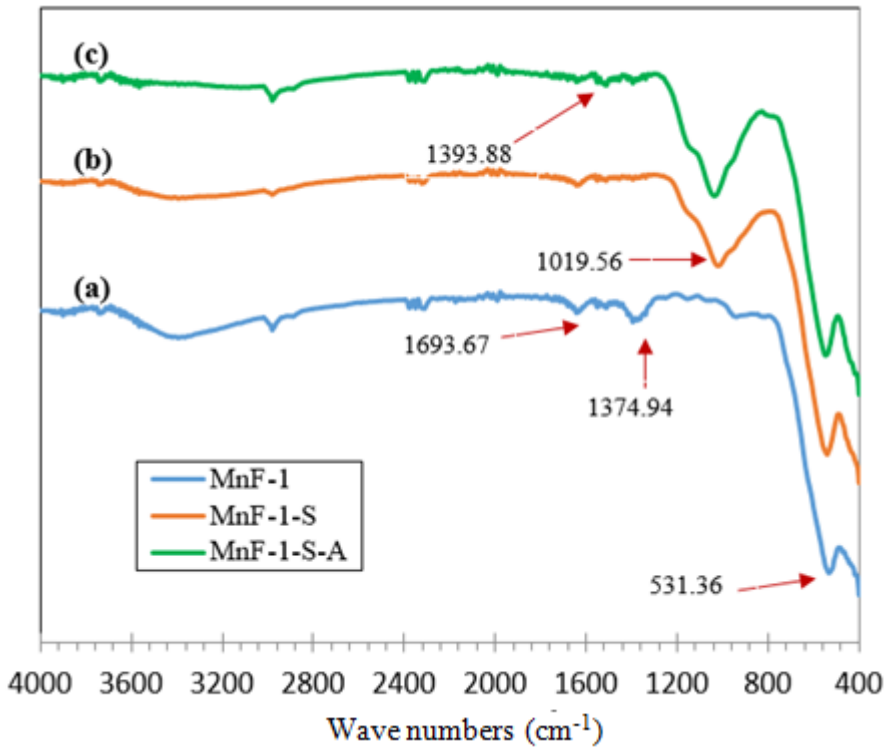

Figure A.37: FTIR analysis results of MnF-1 samples (a) core, (b) silica coated, (c) aminated.

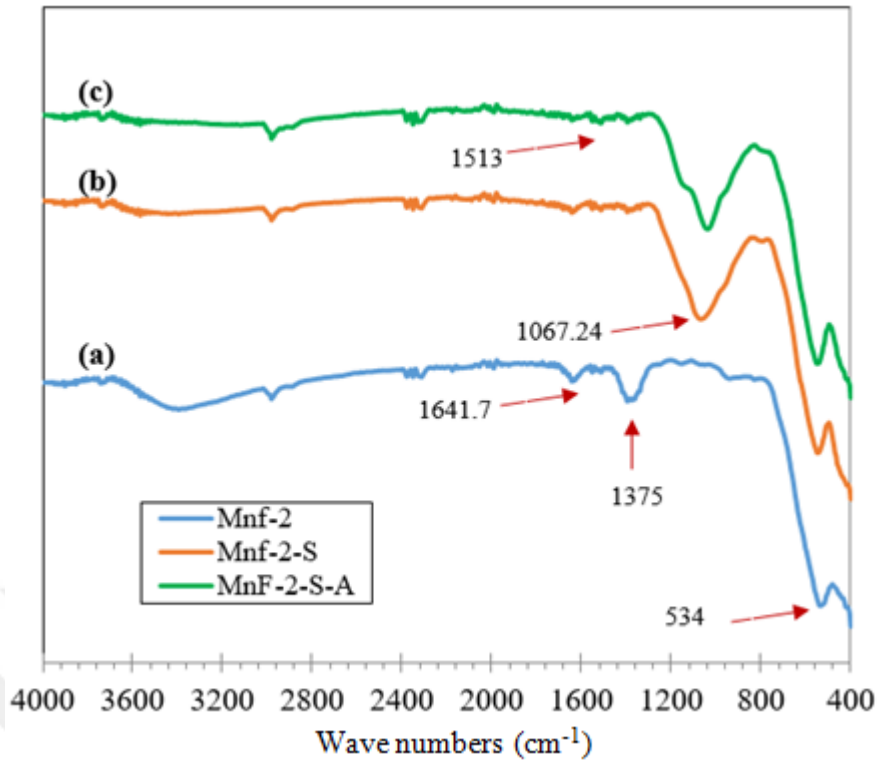

Figure A.38: FTIR analysis results of MnF-2 samples (a) core, (b) silica coated, (c) aminated.

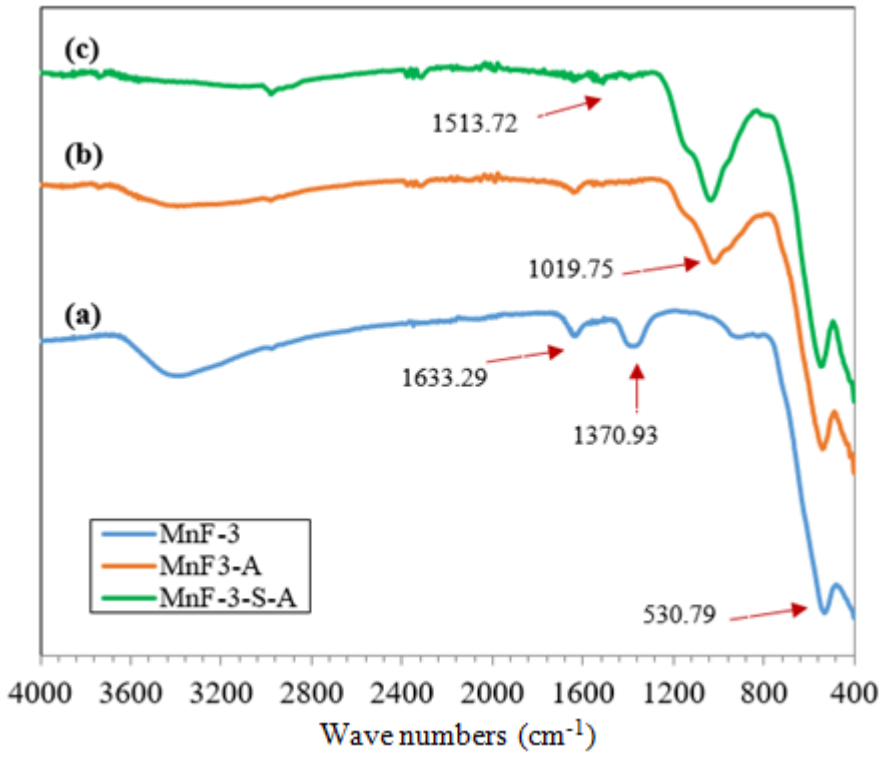

Figure A.39: FTIR analysis results of MnF-3 samples (a) core, (b) silica coated, (c) aminated.

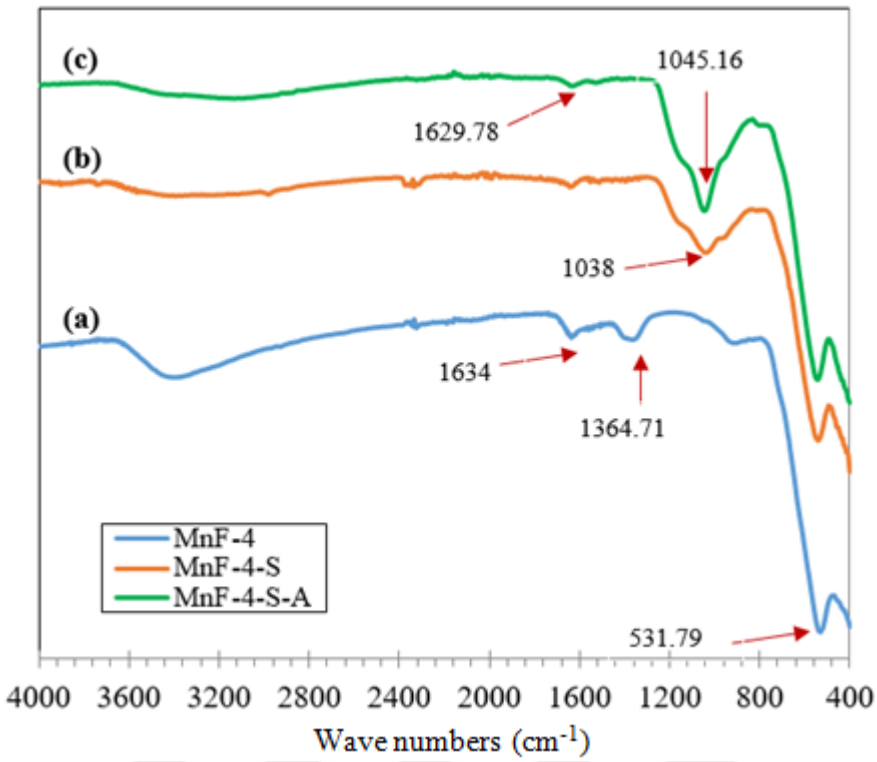

Figure A.40: FTIR analysis results of MnF-4 samples (a) core, (b) silica coated, (c) aminated.

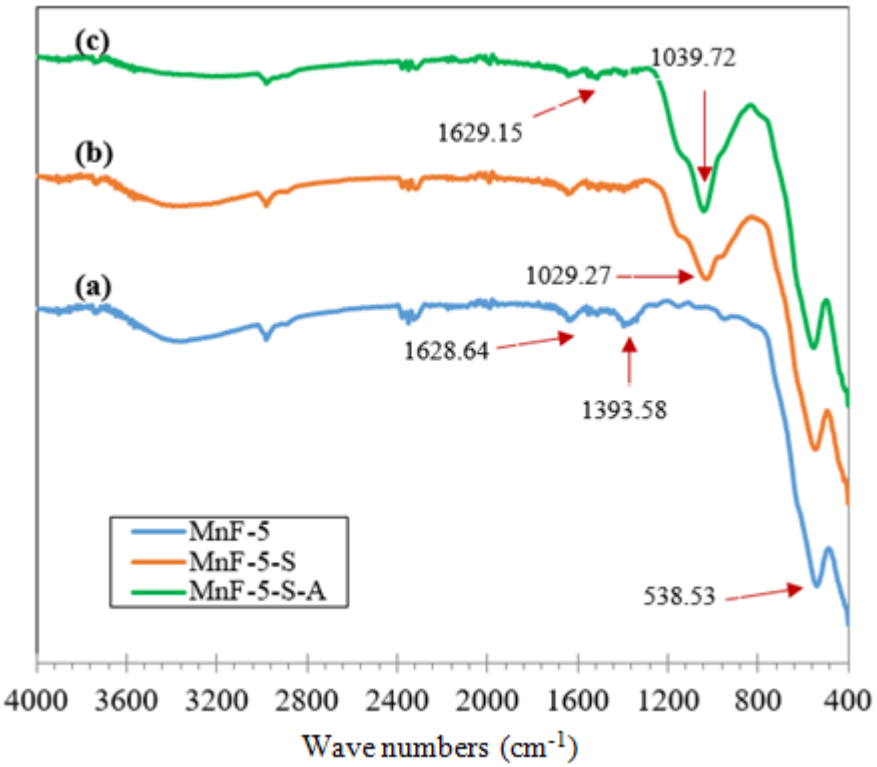

Figure A.41: FTIR analysis results of MnF-2 samples (a) core, (b) silica coated, (c) aminated.

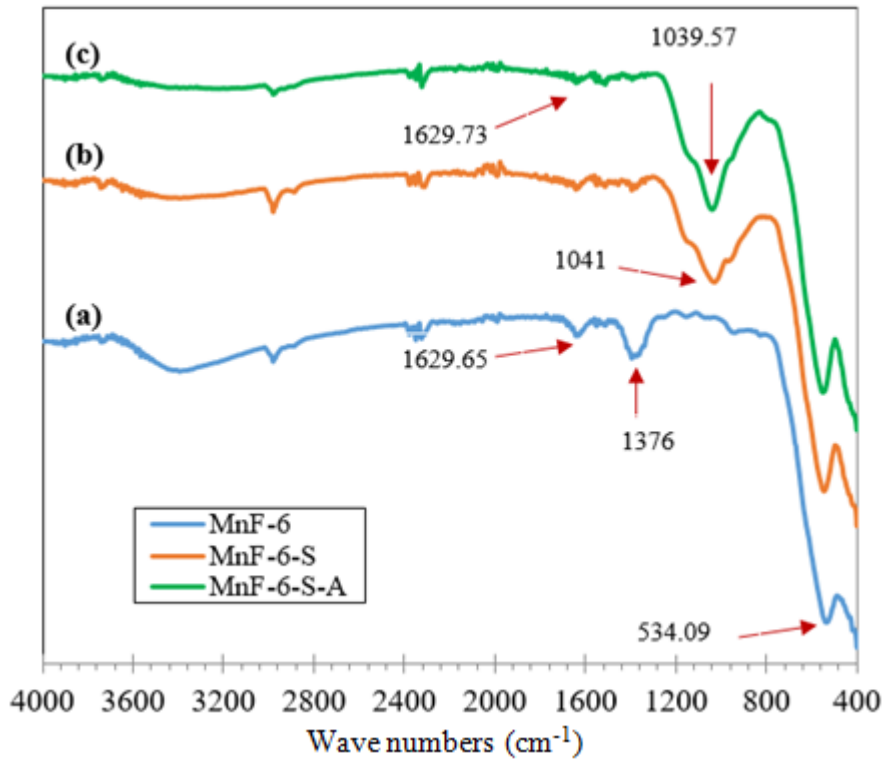

Figure A.42: FTIR analysis results of MnF-2 samples (a) core, (b) silica coated, (c) aminated.

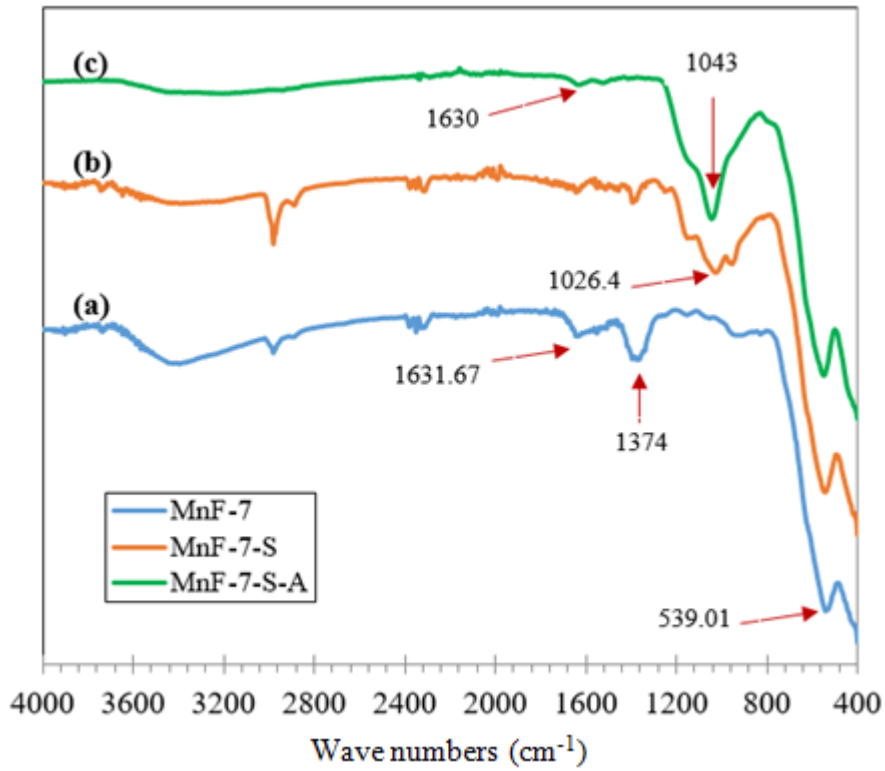

Figure A.43: FTIR analysis results of MnF-7 samples (a) core, (b) silica coated, (c) aminated.

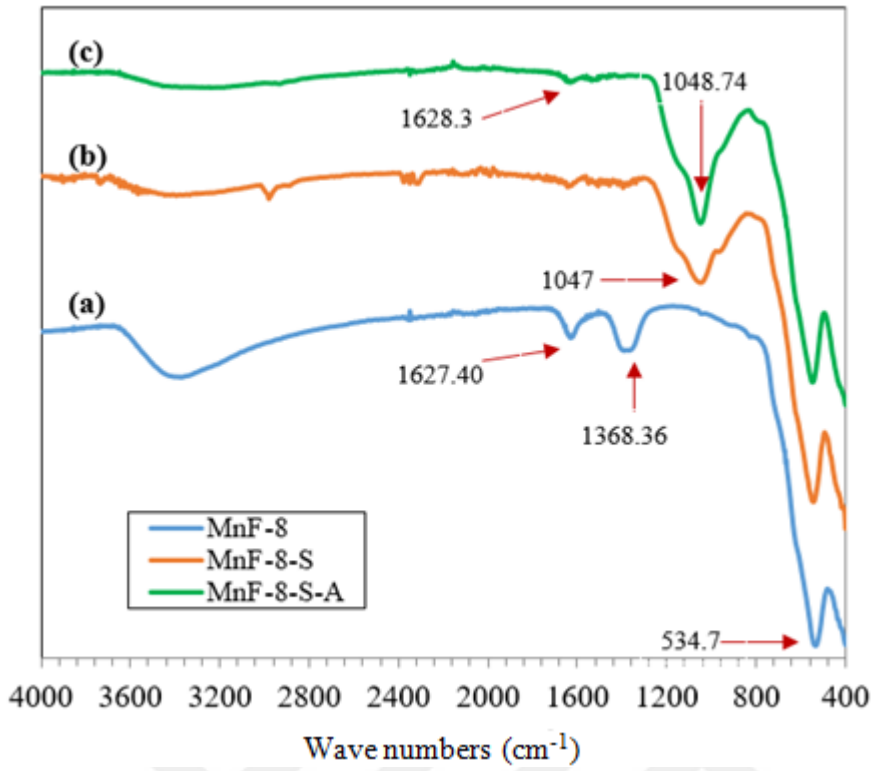

Figure A.44: FTIR analysis results of MnF-8 samples (a) core, (b) silica coated, (c) aminated.

APPENDIX B

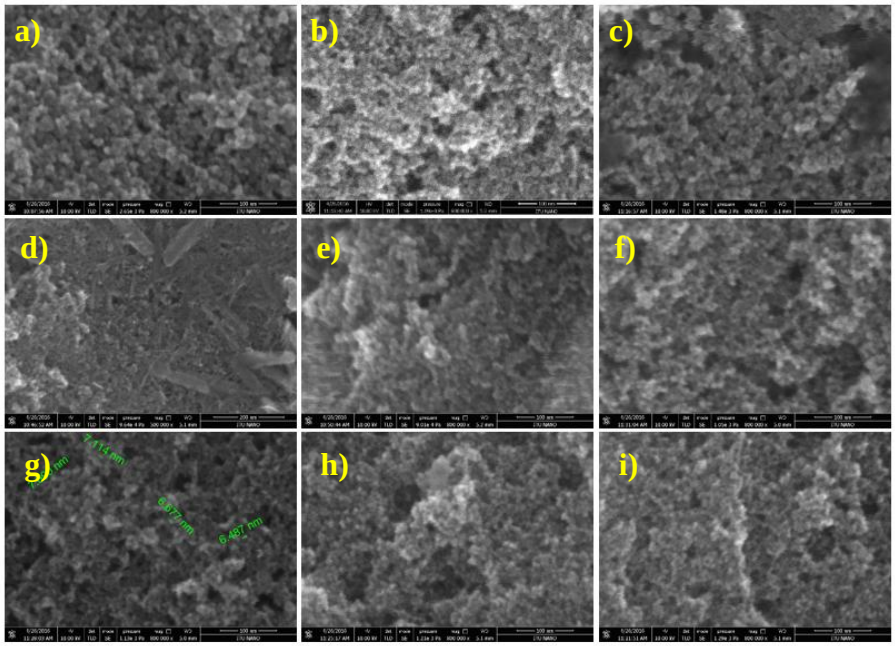

Figure B.1: SEM photographs (a) FO-1, (b) FO-2, (c) FO-3, (d) FO-4, (e) FO-5, (f) FO-6, (g) FO-7, (h) FO-8, (i) FO-9.

Table B.1: Fe_3O_4 Nanoparticles core sized measured in SEM equipment.

Material	Condition	Code	Sythesising NP/Water concentration(mol/L)	Synthesising PH	Diameter(nm)
Fe_3O_4	Core	FO-1	9.64	13	13
Fe_3O_4	Core	FO-2	5.78	13	11
Fe_3O_4	Core	FO-3	3.85	13	
Fe_3O_4	Core	FO-4	9.64	10	8
Fe_3O_4	Core	FO-5	5.78	12	8
Fe_3O_4	Core	FO-6	3.85	12	9
Fe_3O_4	Core	FO-7	9.64	12	7
Fe_3O_4	Core	FO-8	5.78	10	9
Fe_3O_4	Core	FO-9	3.85	12	8

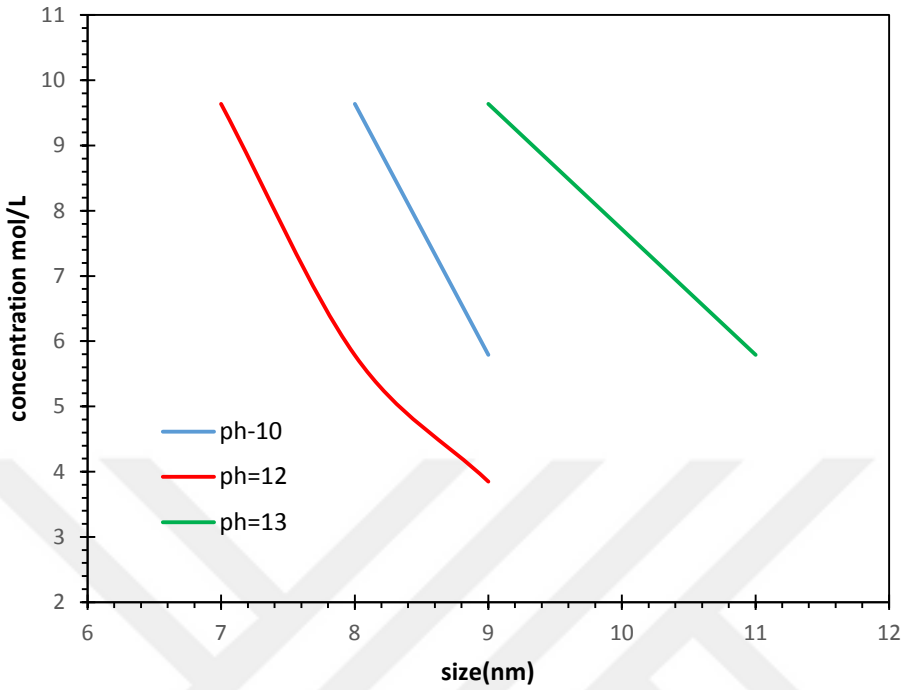

Figure B.2: Fe_3O_4 Nanoparticles core sized measured in SEM equipment.

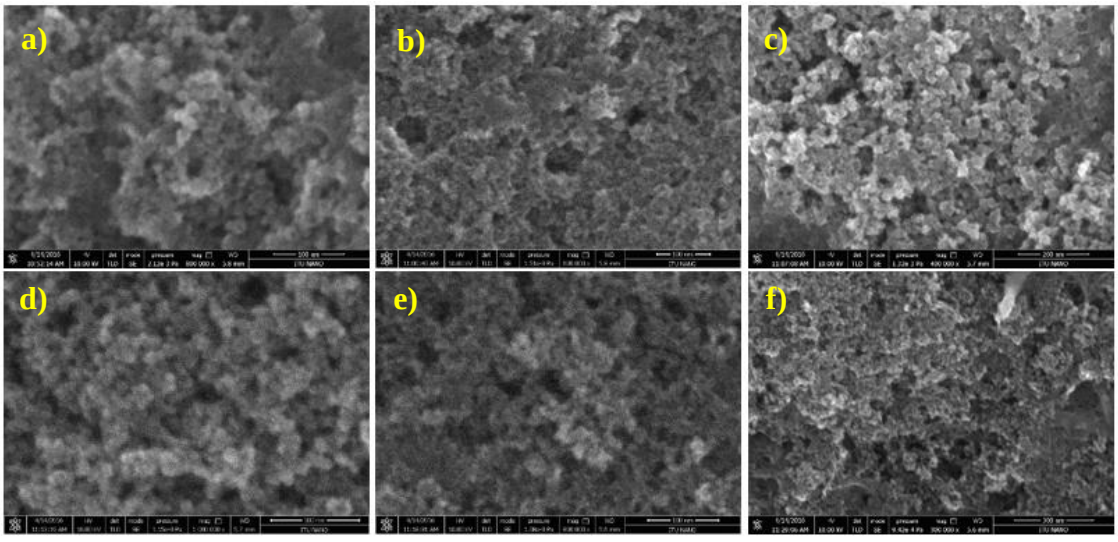

Figure B.3: SEM photographs (a) SF-1, (b) SF-2, (c) SF-3, (d) SF-4, (e) SF-5, (f) SF-6.

Table B.2: $SrFe_{12}O_{19}$ Nanoparticles core sized measured in SEM equipment.

Material	Condition	Code	Sythesising NP/Water concentration(mol/L)	Synthesize PH	Diamater(nm)
$SrFe_{12}O_{19}$	Core	SF-1	26.54	13	12
$SrFe_{12}O_{19}$	Core	SF-2	26.54	14	12
$SrFe_{12}O_{19}$	Core	SF-3	17.7	14	20
$SrFe_{12}O_{19}$	Core	SF-4	17.7	13	13
$SrFe_{12}O_{19}$	Core	SF-5	26.54	12	15
$SrFe_{12}O_{19}$	Core	SF-6	17.7	12	17

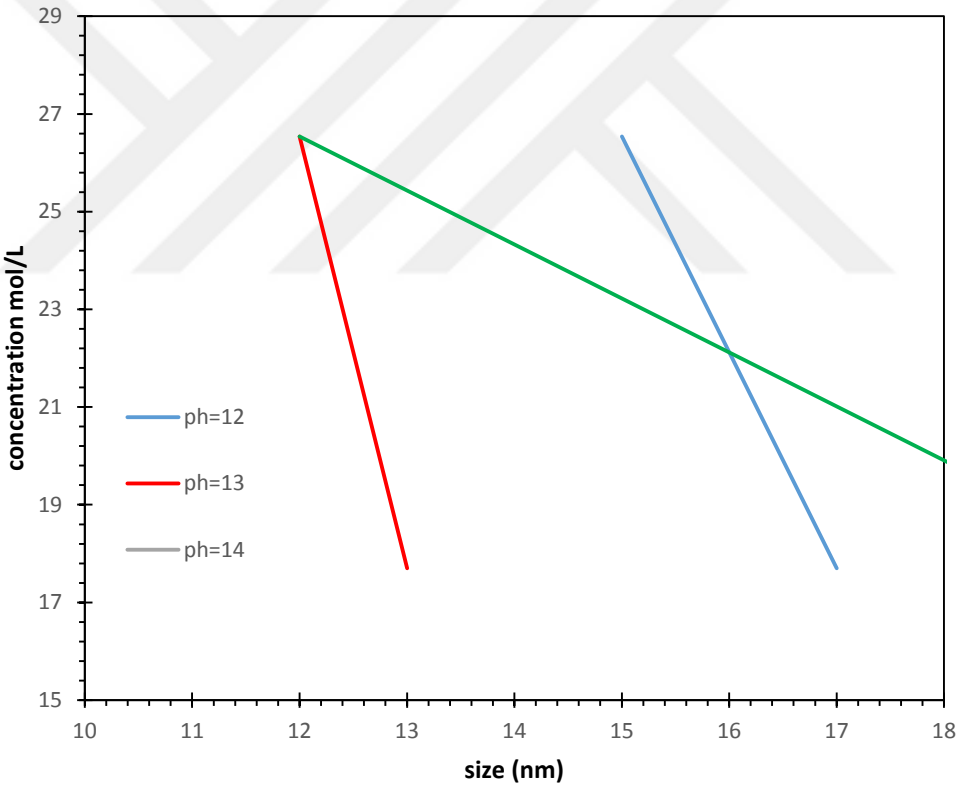

Figure B.4: $SrFe_{12}O_{19}$ Nanoparticles core sized measured in SEM equipment.

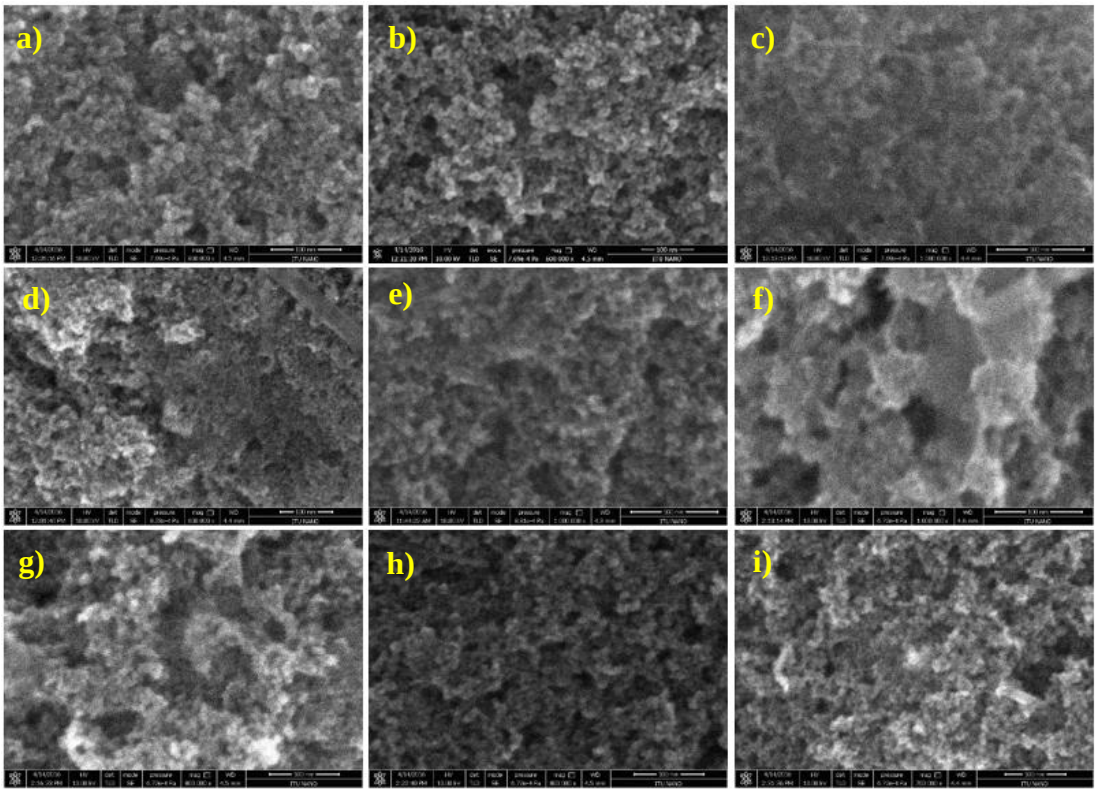

Figure B.5: SEM photographs (a) BF-1, (b) BF-2, (c) BF-3, (d) BF-4, (e) BF-5, (f) BF-6, (g) BF-7, (h) BF-8, (i) BF-9

Table B.3: $BaFe_{12}O_{19}$ Nanoparticles core sized measured in SEM equipment.

Material	Condition	Code	Sythesising NP/Water concentration(mol/L)	Synthesising PH	Diameter (nm)
$BaFe_{12}O_{19}$	Core	BF-1	27.78	13	12
$BaFe_{12}O_{19}$	Core	BF-2	27.78	14	12
$BaFe_{12}O_{19}$	Core	BF-3	18.52	13	11
$BaFe_{12}O_{19}$	Core	BF-4	18.52	14	10
$BaFe_{12}O_{19}$	Core	BF-5	18.52	12	11
$BaFe_{12}O_{19}$	Core	BF-6	46.31	13	10
$BaFe_{12}O_{19}$	Core	BF-7	27.78	11	13
$BaFe_{12}O_{19}$	Core	BF-8	18.52	13	11
$BaFe_{12}O_{19}$	Core	BF-9	46.31	13	10

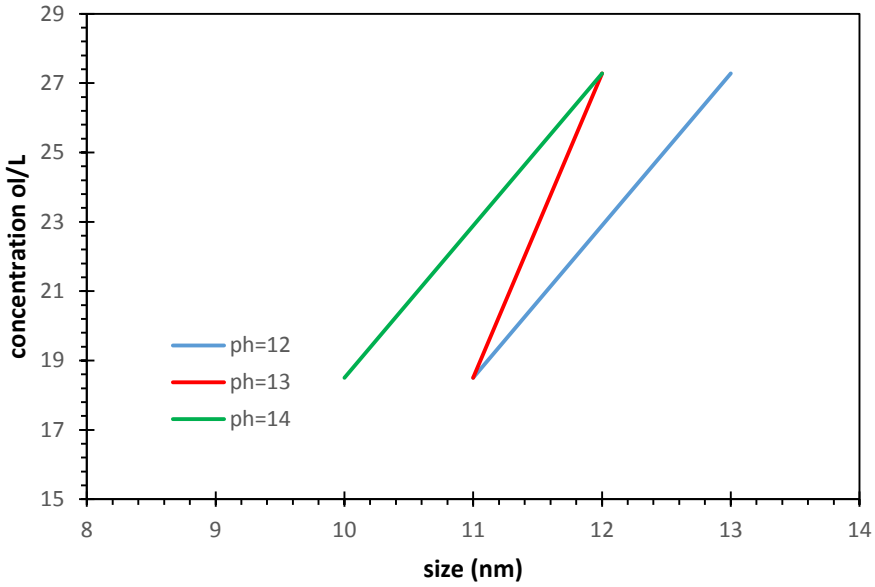

Figure B.6: $BaFe_{12}O_{19}$ Nanoparticles core sized measured in SEM equipment.

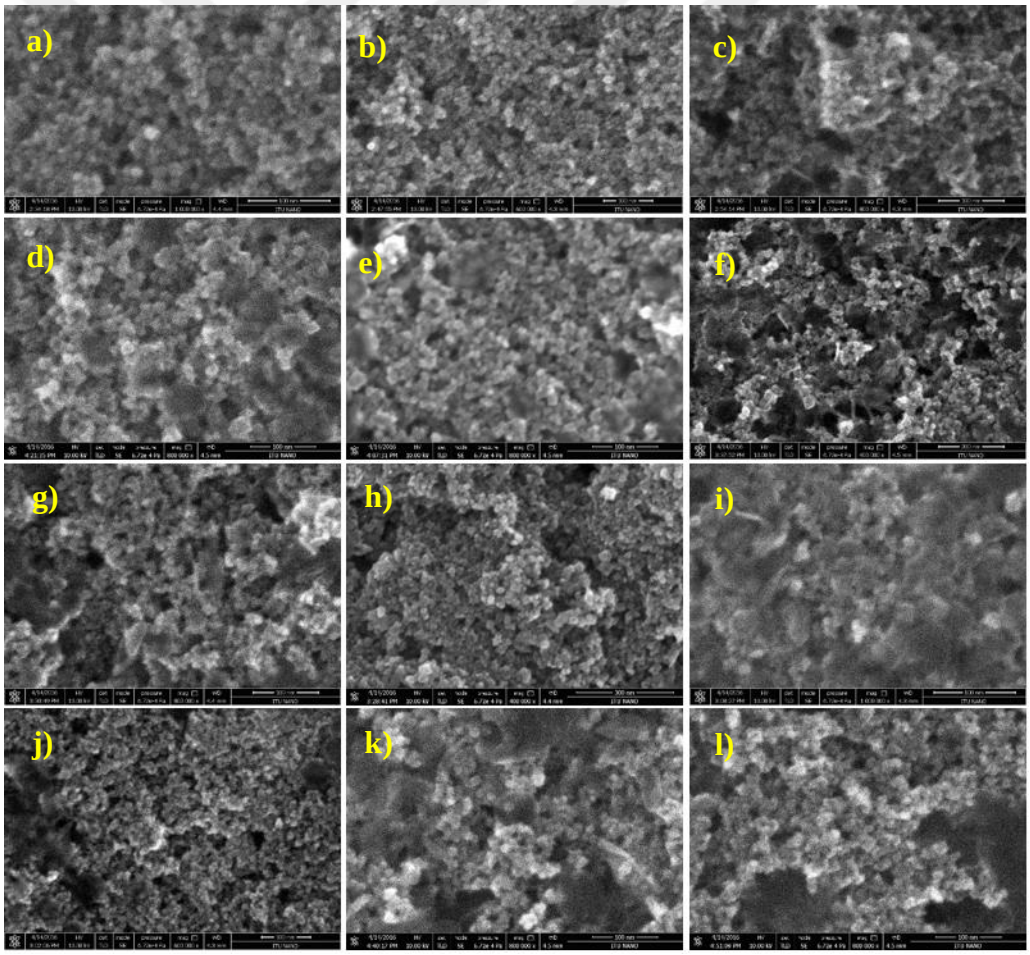

Figure B.7: SEM photographs (a) MgF-1, (b) MgF-2, (c) MgF-3, (d) MgF-4, (e) MgF-5, (f) MgF-6, (g) MgF-7, (h) MgF-8, (i) MgF-9, (j) MgF-10, (k) MgF-11, (l) MgF-12.

Table B.4: $MgFe_2O_4$ Nanoparticles core sized measured in SEM equipment.

Material	Condition	Code	Sythesising NP/Water concentration(mol/L)	Synthesisin PH	Diameter (nm)
$MgFe_2O_4$	Core	MgF-1	5	13	16
$MgFe_2O_4$	Core	MgF-2	3.33	13	18
$MgFe_2O_4$	Core	MgF-3	8.33	6	11
$MgFe_2O_4$	Core	MgF-4	3.33	12	19
$MgFe_2O_4$	Core	MgF-5	5	12	13
$MgFe_2O_4$	Core	MgF-6	3.33	6	21
$MgFe_2O_4$	Core	MgF-7	5	6	19
$MgFe_2O_4$	Core	MgF-8	8.33	6	23
$MgFe_2O_4$	Core	MgF-9	5	6	17
$MgFe_2O_4$	Core	MgF-10	3.33	13	12
$MgFe_2O_4$	Core	MgF-11	5	10	15
$MgFe_2O_4$	Core	MgF-12	3.33	9	17

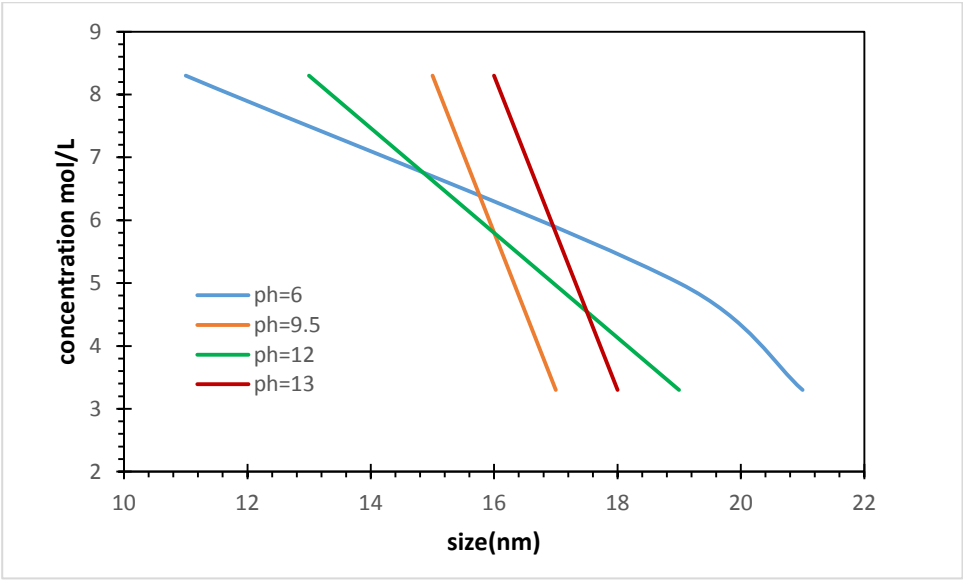

Figure B.8: $MgFe_2O_4$ Nanoparticles core sized measured in SEM equipment.

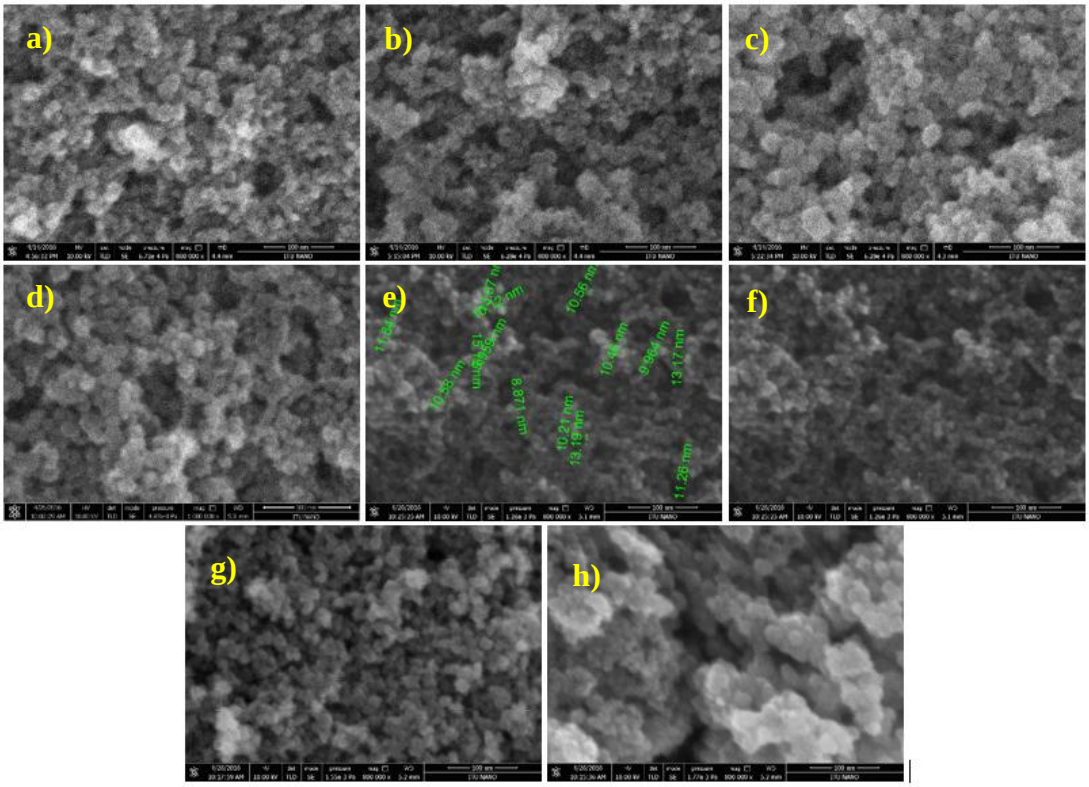

Figure B.9: SEM phptpgraphs (a) MnF-1, (b) MnF-2, (c) MnF-3, (d) MnF-4, (e) MnF-5, (f) MnF-6, (g) MnF-7, (h) MnF-8.

Table B.5: $MnFe_2O_4$ Nanoparticles core sized measured in SEM equipment.

Material	Condition	Code	Sythesising NP/Water concentration(mol/L)	Synthesising PH	Diameter (nm)
$MnFe_2O_4$	Core	MnF-1	5.76	13	17
$MnFe_2O_4$	Core	MnF-2	5.76	12	19
$MnFe_2O_4$	Core	MnF-3	3.84	12	22
$MnFe_2O_4$	Core	MnF-4	3.84	13	13
$MnFe_2O_4$	Core	MnF-5	5.76	6	11
$MnFe_2O_4$	Core	MnF-6	9.6	12	11
$MnFe_2O_4$	Core	MnF-7	9.6	13	13
$MnFe_2O_4$	Core	MnF-8	9.6	6	25

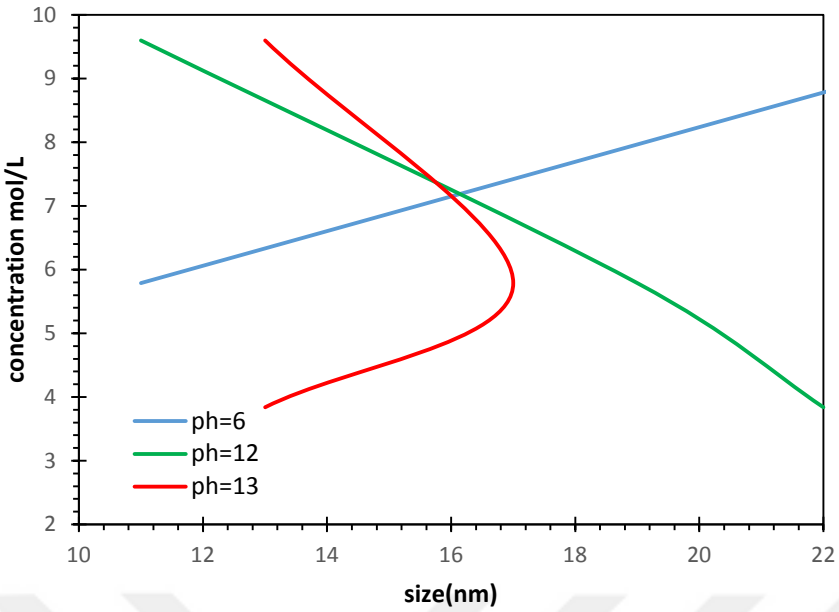

Figure B.10: $MnFe_2O_4$ Nanoparticles core sized measured in SEM equipment.

APPENDIX C

Table C.1: Fe_3O_4 Magneticle nanoparticles core synthesizing conditions and their size and saturation magnetization

Code	Sythesising NP/Water concentration (mol/L)	Synthesising pH	Diameter (nm)	Magnetization (Ms)
FO-1	9.64	13	13	50,56071
FO-2	5.78	13	11	52,72141
FO-3	3.85	13		75,2858
FO-4	9.64	10	8	49,08345
FO-5	5.78	12	8	66,48744
FO-6	3.85	12	9	50,38671
FO-7	9.64	12	7	42,06651
FO-8	5.78	10	9	45,47752
FO-9	3.85	12	8	43,07745

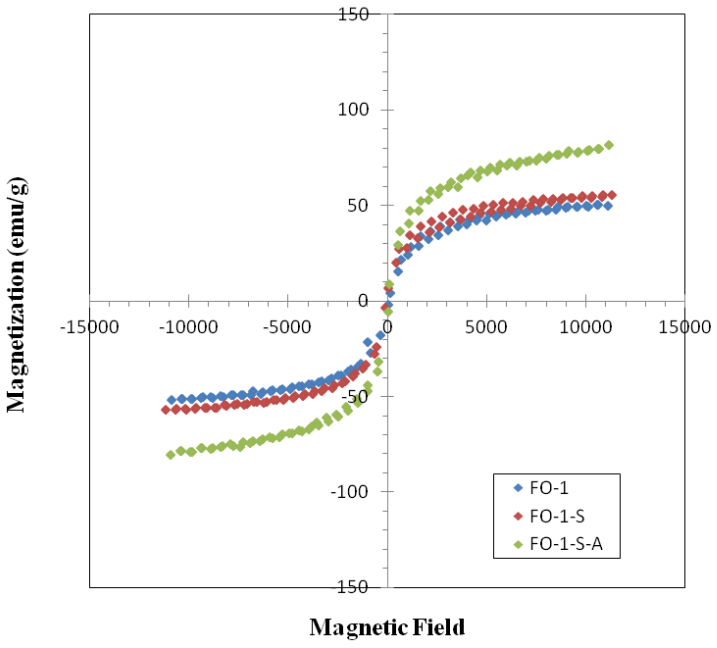

Figure C.1: FO-1, FO-1-S and FO-1-S-A VSM results.

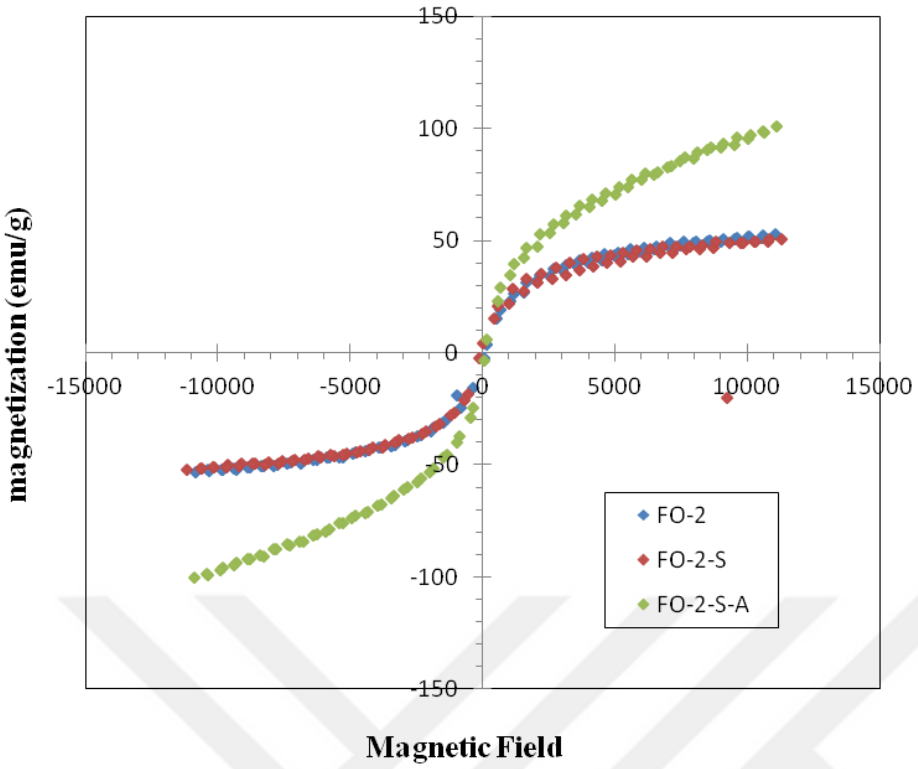

Figure C.2: FO-2, FO-2-S and FO-2-S-A VSM results.

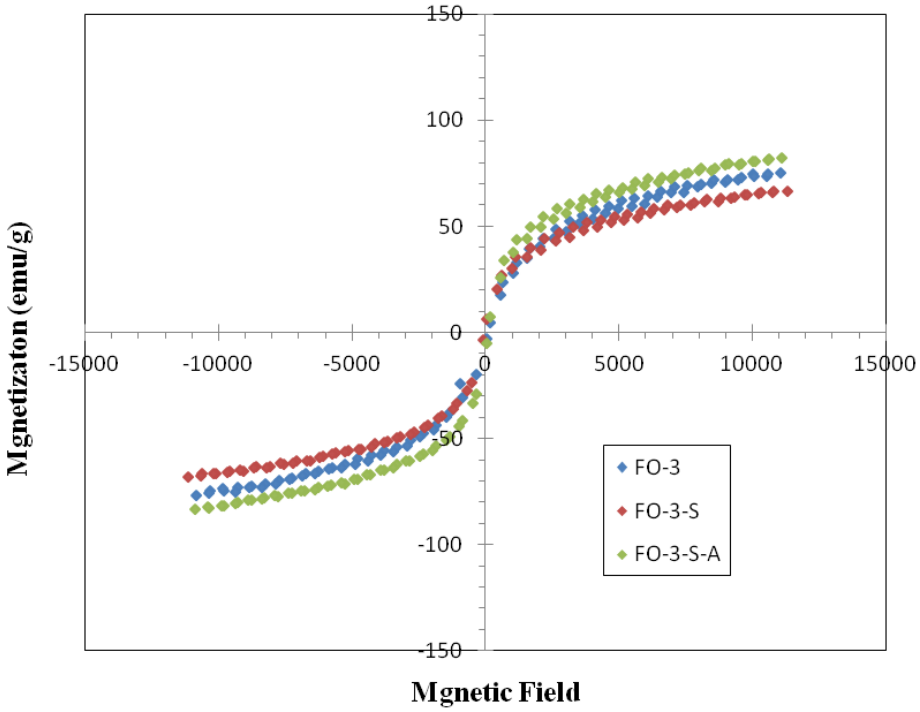

Figure C.3: FO-3, FO-3-S and FO-3-S-A VSM results.

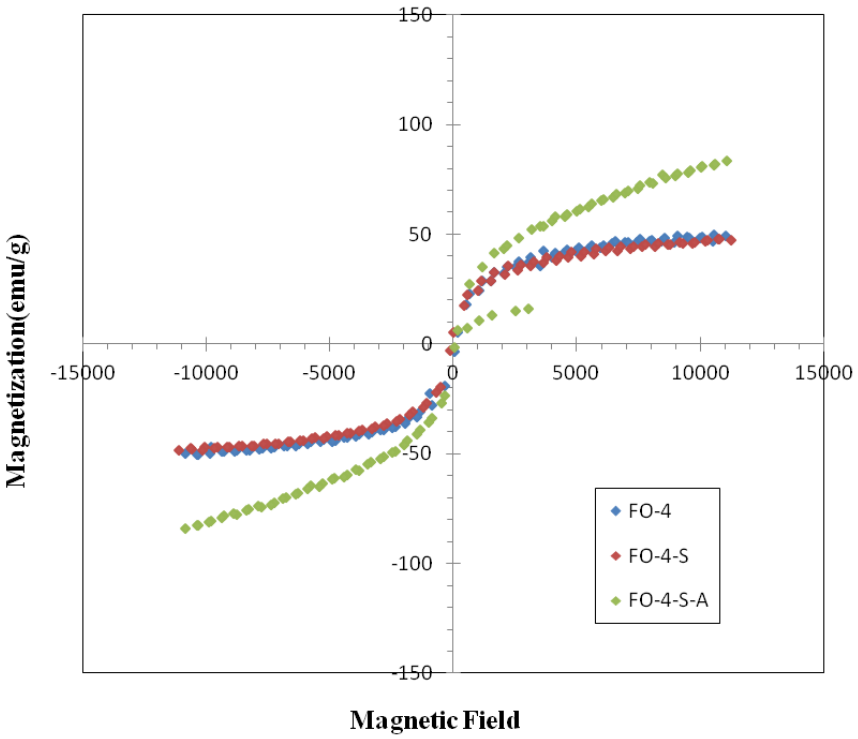

Figure C.4: FO-4, FO-4-S and FO-4-S-A VSM results.

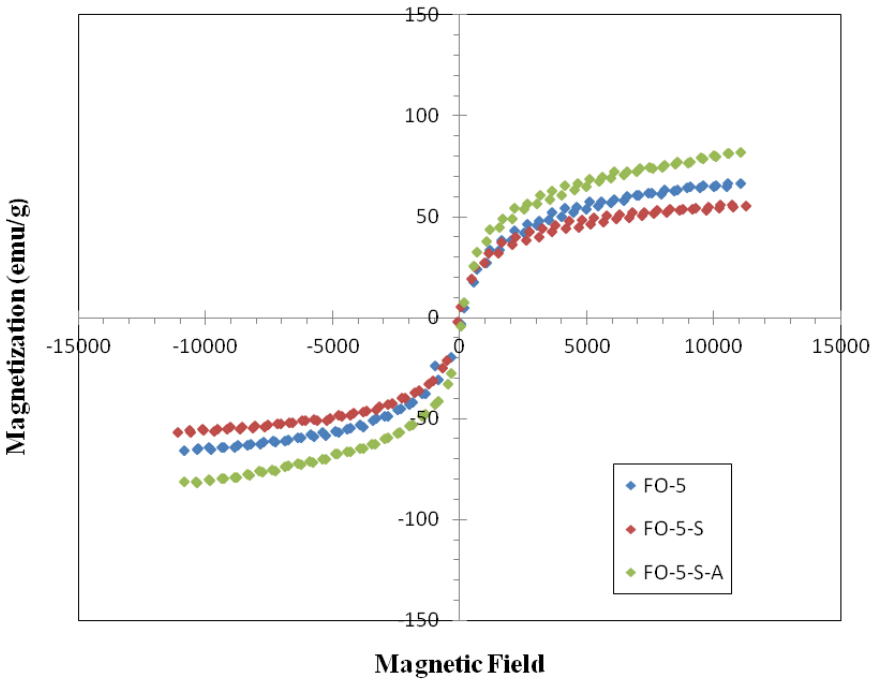

Figure C.5: FO-5, FO-5-S and FO-5-S-A VSM results.

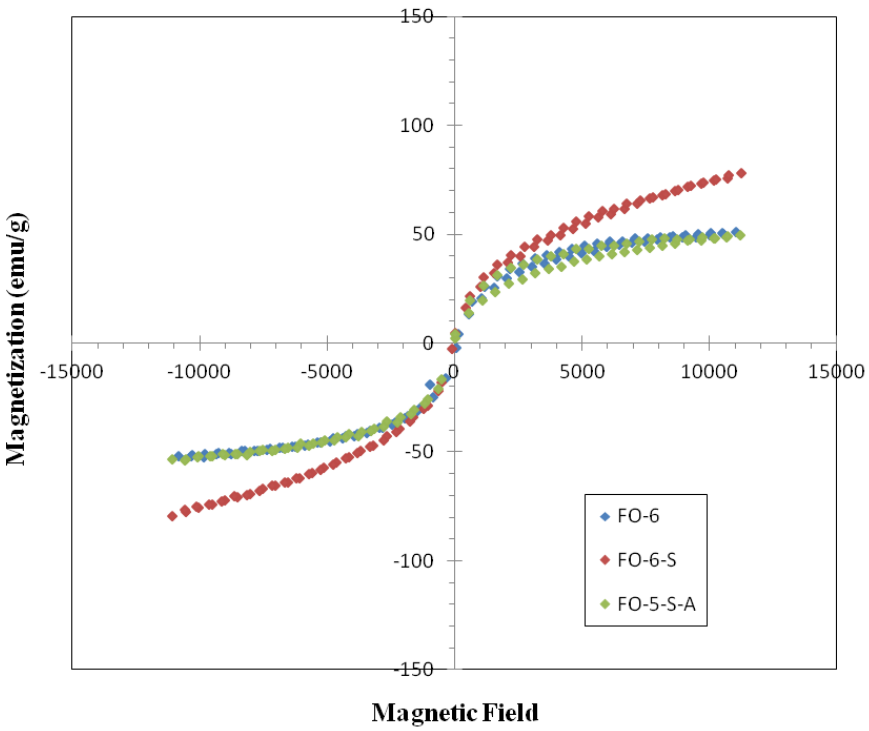

Figure C.6: FO-6, FO-6-S and FO-6-S-A VSM results.

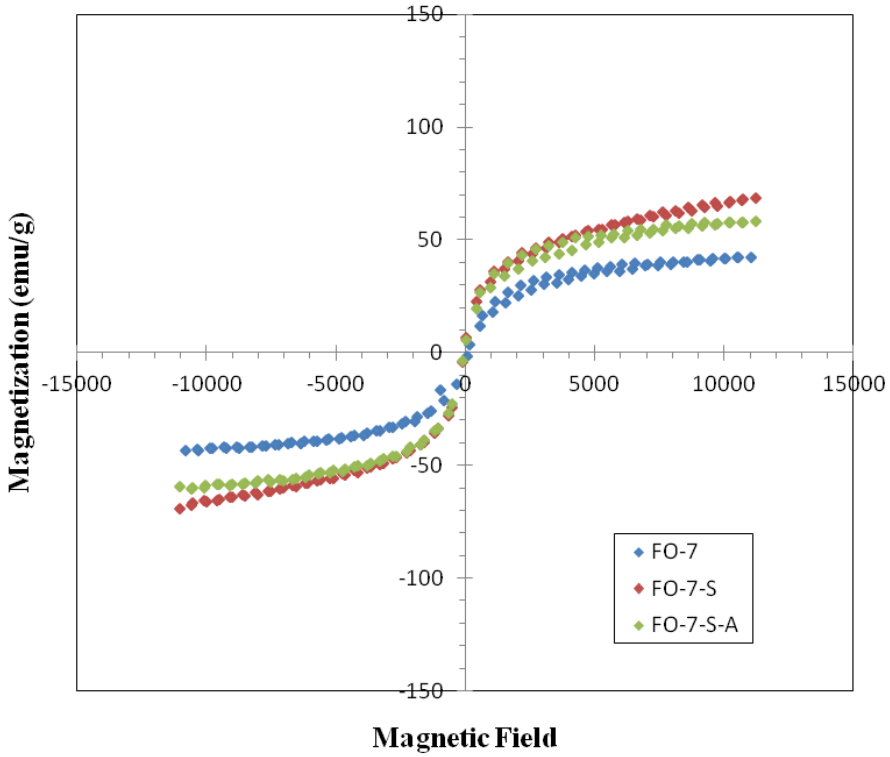

Figure C.7: FO-7, FO-7-S and FO-7-S-A VSM results

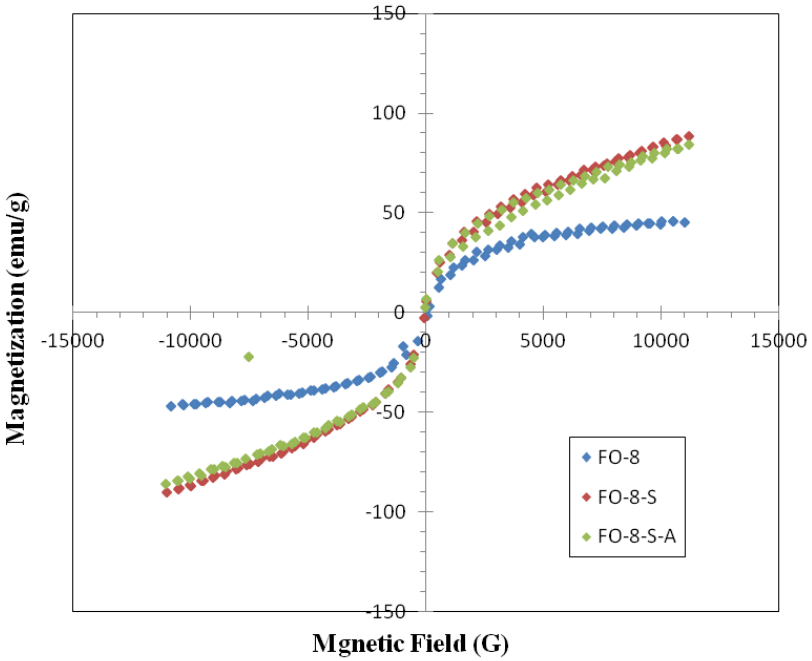

Figure C.8: FO-8, FO-8-S and FO-8-S-A VSM results.

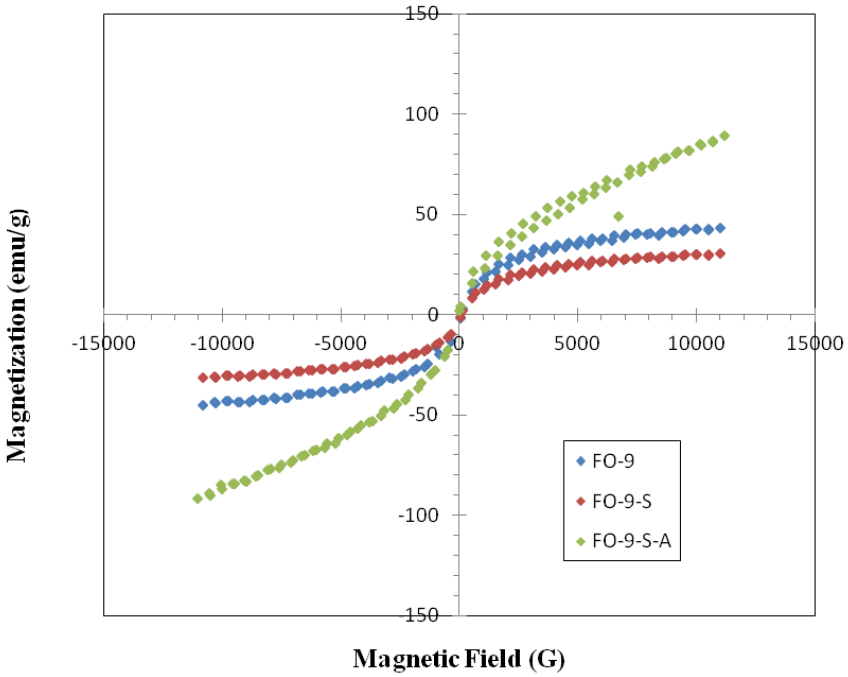

Figure C.9: FO-9, FO-9-S and FO-9-S-A VSM results.

Table C.2: $SrFe_{12}O_{19}$ magneticle nanoparticles core synthesizing conditions and their size and saturation magnetization.

Code	Sythesising NP/Water concentration(mol/L)	Synthesize pH	Diamater (nm)	Magnetization (Ms)
SF-1	26.54	13	12	99,39277
SF-2	26.54	14	12	43,87858
SF-3	17.7	14	20	40,59379
SF-4	17.7	13	13	56,31558
SF-5	26.54	12	15	40,25368
SF-6	17.7	12	17	89,86941

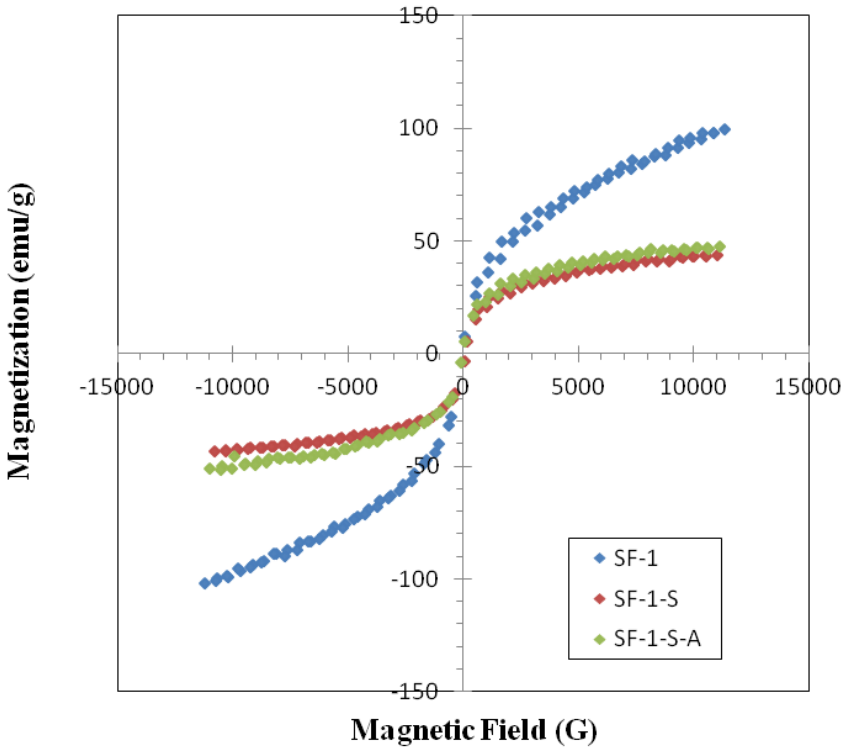

Figure C.10: SF-1, SF-1-S and SF-1-S-A VSM results.

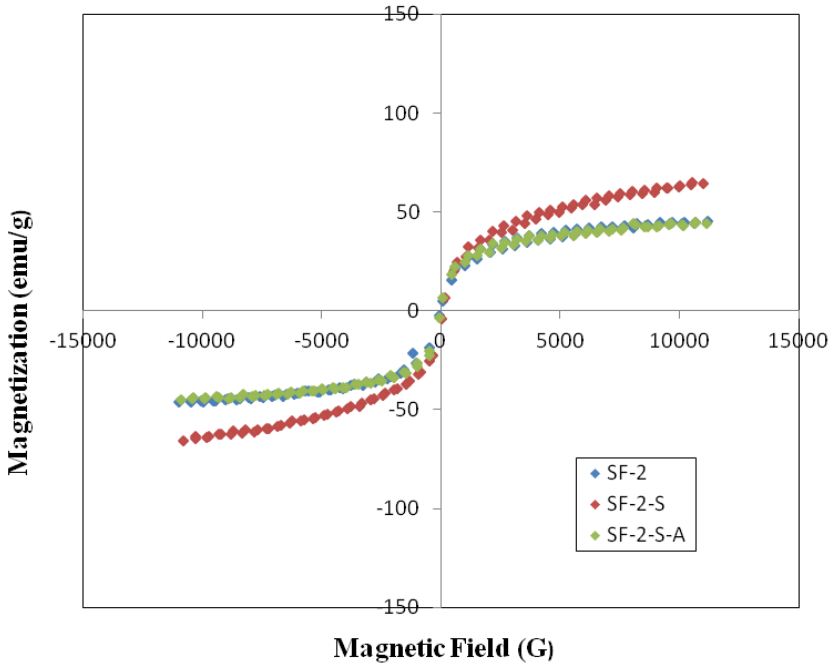

Figure C.11: SF-2, SF-2-S and SF-2-S-A VSM results.

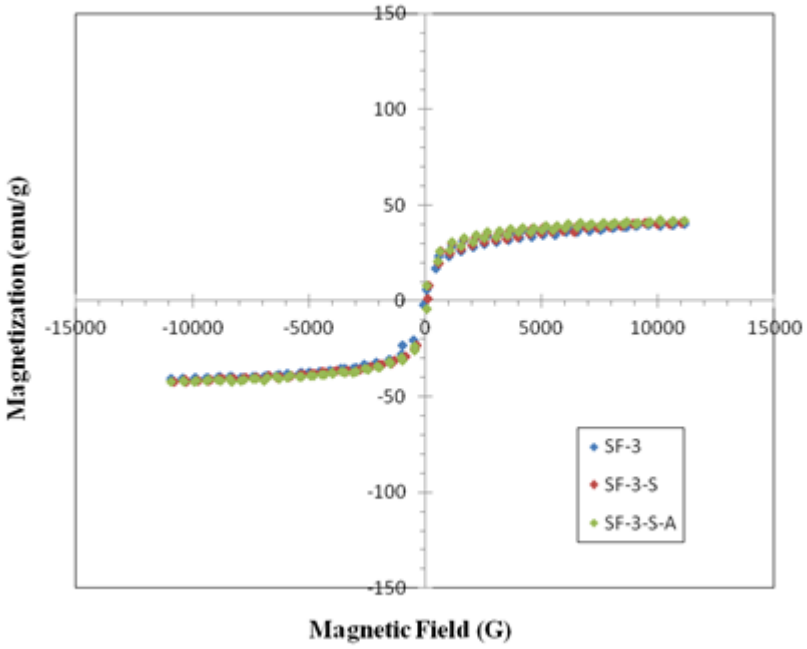

Figure C.12: SF-3, SF-3-S and SF-3-S-A VSM results.

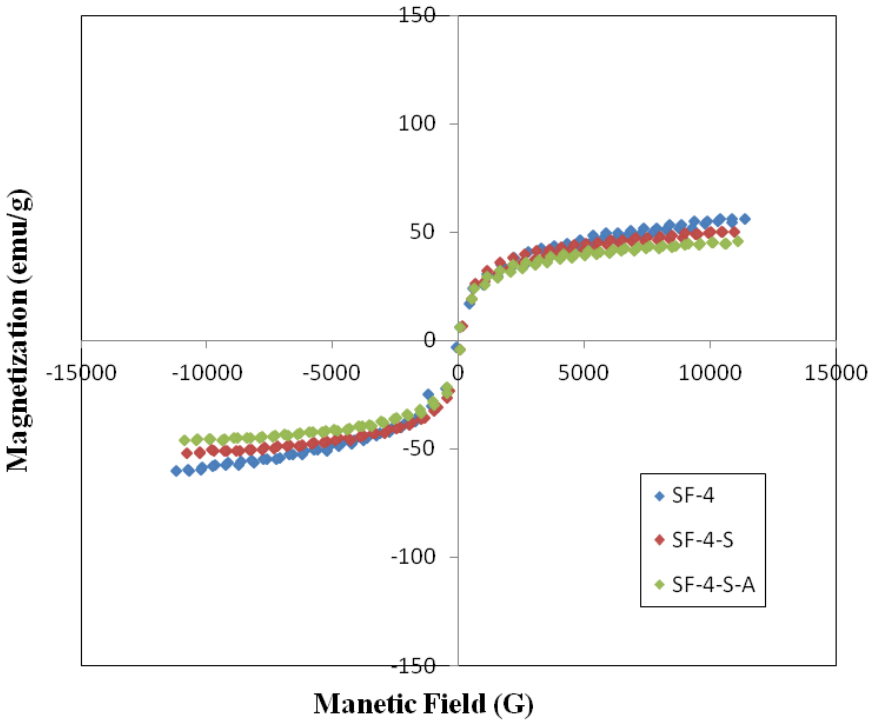

Figure C.13: SF-4, SF-4-S and SF-4-S-A VSM results.

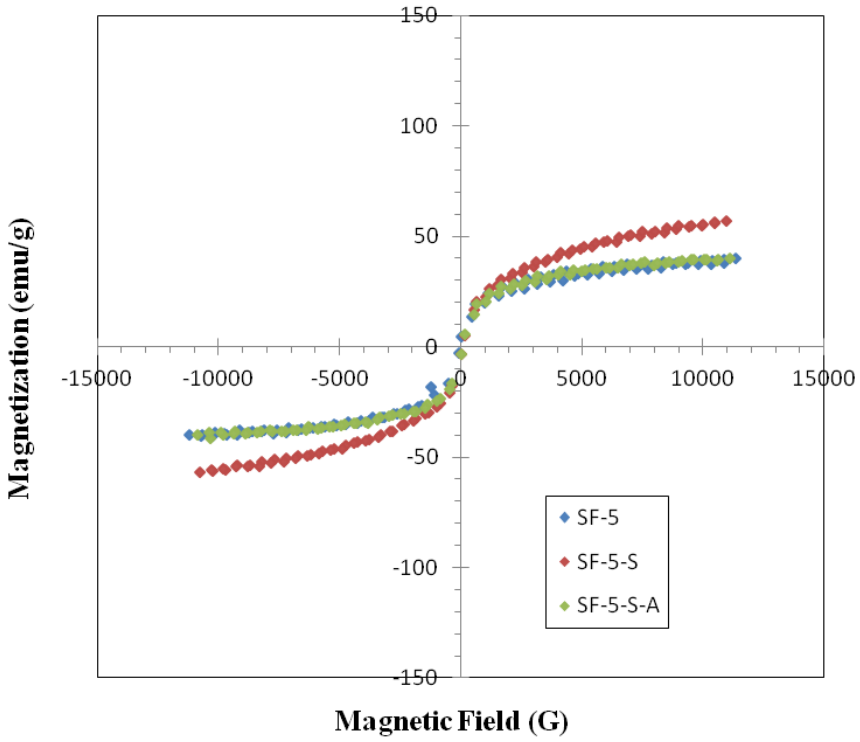

Figure C.14: SF-5, SF-5-S and SF-5-S-A VSM results.

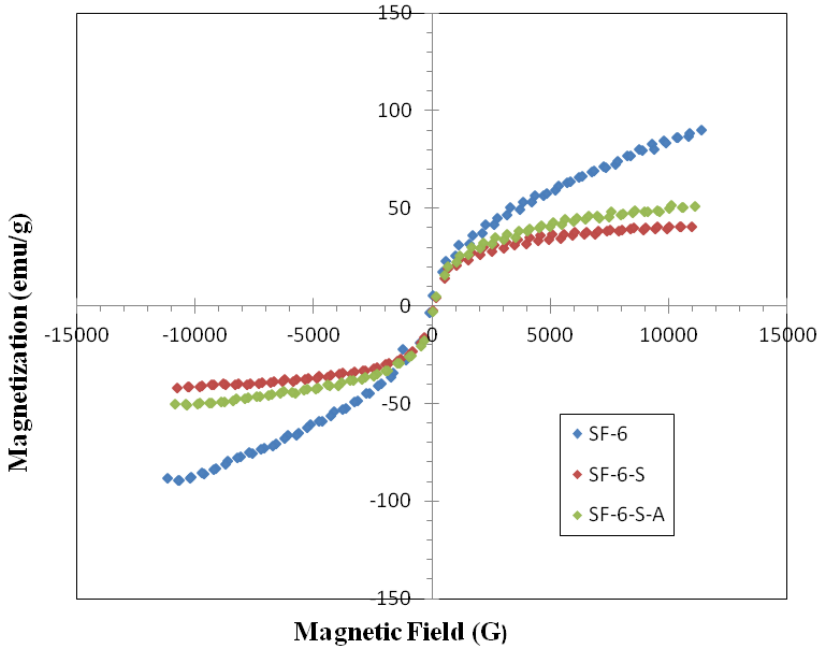

Figure C.15: SF-6, SF-6-S and SF-6-S-A VSM results.

Table C.3: $BaFe_{12}O_{19}$ magneticle nanoparticles core synthesizing conditions and their size and saturation magnetization.

Code	Sythesising NP/Water concentration(mol/L)	Synthesising PH	Diameter (nm)	Magnetization (Ms)
BF-1	27.78	13	12	39,35906
BF-2	27.78	14	12	28,05193
BF-3	18.52	13	11	21,43721
BF-4	18.52	14	10	60,08524
BF-5	18.52	12	11	65,61115
BF-6	46.31	13	10	19,27466
BF-7	27.78	11	13	45,16856
BF-8	18.52	13	11	51,11582
BF-9	46.31	13	10	56,18454

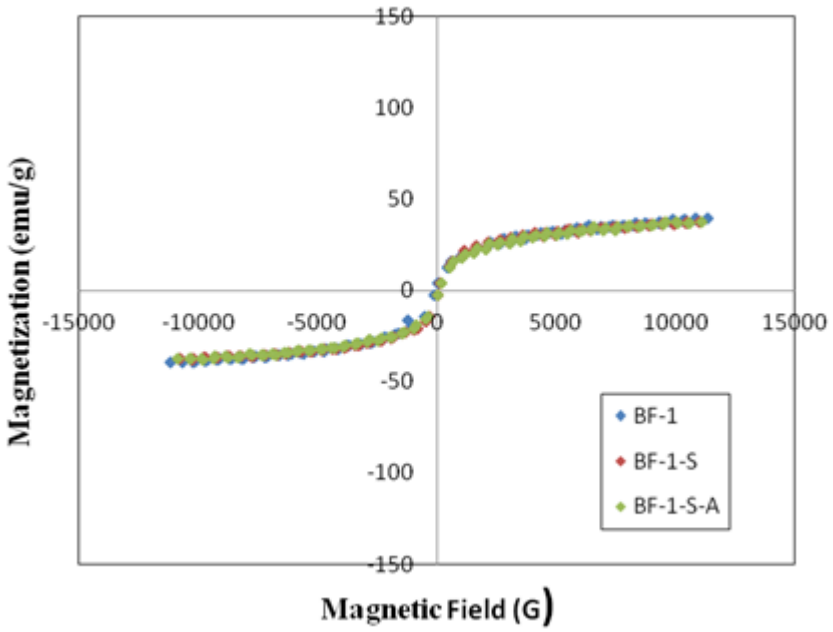

Figure C.16: BF-1, BF-1-S and BF-1-S-A VSM results.

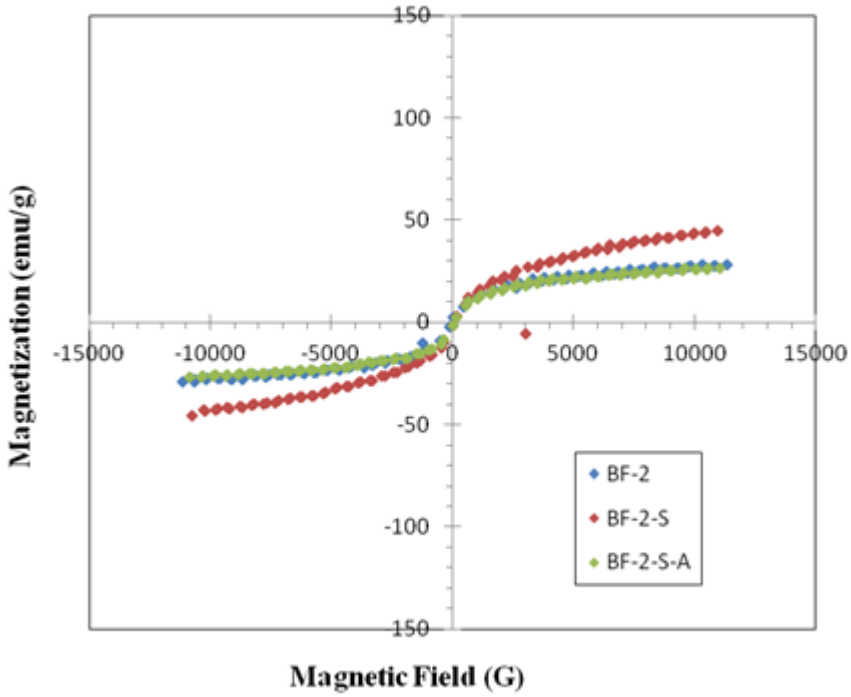

Figure C.17: BF-2, BF-2-S and BF-2-S-A VSM results.

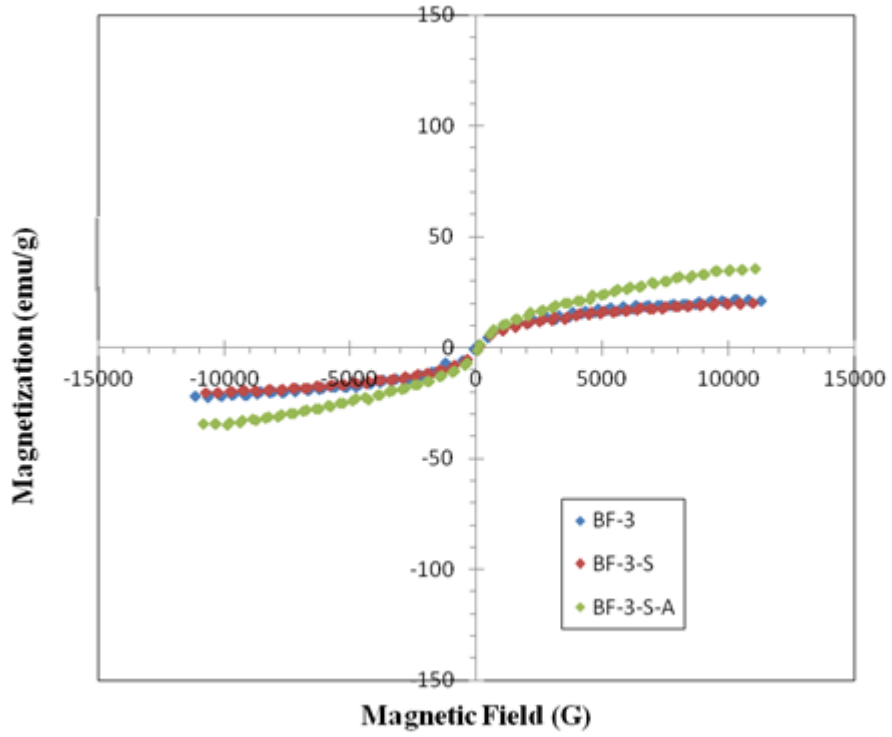

Figure C.18: BF-3, BF-3-S and BF-3-S-A VSM results.

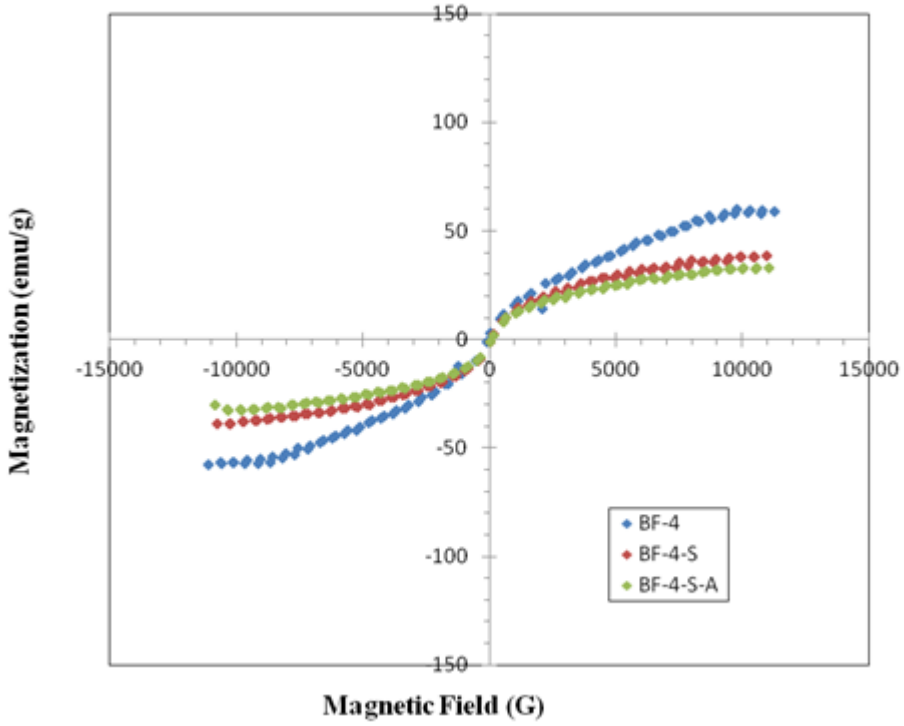

Figure C.19: BF-4, BF-4-S and BF-4-S-A VSM results.

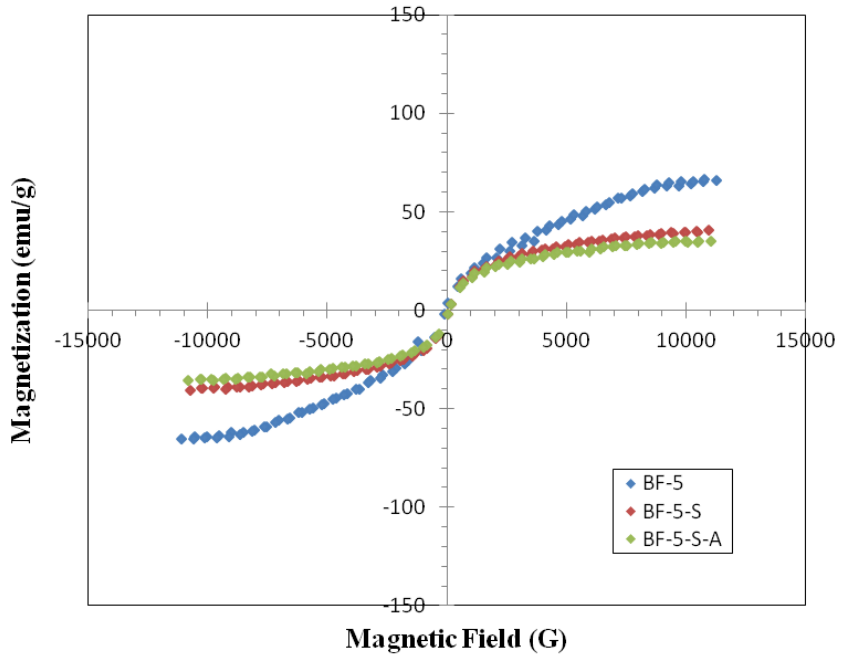

Figure C.20: BF-5, BF-5-S and BF-5-S-A VSM results.

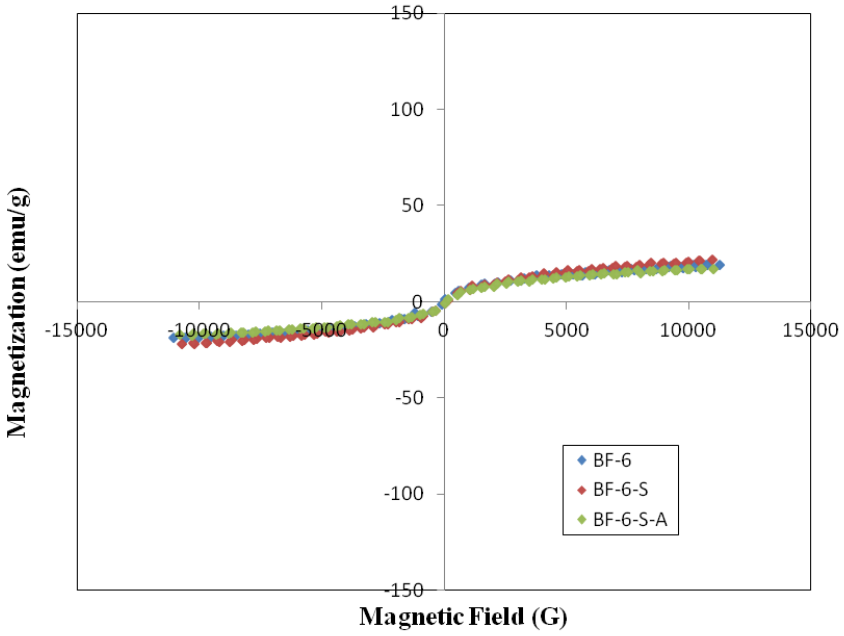

Figure C.21: BF-6, BF-6-S and BF-6-S-A VSM results.

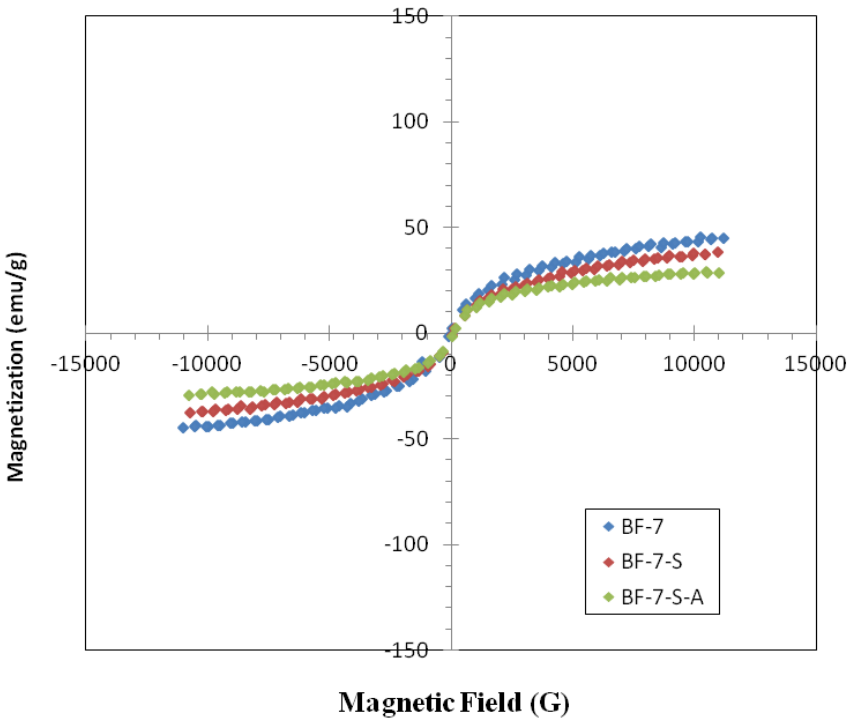

Figure C.22: BF-7, BF-7-S and BF-7-S-A VSM results.

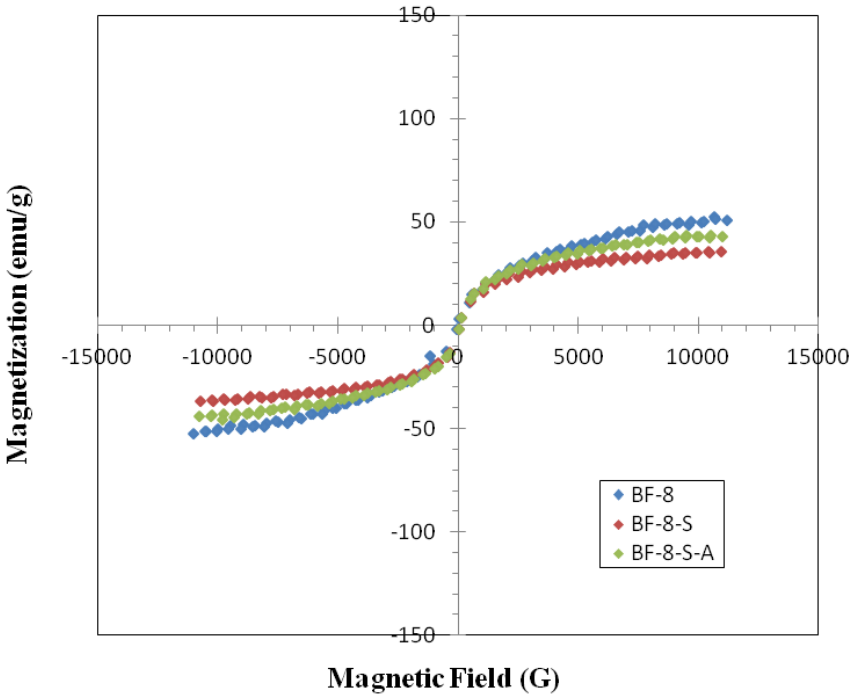

Figure C.23: BF-8, BF-8-S and BF-8-S-A VSM results.

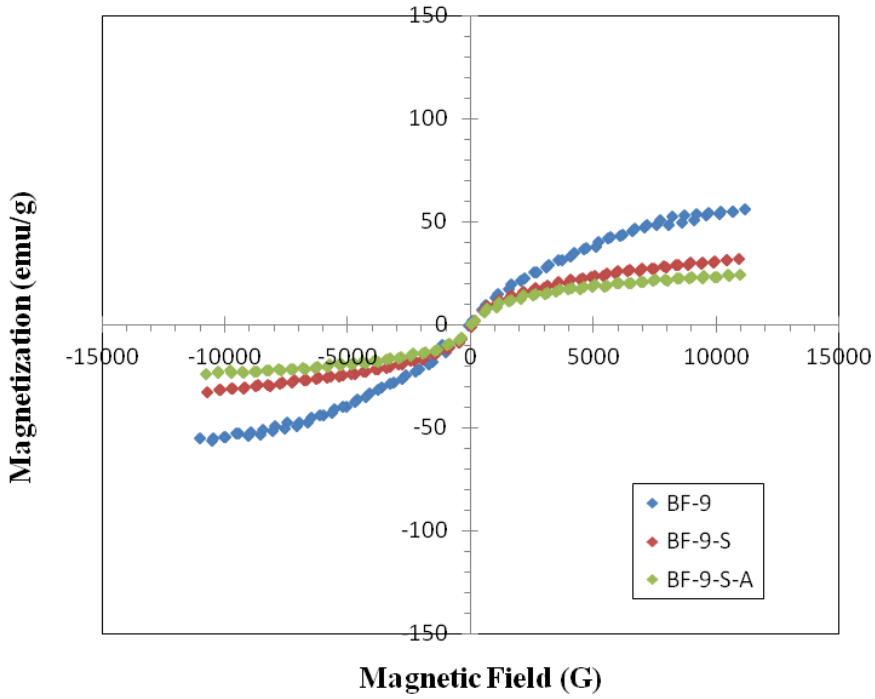

Figure C.24: BF-9, BF-9-S and BF-9-S-A VSM results.

Table C.4: $MgFe_2O_4$ magneticle nanoparticles core synthesizing conditions and their size and saturation magnetization.

Code	Sythesising NP/Water concentration(mol/L)	Synthesising PH	Diameter (nm)	Magnetization (Ms)
MgF-1	5	13	16	67,24344
MgF-2	3.33	13	18	72,84586
MgF-3	8.33	6	11	40,74824
MgF-4	3.33	12	19	35,80814
MgF-5	5	12	13	44,07618
MgF-6	3.33	6	21	56,64277
MgF-7	5	6	19	26,35933
MgF-8	8.33	6	23	65,27278
MgF-9	5	6	17	24,32453
MgF-10	3.33	13	12	22,80322
MgF-11	5	10	15	39,22476
MgF-12	3.33	9	17	31,59831

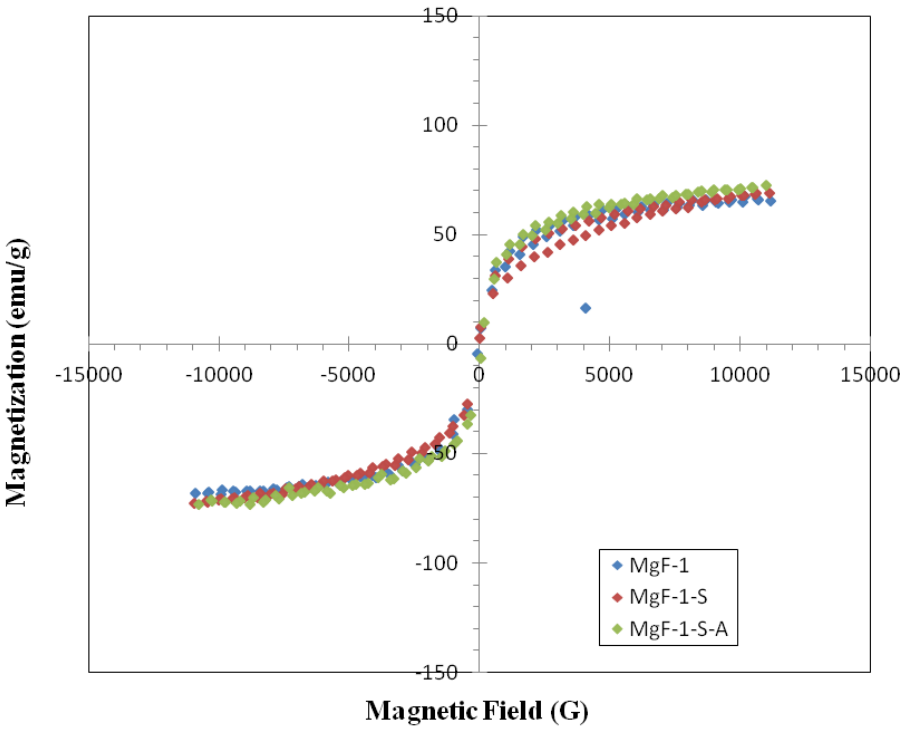

Figure C.25: MgF-1, MgF-1-S and MgF-1-S-A VSM results.

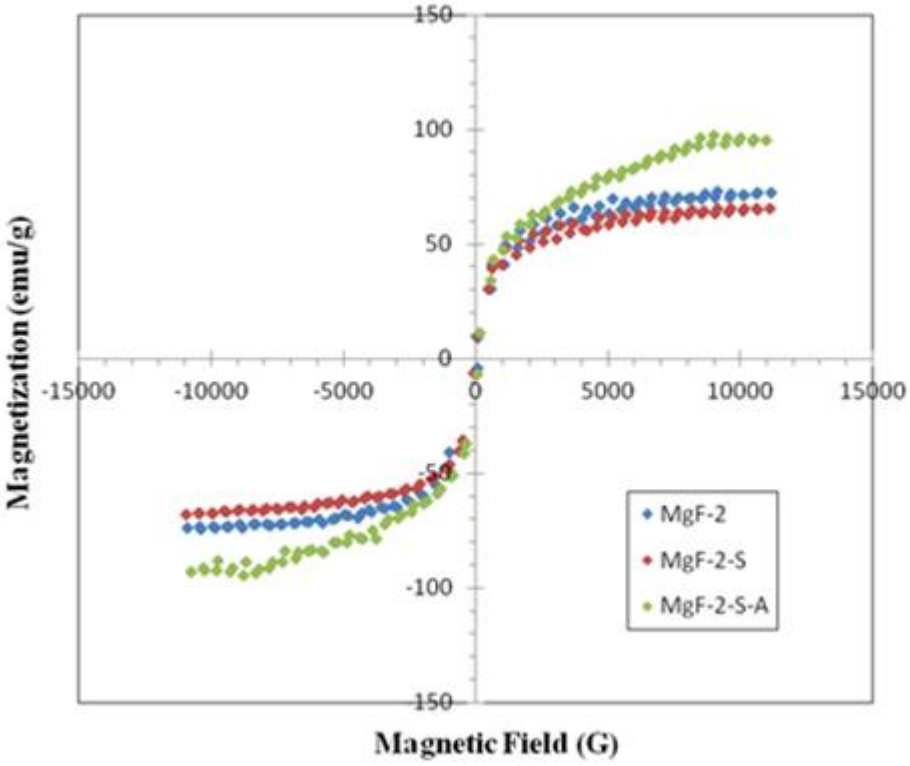

Figure C.26: MgF-2, MgF-2-S and MgF-2-S-A VSM results.

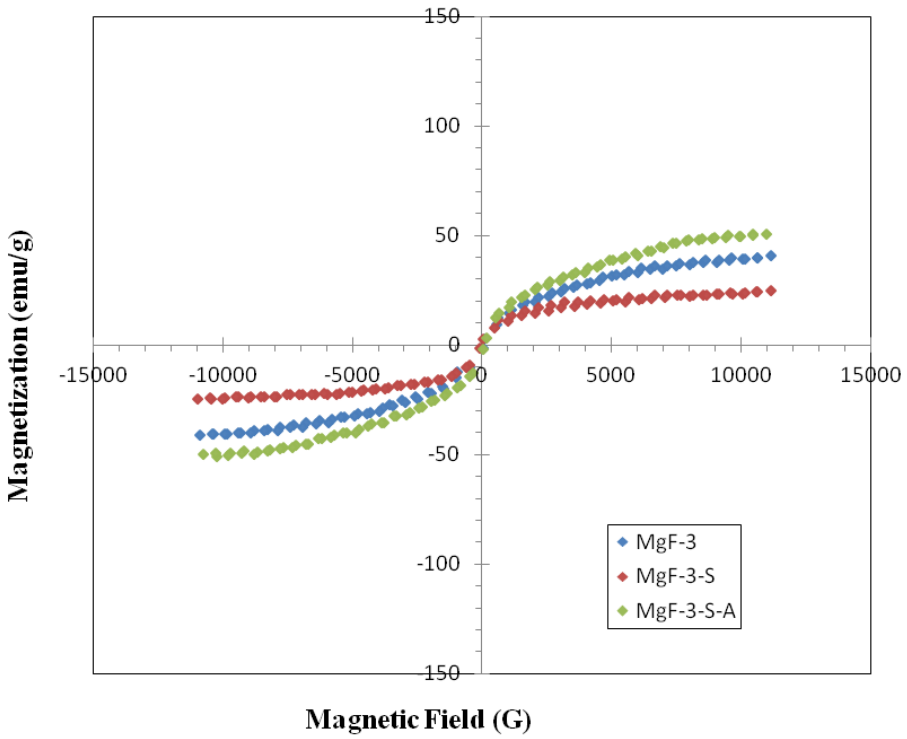

Figure C.27: MgF-3, MgF-3-S and MgF-3-S-A VSM results.

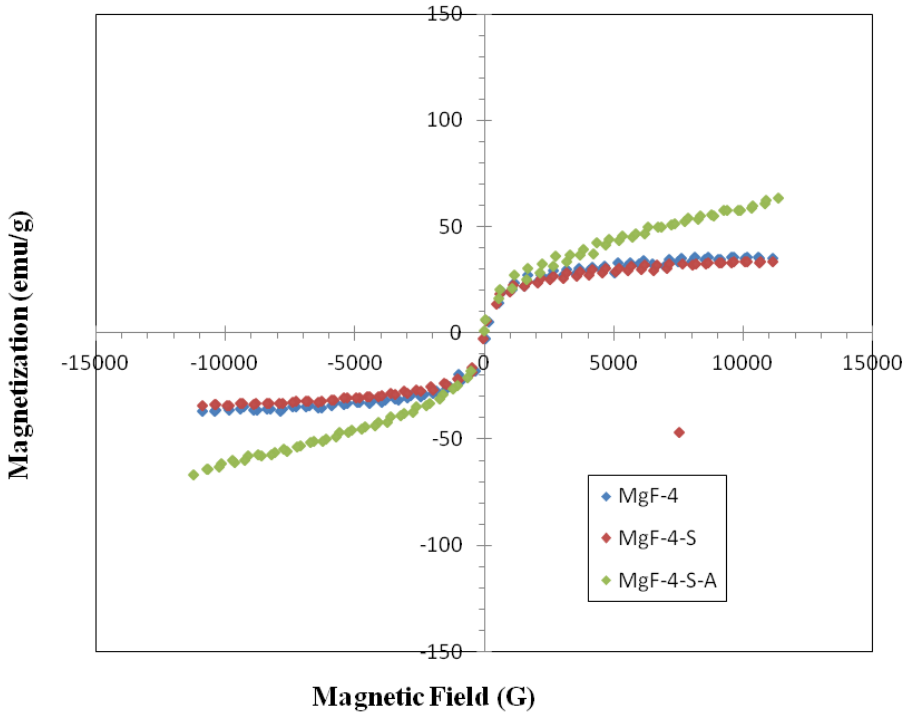

Figure C.28: MgF-4, MgF-4-S and MgF-4-S-A VSM results.

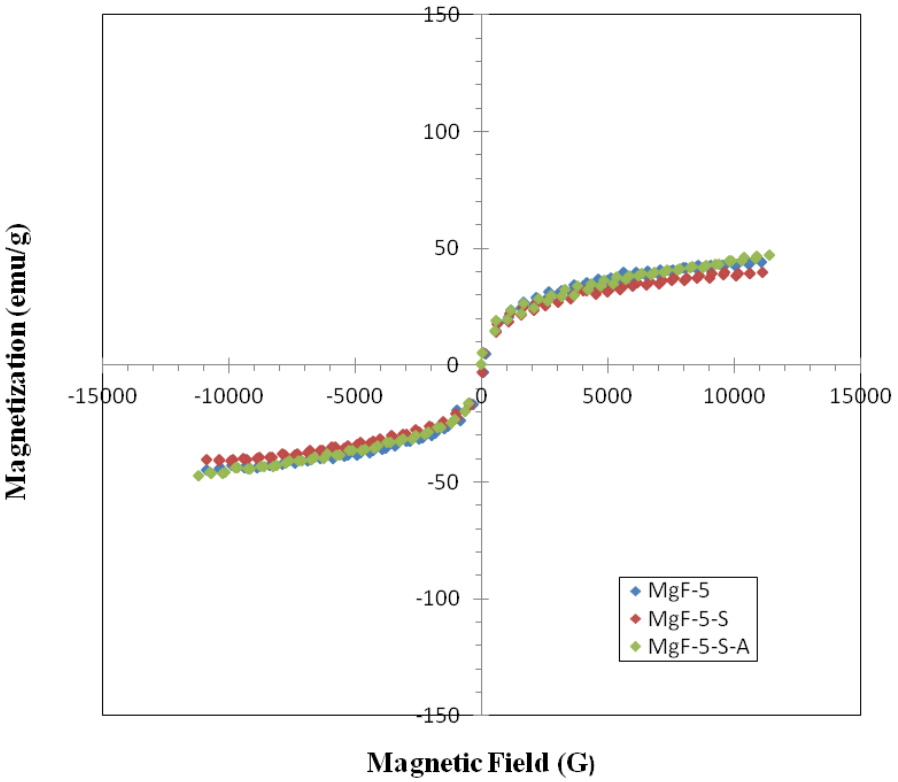

Figure C.29: MgF-5, MgF-5-S and MgF-5-S-A VSM results.

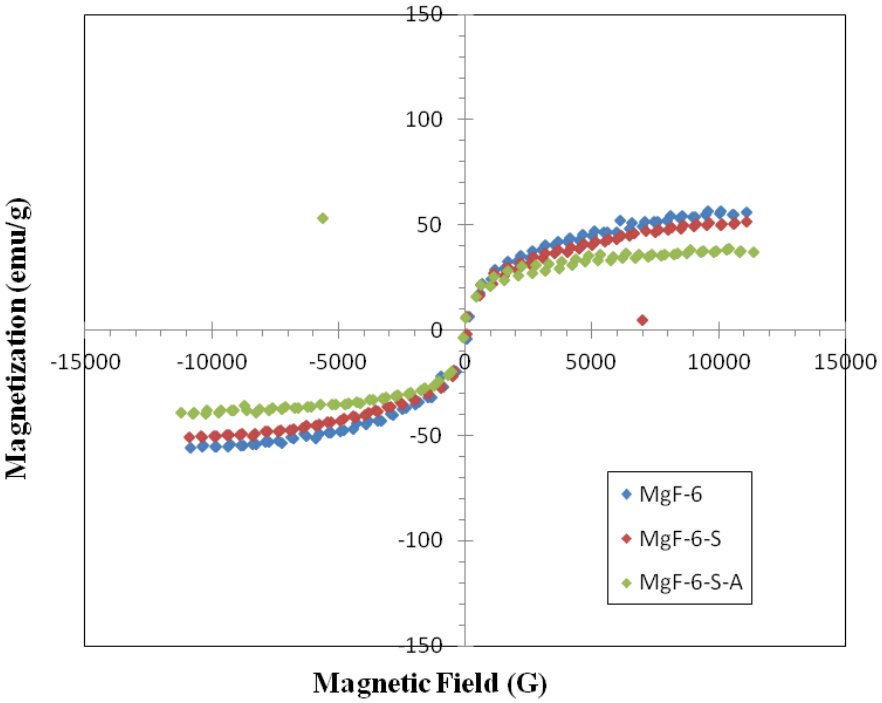

Figure C.30: MgF-6, MgF-6-S and MgF-6-S-A VSM results.

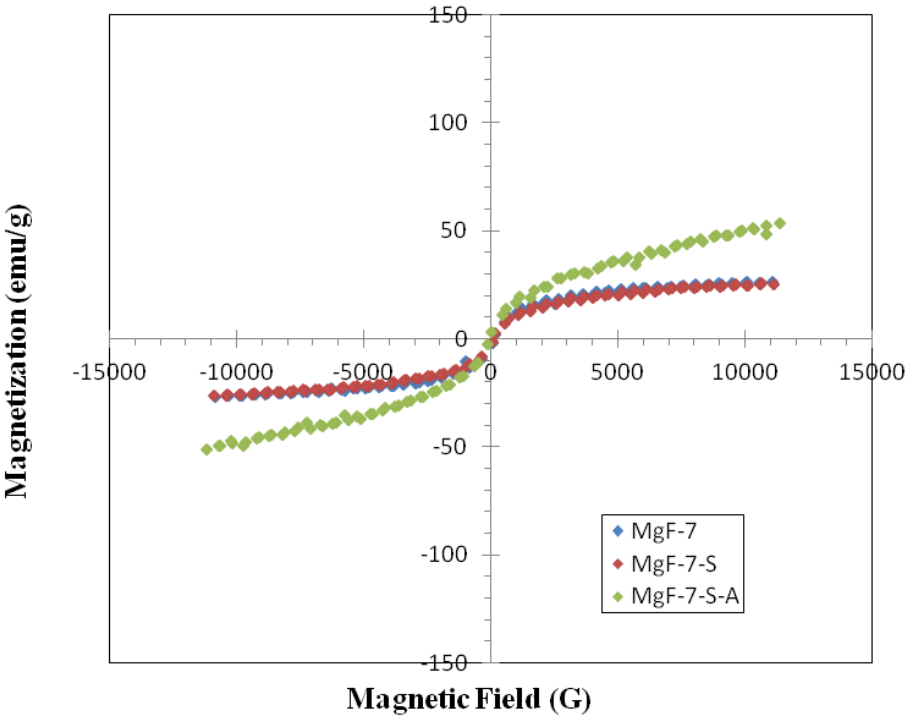

Figure C.31: MgF-7, MgF-7-S and MgF-7-S-A VSM results.

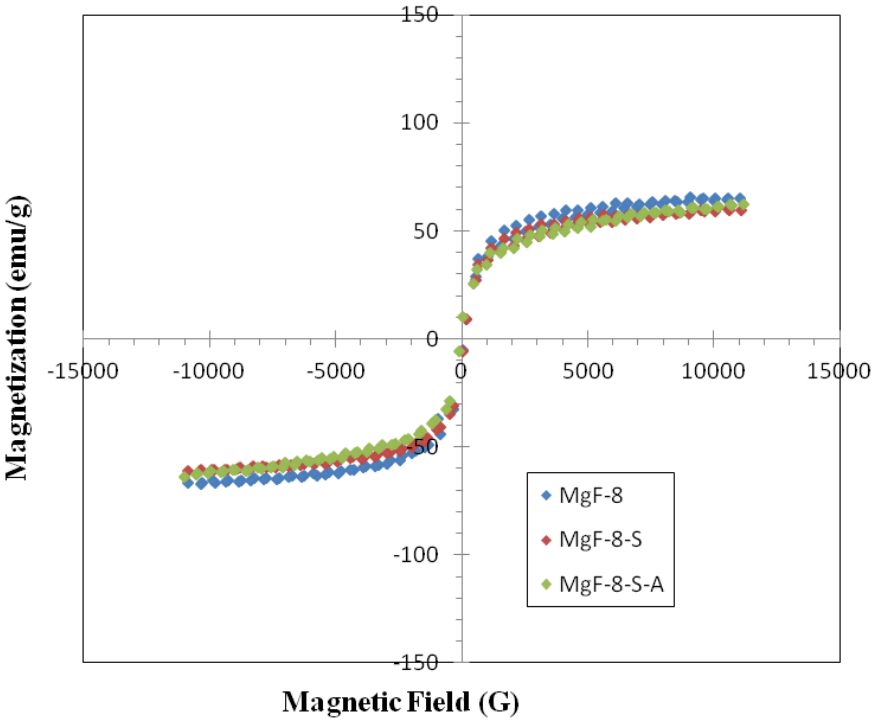

Figure C.32: MgF-8, MgF-8-S and MgF-8-S-A VSM results.

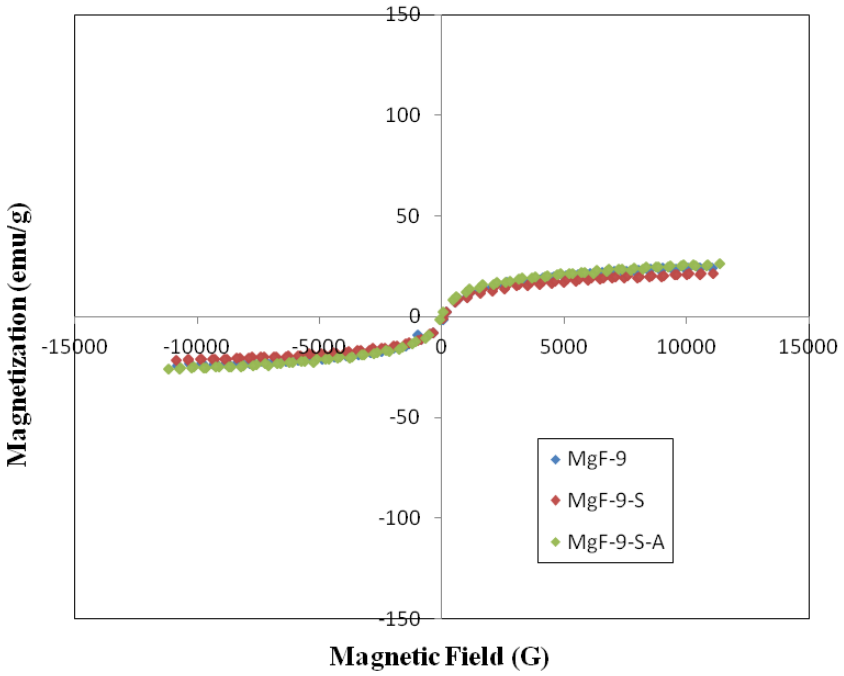

Figure C.33: MgF-9, MgF-9-S and MgF-9-S-A VSM results.

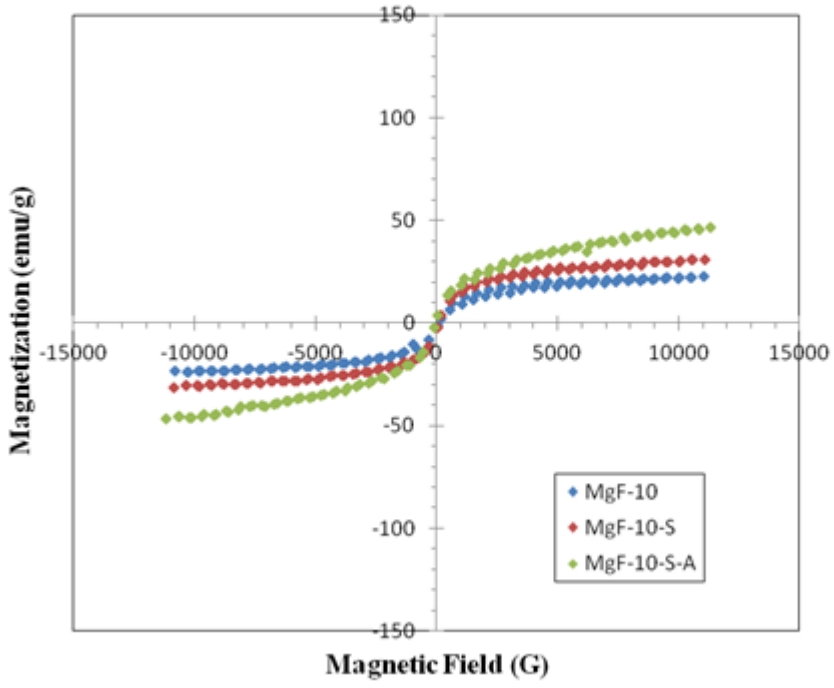

Figure C.34: MgF-10, MgF-10-S and MgF-10-S-A VSM results.

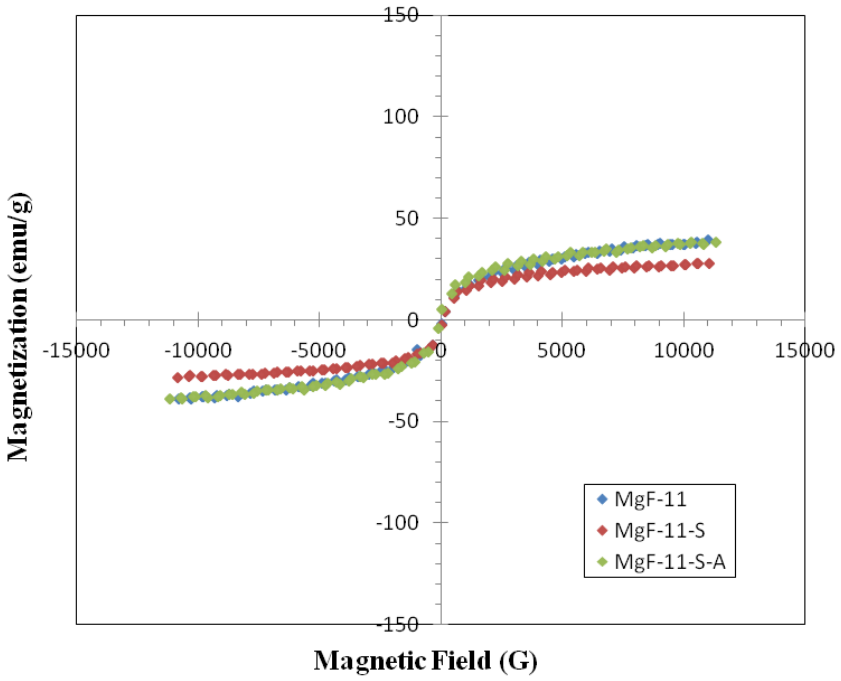

Figure C.35: MgF-11, MgF-11-S and MgF-11-S-A VSM results.

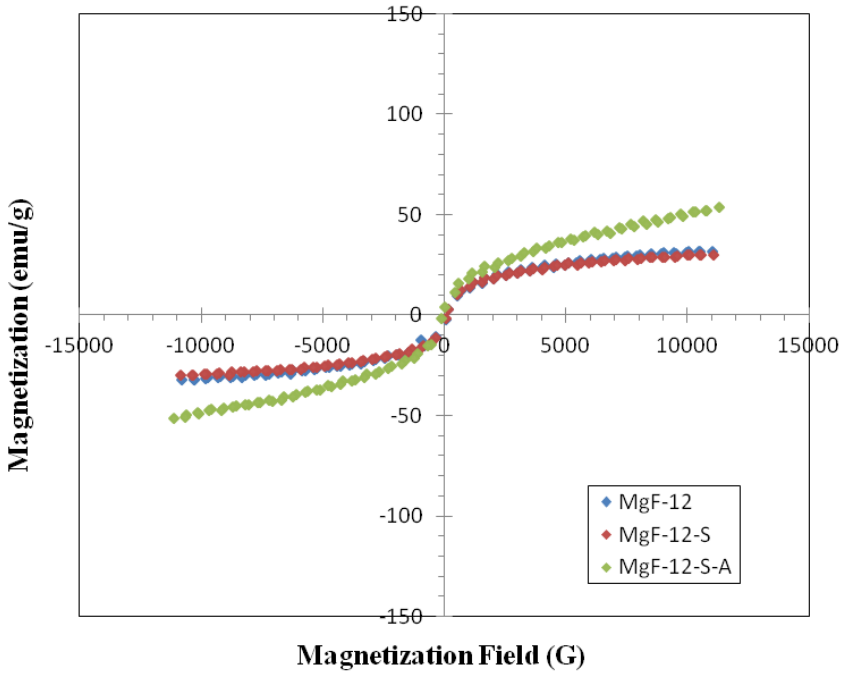

Figure C.36: MgF-12, MgF-12-S and MgF-12-S-A VSM results.

Table C.5: $MnFe_2O_4$ magneticle nanoparticles core synthesizing conditions and their size and saturation magnetization.

Code	Sythesising NP/Water concentration(mol/L)	Synthesising PH	Diameter (nm)	Magnetization (Ms)
MnF-1	5.76	13	17	54,80961
MnF-2	5.76	12	19	55,77094
MnF-3	3.84	12	22	61,42135
MnF-4	3.84	13	13	73,86332
MnF-5	5.76	6	11	53,46002
MnF-6	9.6	12	11	54,65303
MnF-7	9.6	13	13	50,20741
MnF-8	9.6	6	25	75,08439

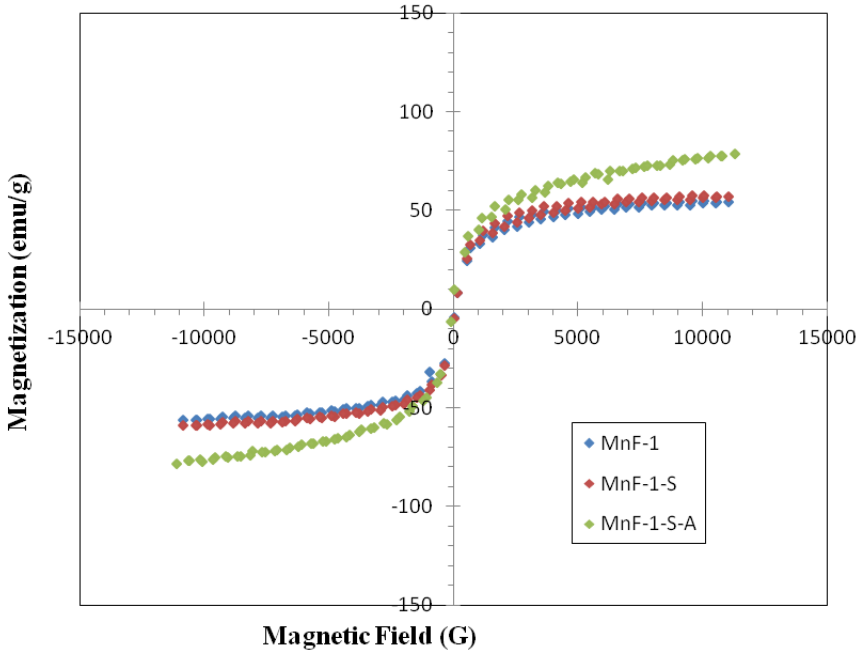

Figure C.37: MnF-1, MnF-1-S and MnF-1-S-A VSM results.

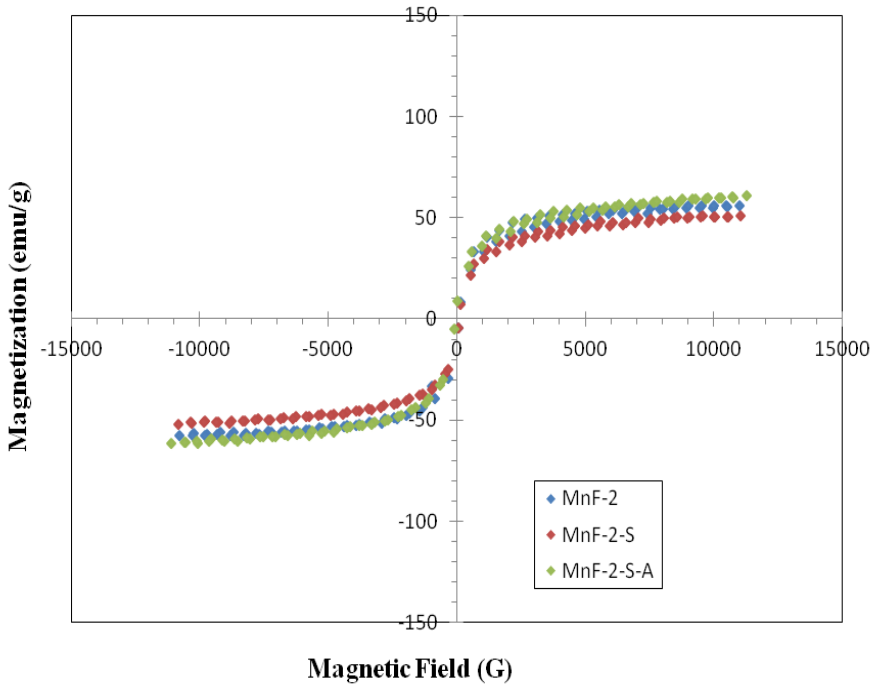

Figure C.38: MnF-2, MnF-2-S and MnF-2-S-A VSM results.

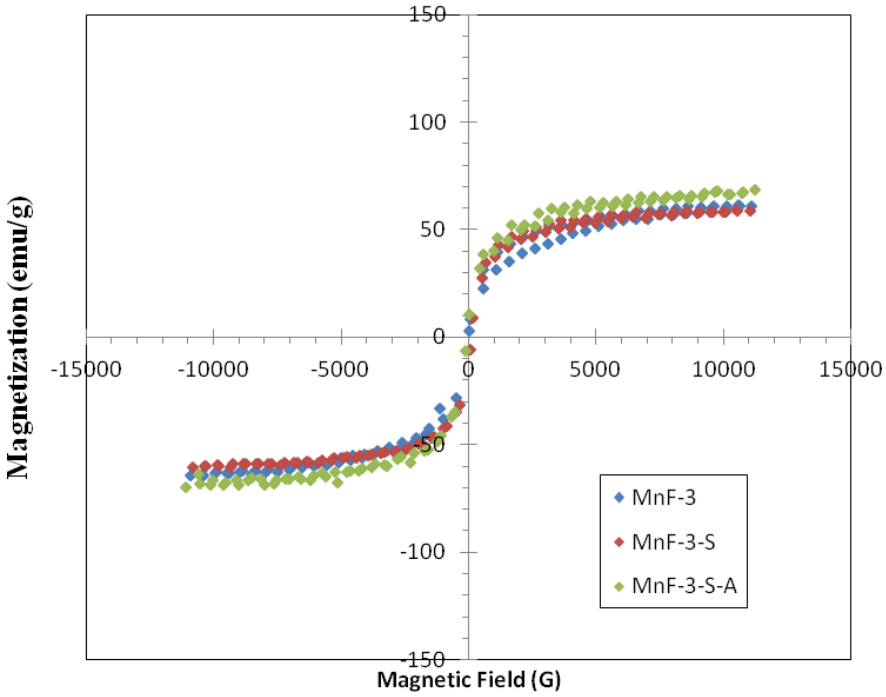

Figure C.39: MnF-3, MnF-3-S and MnF-3-S-A VSM results.

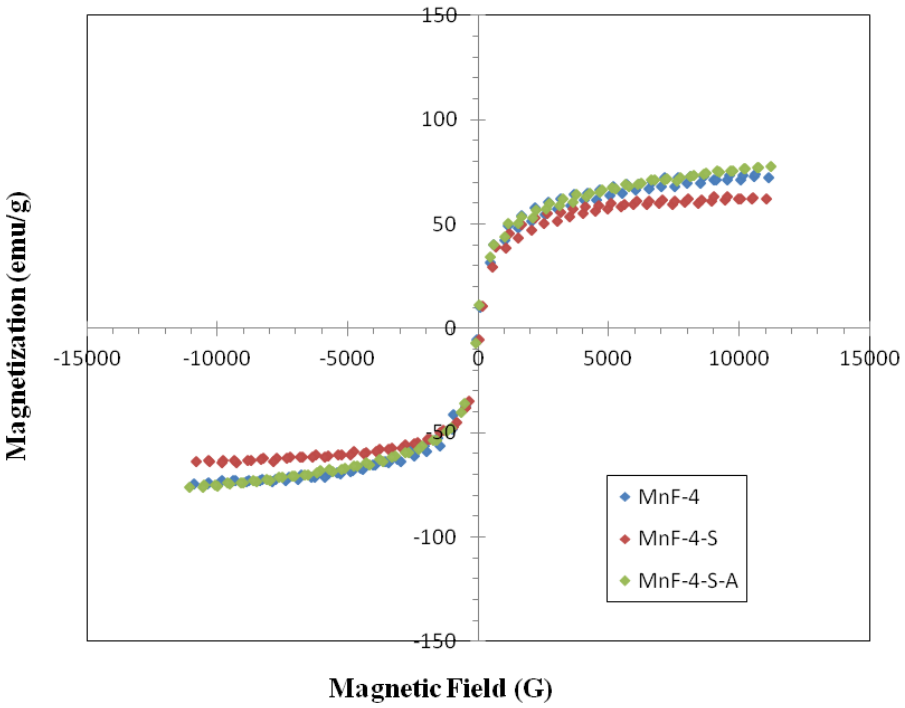

Figure C.40: MnF-4, MnF-4-S and MnF-4-S-A VSM results.

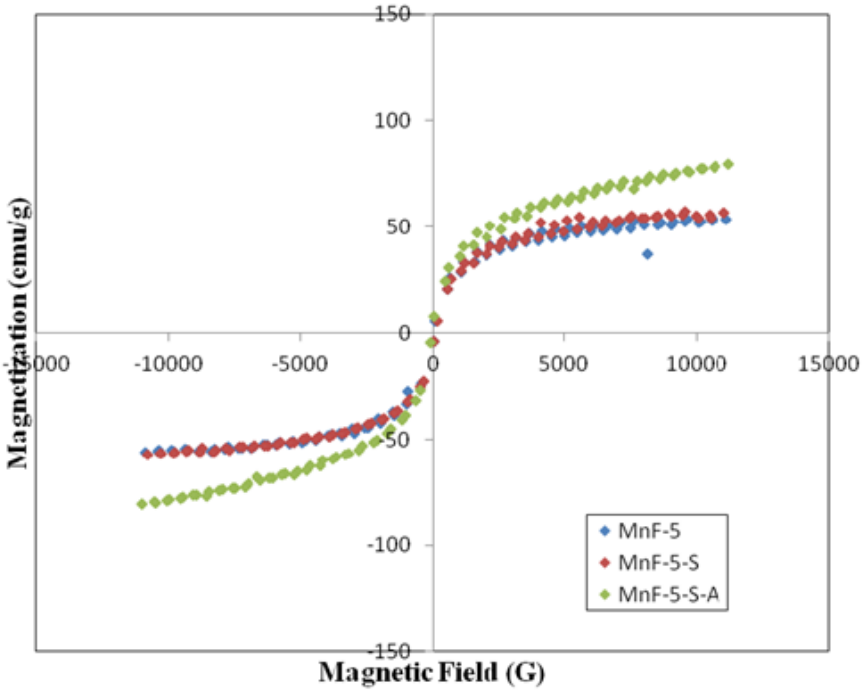

Figure C.41: MnF-5, MnF-5-S and MnF-5-S-A VSM results.

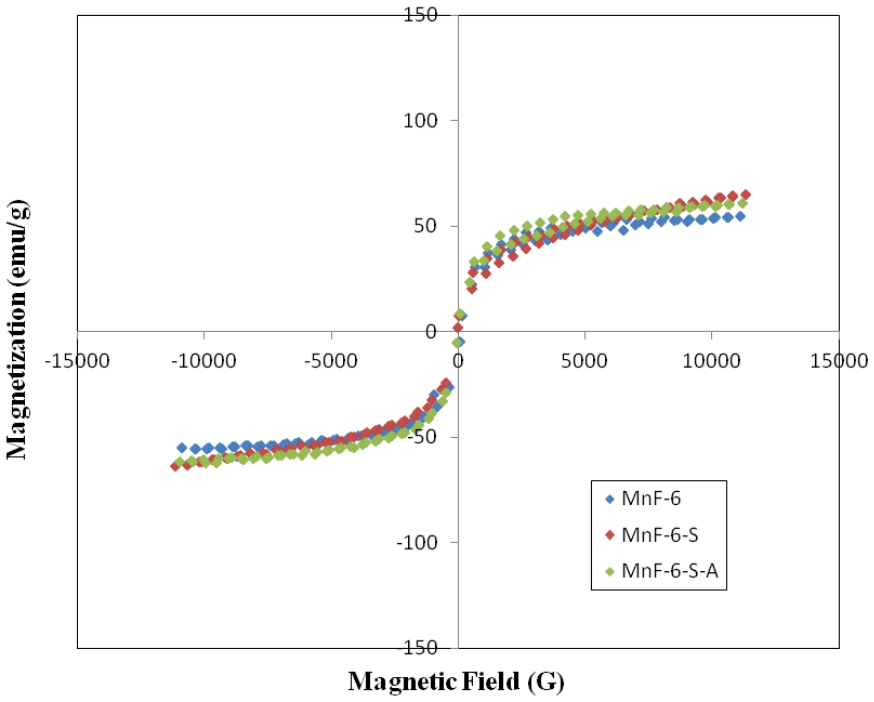

Figure C.42: MnF-6, MnF-6-S and MnF-6-S-A VSM results.

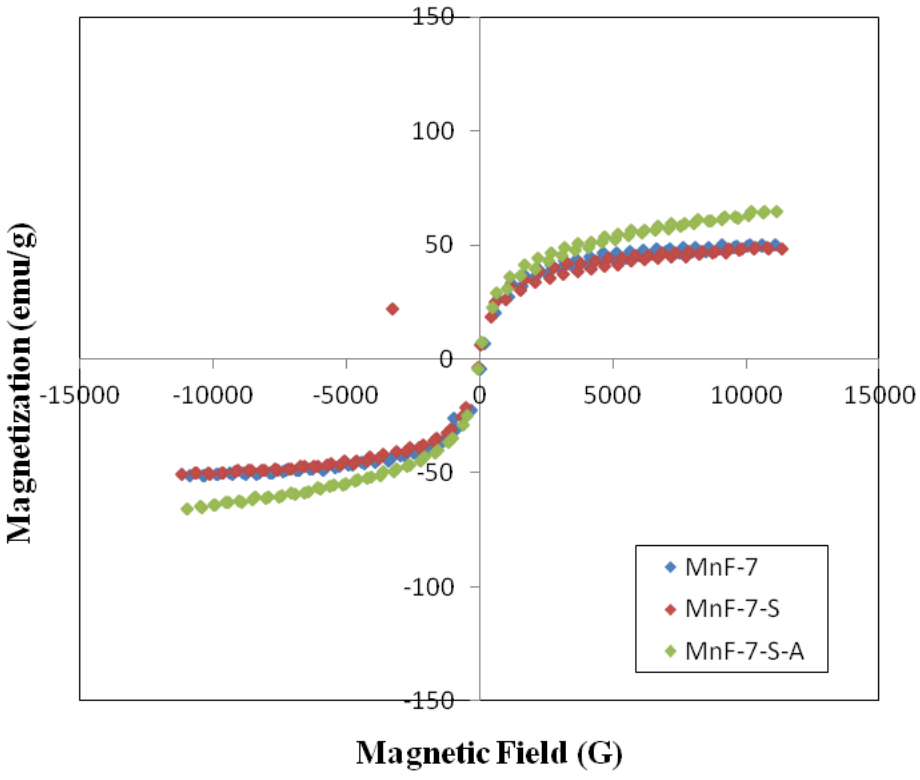

Figure C.43: MnF-7, MnF-7-S and MnF-7-S-A VSM results.

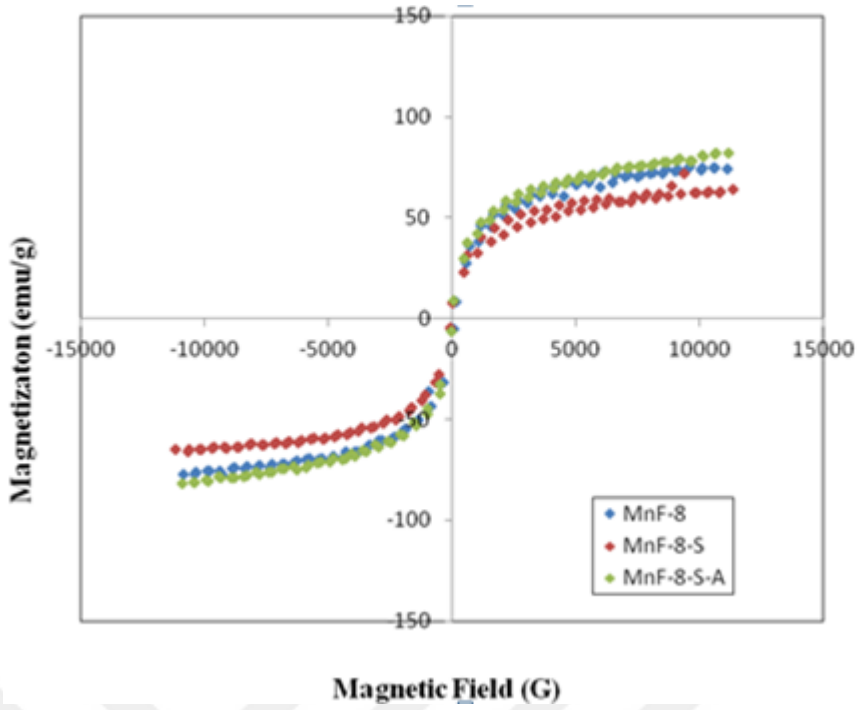

Figure C.44: MnF-8, MnF-8-S and MnF-8-S-A VSM results.

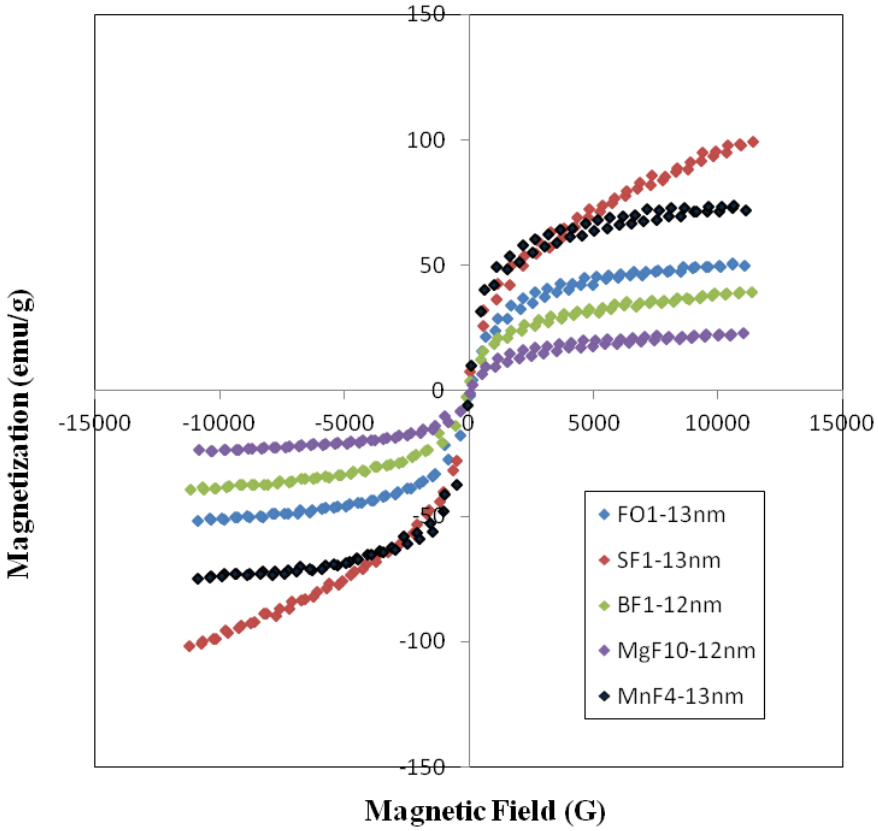

Figure C.45: Comparison of magnetization of all kinds of magnetic nanoparticles with 12 to 13 nm.

CURRICULUM VITAE

Name Surname **:** Mona Nejatpour

Place and Date of Birth **:** Maragheh/ 09.02.1991

E-Mail **:** monanejatpour@gmail.com

EDUCATION **:**

- **B.Sc.** **:** 2014, Tabriz University, Faculty of Mechanical Engineering, Mechanical Engineering